Mathematical Models for the Coinfection Dynamics of Cholera and Typhoid

by

Lunga Masiza Matsebula

THESIS

Submitted in fulfillment of the requirements for the degree of

DOCTOR OF PHILOSOPHY

in the

Department of Mathematics and Applied Mathematics

of the

Faculty of Science

UNIVERSITY OF JOHANNESBURG

Supervisor: **Prof. Farai Nyabadza**

Declaration

The work presented in this thesis was carried out in the Department of Mathematics and Applied Mathematics at the University of Johannesburg. The thesis was done under the supervision of Professor Farai Nyabadza. I declare that this work is in line with the plagiarism policy of the University of Johannesburg. This means that the work is authentic and original, and it has no copy right infringement. I further declare that no unethical research practises were used, nor was any material gained through dishonest means. I understand that plagiarism is a serious offence.

Lunga Masiza Matsebula

Prof. Farai Nyabandza

Abstract

Due to deteriorating infrastructure and declining infrastructure funding in African countries, There is a resurgence of cholera and typhoid fever. Poor waste disposal systems, poor hygiene and seasonal rains have been the main drivers of these two infections. Recently in Zimbabwe, an outbreak of the two infections was observed. Given that both infections are water-borne, a logical question is: was the outbreak of these two diseases a coincidence, or is there more structural mechanism to explain the observed coinfection? In this work, we attempt to answer such a question. We develop a system of ordinary differential equations to model the transmission dynamics of both diseases. We further add time dependant infection rates to model the dynamics of diseases in fluctuating environments. The model steady states are determined and analysed, and the role of fear is incorporated into the models. Impact analysis - how the diseases impact each other - is carried out. Numerical simulations and sensitivity analysis are used to verify the analytic results. We discover that for the greatest impact of disease control, the management of the diseases should be carried out in tandem. The public health implications of these results are articulated.

Keywords: Fear, Seasonality, Stability analysis, Basic reproduction number, Cholera, Typhoid, Coinfection, Impact analysis.

Contents

List of Figures

List of Tables

Chapter 1

Introduction

1.1 Background

Cholera is a bacterial infection with two modes of transmission: direct transmission, which is human to human transmission; and indirect transmission, which results from ingesting contaminated food. The latter form of transmission is more common in cholera endemic areas. Cholera infects a maximum of 4 million people annually, and of those that are infected, 21,000 to 143,000 people die from the disease [92]. Known estimates for the incubation period for cholera range between one and five days. Cholera is associated with watery diarrhoea, vomiting, and severe dehydration. At its worst form, the disease can cause a previously healthy person: to lose as much as one liter per hour of fluids, to become hypertensive in under four hours, and to die in within a day [40]. Death is usually preceded by renal failure, shock, pulmonary oedema and hypokalaemia due to dehydration.

Typhoid Fever is a life-threatening bacterial infection caused by *Salmonella Typhi* [84]. The transmission modes of typhoid are identical to those of cholera: direct transmission and indirect transmission. This disease adversely affects the recticuloendothelical system, the gall bladder and the intestinal lymphoid [52]. Known

estimates of the incubation period for the typhoid fever disease range from ten to fourteen days [52]. The case fatality rate of typhoid fever was $10 - 20\%$ before the advent of treatment, whilst, with prompt treatment, the case fatality rate was reduced to less than 1% [29]. It was observed that the total number of deaths, throughout the world, caused by typhoid fever in the year 1990 was 181 000 [1]; in the year 2000, it was 217 000 [21]; and in the year 2013, it was 161 000 [1]. In the Democratic Republic of Congo, more than 42 000 people contracted the typhoid fever disease during the years 2004 and 2005 [94]; whilst in Zimbabwe, Harare, there were 3187 suspected cases of typhoid and 191 confirmed cases of typhoid in the year 2018 [61].

1.2 Cholera

1.2.1 Classification of Cholera Strains

Several strains of the cholera bacteria have been discovered recently. The *V. cholerae* serogroup is divided into three subclasses, namely: *V. cholerae* 01, *V. cholerae* 0139, and others [40] (see Figure 1.1). The *V. cholerae* 01 serogroup has two biotypes: the El Tor biotype and the classical biotype. Each of the biotypes contain three Serotypes, and they are: Ogawa, Inaba, Hikojima [47]. Serotypes further divide into antigens. The known antigens are A,B; A,C; and A,B,C. Figure 1.1 summarizes the classification. It has been shown that the *V. cholerae* 01 Serogroup, El Tor biotype is the most common strain of *V. cholerae*, and the *V. cholerae* 0139 is the least common strain of cholera. Both of these strains are resistant to drugs, and the *V. cholerae*, El Tor biotype strain was responsible for the most recent cholera pandemic [49].

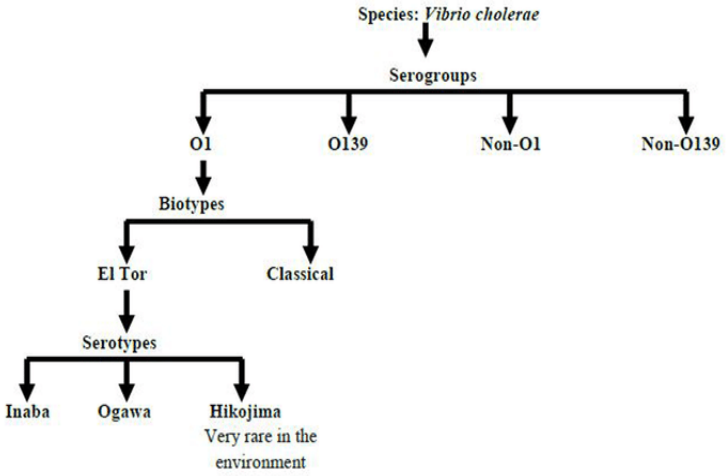

Figure 1.1: Source: [47]. The classification of *V. cholerae* strains.

1.2.2 History of Cholera

Records from the World Health Organisation show that, in the past two centuries, cholera has been responsible for seven pandemics [92]. The first six pandemics were caused by a strain of the bacteria emanating from the serogroup *V. cholerae* 01 and the classical biotype, whilst the last strain of the bacteria came from the serogroup *V. cholerae* 01 and the El Tor biotype [49]. Figure 1.2 shows the different pandemics [43]. Figure 1.3 attests to how the African continent has been disproportionately affected by the cholera disease [4]. The African continent accounted for 90% of the global cholera cases in 1990 [25]. We note that the reported cases, reporting countries, and the number of deaths were on an upward trend, whilst the case fatality ratio showed the opposite trend. A possible explanation for such observations is that improvements in reporting could have led to better management of the disease. Indeed, it can be noted that after the year

1990, the number of reporting countries increased, suggesting that there was better data collection. Better data collection inevitably leads to more reported cases and more reported deaths. The downward trend of the case fatality ratio suggests an improvement in the management of the disease despite the overall increase in deaths.

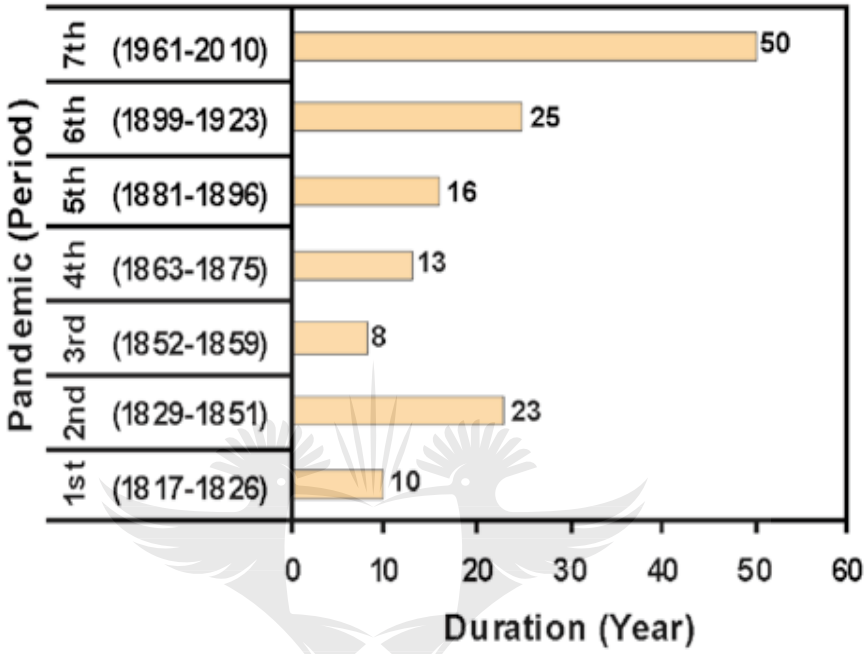

Figure 1.2: Soure: [43]. The seven cholera pandemics and their durations in years.

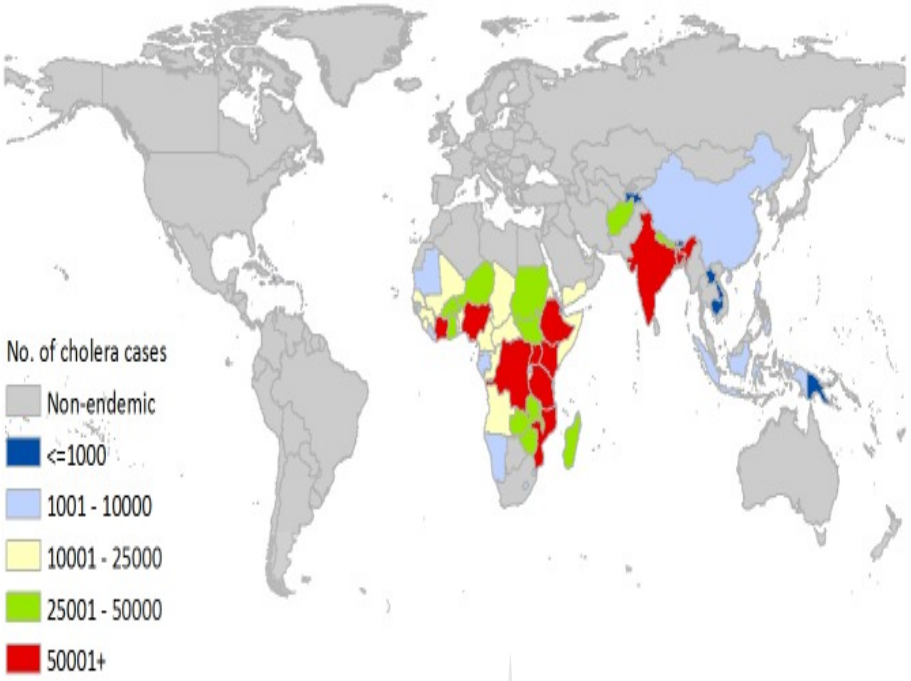

Figure 1.3: Soure: [4]. Annual number of cholera cases in endemic countries.

1.3 Typhoid Fever

1.3.1 Classification of Typhoid Fever Strains

Salmonella comes from the Kingdom and phylum Eubacteria and Proteobacteria [42] (See Figure 1.4). The bacteria's class, order and family, respectively, are Gammaproteobacteria, Enterobacteriales and Enterobacteriaceae. Salmonella has two species and six subspecies. The subspecies are bongori and enterica, whilst the subspecies are enterica (I), salamae (II), arizonae (IIIa), diarizonae (IIIb), houtenae (IV), indica (VI). All six subspecies come from the species enterica. The enterica (I) subspecies has two Serovars, namely nontyphoidal and typhoidal. The nontyphoidal salmonella is characterized by gastroenteritis and food poisoning, whilst typhoidal Salmonella is characterized by typhoid fever and paratyphoid

fever [93].

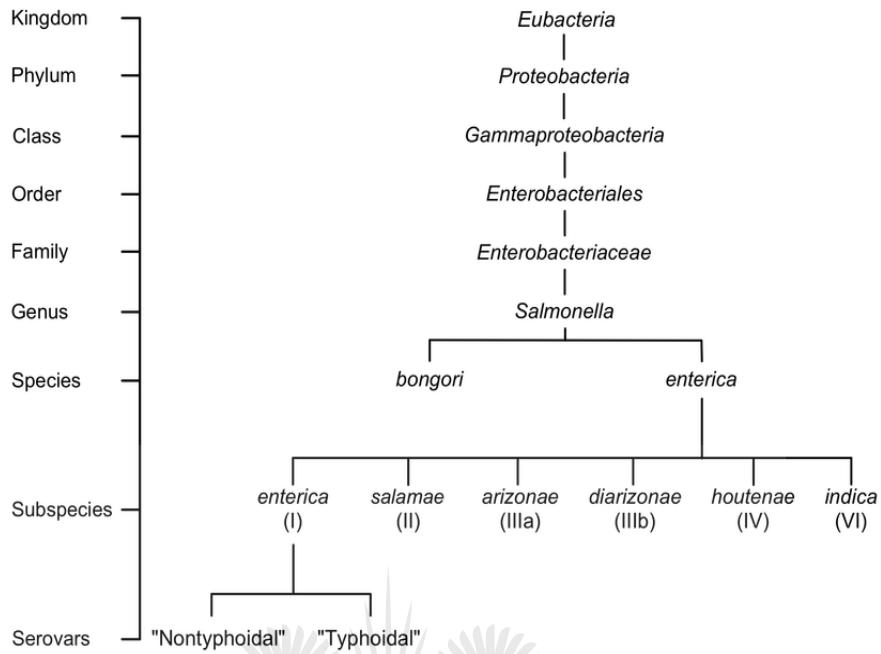

Figure 1.4: Source: [42]. The classification of Salmonella strains.

1.3.2 History of Typhoid Fever

The African continent has been disproportionately affected by typhoid fever. Although the total duration of the outbreaks in the African continent was the second shortest, the continent still managed to record the highest number of cases of the disease [5] (see Table 1.1). More than half (54%) of cases were recorded in the African continent, and the highest number of reporting countries were also under resourced African countries. Countries such as Uganda, Zimbabwe, Democratic Republic of Congo, Ethiopia, Kenya, The Malawi-Mozambique border and Zambia represented 32% of all countries reporting the outbreaks. Southeast Asia recorded highest number of outbreaks globally (13 outbreaks) within a period of 27 years, whereas the African continent recorded 12 outbreaks in nearly half that time (14 years) [5]. This underscores the severity of the infection within the

African continent, and it suggests that the African continent is key to the global management of typhoid fever.

Characteristic	WHO region*						Total
	African	Eastern Mediterranean	European	Region of the Americas	Southeast Asia	Western Pacific	
Outbreak years	2004–2018	1992–2017	1996–2008	1989–2015	1989–2016	1990–2014	1989–2018
Number of countries reporting outbreaks	8	3	4	1	4	5	25
Number of outbreaks	12	5	5	7	13	6	48
Number multidrug resistant	6	3	2	0	4	1	16
Number fluoroquinolone non-susceptible	6	1	0	0	2	2	11
Total number of cases	24,513	1,081	11,603	154	7,390	474	45,215
Median cases (range)	1,101 (98–10,230)	185 (27–486)	332 (6–10,677)	12 (3–68)	91 (11–5,963)	48 (7–253)	101 (3–10,677)
Number of confirmed cases	848	630	3,370	110	607	212	5,777
Median duration days (range)	140 (13–989)	60 (11–390)	23 (6–539)	50 (23–139)	36 (11–304)	101 (15–219)	57 (6–989)
Median incidence proportion (range)	0.2% (0–0.3%)	60% (60–60%)	16% (14–40%)	8% (8–8%)	3% (0.7–14%)	3% (1–5%)	5% (0–60%)
Median proportion hospitalized (range)**	27% (17–50%)	20% (20–20%)	34% (12–78%)	62% (31–82%)	63% (6–71%)	58% (3–64%)	50% (3–82%)
Median case fatality ratio (range)	1% (0.1–44%)	0% (0–1%)	0% (0–1%)	0% (0–4%)	0% (0–9%)	0% (0–0%)	0% (0–44%)

Table 1.1: Source: [5]. CFR indicates proportion of all cases that died.
*Twenty-five countries [number of outbreaks] reviewed by WHO region: African (Uganda [3], Zimbabwe [3], Democratic Republic of Congo [2], Ethiopia, Kenya, Malawi–Mozambique border, and Zambia), Eastern Mediterranean (Pakistan [2], Saudi Arabia [2], and Jordan), European (France [2], Turkey, Tajikistan, and Germany), region of the Americas (the United States [7]), Southeast Asia (India [8], Thailand [2], Thai–Myanmar border, Myanmar, and Nepal), and Western Pacific (China [2], Japan, Malaysia, Nauru, and Singapore).
∗∗ Incidence proportion, or attack rate, is the number of ill persons in the exposed population.

1.4 Significance of the Study

The significance of the study lies in understanding the transmission dynamics and intervention strategies for cholera and typhoid. Most specifically, the importance is captured in the following aspects of the work. First, the models discussed in this investigation add to the mathematical modelling of cholera and typhoid. Factors such as seasonality and the coinfection of the diseases are discussed in detail. Second, this investigation shows the interplay between the two infections. This is achieved through answering the following question: Are the two infections in conflict with one another, or are they symbiotic? Third, the work shows how the multiple transmission routes affect the disease prevalence, and how they affect the prevalence of coinfected individuals. Four, the results obtained in this investigation can be used to guide policy. Five, our work adds to the repository of mathematical techniques for modelling cholera and typhoid,
To this end, no effort is insignificant in modelling aspects of the diseases that are not well documented. Transmission of the diseases is driven by factors such as human movement, lifestyle, socio-economic status, climate, the presence of other infections and policies. Indeed, models that incorporate such factors can greatly enhance our understanding of these diseases. Future projections would have been possible had data been available. However due to this limitation, the models discussed in this work are not an alternative to the data, instead they should be viewed as a tool to make sense of the transmission of these diseases,

1.5 Aims and Objectives

In a broad sense, this study is themed around the construction and the analysis of mathematical models of typhoid and cholera. Poorly understood aspects of the transmission dynamics of cholera and typhoid are investigated. More specifically,

some of the objectives that are found in the various chapters in the thesis are:

I) To give an outline of the epidemiology of cholera, typhoid and their coinfection.

II) To uncover sufficient conditions that are required for the management of the diseases.

III) To justify, through software implementation and graphs, all analytic results produced by the study.

IV) To investigate the impact of seasonality on the prevalence of typhoid fever, and on the speed with which the disease propagates.

V) To design mathematical models on the coinfection of typhoid and cholera.

1.6 Motivation

Despite several models being dedicated to the study of cholera and typhoid fever in the literature, a number of open problems still persist. Aspects such as periodicity, human behaviour, age structure, vaccination, hyper-infectivity and lack thereof, and multiple transmission pathways have been modelled in order to understand and quantify their correlation with the prevalence of cholera [14, 22, 38, 39, 83, 90]. Factors such as treatments, carriers, and protected classes have also been modelled to understand how they affect typhoid prevalence [17, 58, 88]. Seasonality has been modelled for diseases such as cholera and schistosomiasis [11, 41, 71]. coinfection models have been developed for HIV and HCV, HIV and malaria, malaria and cholera, and listeriosis and anthrax [15, 63, 65, 68]. Although our work sits within the span of the factors mentioned above, it also differs in some respects. To the best of our knowledge, the following aspects of the two infections have not been considered in the literature: first, seasonality in typhoid; second, coinfection between typhoid and cholera; and last, seasonality

arising from the cholera-typhoid coinfection. Hence, these differences form the basis for our research.

1.7 Outline

This thesis consists of six chapters. Three of these chapters resulted in publications. The first chapter gives the background of the two infections. We outline the aims and the objectives of the study here, as well as to motivate why this study was carried out. The epidemiology of both diseases is also discussed in this chapter.

We carry out a review of the literature in the second chapter. The mathematical modelling techniques used by other modellers to study cholera, typhoid, seasonality and coinfection are documented. These techniques are then applied to our own models containing cholera, typhoid, seasonality and coinfection in the subsequent chapters.

A coinfection model for cholera and typhoid is developed and analysed in the third chapter. Numerical simulations are conducted to verify the analytic results obtained in this chapter.

The effects of seasonality and fear on typhoid fever are investigated in chapter 4. We compare a seasonal model and a non seasonal model, and changes to the basic reproduction number are documented. The work from this chapter yielded a publication.

A summary and conclusion for this investigation is provided in chapter 5. We make recommendations for the management of the diseases, and we discuss the limitations of this thesis in this chapter.

In the next chapter, a brief literature review of work that is closely related to our topic is provided.

Chapter 2

Literature Review

Since the emergence of the first cholera pandemic and the emergence of the first typhoid epidemic, numerous mathematical models have been created to gain insights into how these diseases propagate. The rationale behind the modelling was that knowledge of these diseases' transmission patterns would unravel clues on how to break the transmission routes. In this chapter, we discuss the mathematical methods employed in the study of cholera, typhoid, seasonality, and coinfections.

2.1 Mathematical Models on Cholera

Tian and Wang [83] proposed a few models to study the global stability for cholera. One such model is the following,

$$\begin{aligned}\frac{\mathrm{d}S}{\mathrm{d}t} &= bN - Sf(B) - bS,\\ \frac{\mathrm{d}I}{\mathrm{d}t} &= Sf(B) - (\gamma + b)I,\\ \frac{\mathrm{d}B}{\mathrm{d}t} &= eI - mB.\end{aligned}$$

All variables and parameters are as defined in [83]. The cholera models that are analysed in this paper derive their uniqueness from the incorporation of environ-

mental factors and multiple transmission routes. Using three methods, new global stability results were obtained for the cholera models. The method of monotone dynamical systems converts a three-dimensional autonomous dynamical system into a two-dimensional one. The application of this method is easier than the geometric method. However, most high dimensional systems do not meet the conditions required for the applications of the method of monotone dynamical systems. The geometric approach imposes fewer constraints on a model, however its implementation is significantly more cumbersome than the implementation of the method of monotone dynamical systems. The Lyapunov functions method has been widely used to study global stability, despite its weakness of relying heavily on trial and error for the construction of the Lyapunov function. Using Volterra Lyapunov matrix analysis, the authors extended the Lyapunov function framework for analysing global stability.

A cholera model with vaccination was formulated by Cui *et al.*[22]. The model proposed was the following,

$$\begin{aligned}
\frac{\mathrm{d}S}{\mathrm{d}t} &= \mu_1 - \frac{\beta_1 SB}{1+\alpha_1 B} - \frac{\beta_2 SI}{1+\alpha_2 I} - \phi S - \mu_1 S + \theta V,\\
\frac{\mathrm{d}V}{\mathrm{d}t} &= \phi S - \theta V - \mu_1 V,\\
\frac{\mathrm{d}I}{\mathrm{d}t} &= \frac{\beta_1 SB}{1+\alpha_1 B} + \frac{\beta_2 SI}{1+\alpha_2 I} - (d+\alpha+\mu_1)I,\\
\frac{\mathrm{d}R}{\mathrm{d}t} &= \alpha I - \mu_1 R,\\
\frac{\mathrm{d}B}{\mathrm{d}t} &= \eta I - \mu_2 B.
\end{aligned}$$

All variables and parameters are as defined in [22]. In this work, a $SVIR - B$ cholera model was developed and analysed. This model justifies the use of an imperfect vaccine. It also considers environmental components and multiple transmission routes. Under certain conditions, the control reproduction number has to be less than unity for global asymptotic stability at the disease free equilibrium. The control reproduction number has to be greater than one for global stability at the endemic equilibrium. It is observed that in the absence of vaccination (perfect or otherwise), the model showed that disease transmission was high. Parameters that are most sensitive to change to the control reproduction number are the vac-

cination rate and the immunity waning rate. A necessary and sufficient condition for the eradication of cholera is that the vaccination rate and the waning rate must exceed a certain threshold, whilst the control reproduction number must be less than unity.

Kokomo and Emvudu [38] developed an age structured model for cholera with vaccination. The model they introduced was a coupled system of PDEs and ODEs, such as

$$\begin{aligned}
&\frac{\partial S}{\partial t}(a,t) + \alpha \frac{\partial S}{\partial a}(a,t) = \Lambda(a,t) - [\lambda_i(a,t) + \lambda_d(a,t) + \psi(a) + \mu(a)]S(a,t),\\
&\frac{\partial I}{\partial t}(a,t) + \alpha \frac{\partial I}{\partial a}(a,t) = (\lambda_i(a,t) + \lambda_d(a,t))(S(a,t) + \sigma V(a,t)) - [\gamma(a) + \mu(a)]I(a,t),\\
&\frac{\partial V}{\partial t}(a,t) + \alpha \frac{\partial V}{\partial a}(a,t) = \psi(a)S(a,t) - (\lambda_i(a,t) + \lambda_d(a,t))\sigma V(a,t) - \mu(a)V(a,t), \quad (2.1)\\
&\frac{\partial R}{\partial t}(a,t) + \alpha \frac{\partial R}{\partial a}(a,t) = \gamma(a)I(a,t) - \mu(a)R(a,t),\\
&\frac{\mathrm{d}B_H(t)}{\mathrm{d}t} = \int_0^A \xi(a)\eta I(a,t)\,\mathrm{d}a - \chi B_H(t),\\
&\frac{\mathrm{d}B_H(t)}{\mathrm{d}t} = \chi B_H(t) - \delta_L B_L(t).
\end{aligned}$$

All variables and parameters are as defined in [38]. In model (2.1), work by Cai *et al.* [14] was extended. The extension was carried out through the inclusion of a hyper-infective class and a less-hyper infective class. The model consists of four PDEs and two ODEs. Semigroup theory was used to show that the model has a unique positively bounded solution. The existence of a unique equilibrium was established. The model showed that the disease free equilibrium was locally asymptotically stable whenever the reproduction number was less than one and it was unstable whenever it was greater than one. Whenever the endemic equilibrium was unstable, the disease was alleviated under certain conditions. These conditions include the basic reproduction number being greater than one and the threshold parameter $\mathcal{R}^*$ being less than one. On the other hand, vaccinations were ineffective whenever the reproduction number and $\mathcal{R}^*$ were greater than one.

The influence of human behaviour on the dynamics of cholera was modelled by

Wang *et al.* [90]. The model formulated has the following structure,

$$\begin{aligned}
\frac{\mathrm{d}S}{\mathrm{d}t} &= \mu N - \beta_1(I)SI - \beta_2(I)\frac{SB}{B+K} - \mu S + \sigma R,\\
\frac{\mathrm{d}I}{\mathrm{d}t} &= \beta_1(I)SI + \beta_2(I)\frac{SB}{B+K} - (\gamma+\mu)I,\\
\frac{\mathrm{d}R}{\mathrm{d}t} &= \gamma I - (\mu+\sigma)R,\\
\frac{\mathrm{d}B}{\mathrm{d}t} &= \beta_3(I)I - \delta B.
\end{aligned}$$

All variables and parameters are as defined in [90]. Human behaviour and how it affects the dynamics of cholera are documented in this article. These models give a mathematical justification for reducing the prevalence levels of cholera, reducing the speed of spreading the disease, and reducing infection risk factors for heterogeneous and homogeneously mixing individuals. An assumption made for these models was that human behaviour can be influenced by media coverage, and by extension, media coverage also influences cholera dynamics. The force of infection and the shedding rate are also assumed to be decreasing functions of the infection size. The homogeneously mixing individuals and bacteria are modelled through a set of ODEs, whilst the heterogeneous mixing hosts and bacteria are modelled through PDEs. A consistent finding in both models was that when the basic reproduction number was greater than one, the disease would persist and the endemic equilibrium was asymptotically stable. A comparison between the reproduction numbers of the PDE model and the ODE model was carried out, and the major finding was that the different models predict different risk structures. The models' limitations include: the failure to incorporate fake news, the failure to incorporate non-random movement and the failure to factor in seasonality.

A mathematical model of cholera in a periodic environment with control actions

was studied by Kolaye *et al.* [39]. The following model was presented,

$$\begin{aligned}
\frac{\mathrm{d}S}{\mathrm{d}t} &= \lambda - \left(\beta \frac{B_H + \epsilon B_L}{K_c + B_H + B_L} + \mu\right) S + \gamma R. \\
\frac{\mathrm{d}I}{\mathrm{d}t} &= \left(\beta \frac{B_H + \epsilon B_L}{K_c + B_H + B_L}\right) S - (\mu + d + \alpha) I, \\
\frac{\mathrm{d}R}{\mathrm{d}t} &= \alpha I - (\mu + \gamma) R, \\
\frac{\mathrm{d}B_H}{\mathrm{d}t} &= r B_L \left(1 - \frac{B_H}{K + C}\right) - (\mu_H + v) B_H + \delta I, \\
\frac{\mathrm{d}B_L}{\mathrm{d}t} &= v B_H - \mu_L B_L.
\end{aligned}$$

All variables and parameters are as defined in [39]. The controls are introduced for this model, and they include sensitization and sanitation. To model these controls, impulsive differential equations are utilised. An effective control strategy would be the implementation of campaigns for both sensitization and sanitation. The model showed that when the basic reproduction number was greater than one, the disease persisted, and the endemic equilibrium was globally asymptotically stable. It is observed that sensitisation alone was insufficient for the control of cholera. Kolaye *et al.* concluded that the fight against cholera should consider both controls, that is sensitisation and sanitation.

2.2 Mathematical Models on Typhoid

Analytic solutions to a typhoid fever model (2.2) were calculated by Peter *et al.* [66] using the Variational Iteration Method (VIM). The model presented in [66] is given by,

$$\begin{aligned}
\frac{\mathrm{d}S}{\mathrm{d}t} &= \theta - \mu_1 S - \lambda S, \\
\frac{\mathrm{d}I_c}{\mathrm{d}t} &= \rho \lambda S - (\mu_2 + \epsilon_1) I_c, \\
\frac{\mathrm{d}I}{\mathrm{d}t} &= (1 - \rho) \lambda S - (\mu_3 + \delta + \epsilon) I, \\
\frac{\mathrm{d}R}{\mathrm{d}t} &= \delta I - \mu_4 R, \\
\frac{\mathrm{d}W}{\mathrm{d}t} &= \epsilon_1 I_c + \epsilon_2 I - \mu_b W.
\end{aligned} \tag{2.2}$$

All variables and parameters are as defined in [66]. In this model, a direct and indirect transmission pathway was considered for typhoid fever. A series solution was presented for the model using the Variational Iteration Method (VIM). The VIM produced series solution was then compared to the fourth order Runge Kutta method to determine the accuracy of the VIM. The major result was that the VIM was just as accurate as the fourth order Runge Kutta method in calculating the trajectories of the typhoid fever model.

The modelling of typhoid fever with a protected class was carried out by Nthiiri *et al.* [58]. The model they developed and analysed was the following,

$$\begin{aligned}
\frac{\mathrm{d}P}{\mathrm{d}t} &= \alpha\Lambda - (\gamma + \mu)P, \\
\frac{\mathrm{d}S}{\mathrm{d}t} &= (1-\alpha)\Lambda + \gamma P - (\lambda + \mu)S, \\
\frac{\mathrm{d}I}{\mathrm{d}t} &= \gamma S - (\delta + \beta + \mu)I, \\
\frac{\mathrm{d}T}{\mathrm{d}t} &= \beta I - \mu T.
\end{aligned}$$

All variables and parameters are as defined in [58]. The model shows that effective control prevents infection especially in resource scarce areas. For example, vaccination lowers the disease induced mortality; the improvement of life standards, through better health care and sanitation, leads to a reduction in the infection rate; and controls applied to susceptible individuals, through prevention strategies, keep the susceptible individuals from getting infected. Indeed, the evidence seems to suggest that controls are vital for the prevention of the disease.

Chamuchi *et al.* [17] formulated a typhoid fever model with carriers. The model they formulated was as follows,

$$\begin{aligned}
\frac{\mathrm{d}S}{\mathrm{d}t} &= b - d_1 S - (\beta I_c + \gamma I)S - \theta S, \\
\frac{\mathrm{d}I_c}{\mathrm{d}t} &= p(\beta I_c + \gamma I)S - (d_2 + \alpha)I_c, \\
\frac{\mathrm{d}I}{\mathrm{d}t} &= (1-p)(\beta I_c + \gamma I)S - (d_3 + \pi)I + \alpha I_c, \\
\frac{\mathrm{d}R}{\mathrm{d}t} &= \pi I - \theta S - d_4.
\end{aligned}$$

All variables and parameters are as defined in [17]. In this model, the effects of carriers on the transmission dynamics of typhoid fever are analysed. It was discovered that when the reproduction number was less than one, the disease free equilibrium was stable. The basic reproduction number was most sensitive to the following parameters: the human recruitment rate; and the typhoid transmission by non-symptomatic individuals, symptomatic individuals, and the proportion of individuals who become non symptomatic upon infection. The cumulative typhoid cases are most sensitive to treatment. High prevalence of typhoid can be observed whenever the carriers outnumber the treated individuals. Some of the limitations of the model include: firstly, all recruited individuals are assumed to be susceptible; secondly, treatment is less effective whenever there is a high number of carriers.

The optimal control mathematical model (2.3) for the transmission dynamics of typhoid fever with treatment was analyzed by Wameko *et al.* [88].

$$\begin{aligned}
\frac{\mathrm{d}E}{\mathrm{d}t} &= p\pi - (\varphi + \mu)E, \\
\frac{\mathrm{d}S}{\mathrm{d}t} &= (1-p)\pi = \varphi E + \alpha R - (\lambda + \mu)S, \\
\frac{\mathrm{d}C}{\mathrm{d}t} &= p\lambda S - (\gamma + \theta + d_1 + \mu)C, \\
\frac{\mathrm{d}I}{\mathrm{d}t} &= (1-p)\lambda S + \gamma C - (\beta + d_2 + \mu)I, \\
\frac{\mathrm{d}R}{\mathrm{d}t} &= \theta C + \beta I - (\alpha + \mu)R, \\
\frac{\mathrm{d}B}{\mathrm{d}t} &= r\left(1 - \frac{B}{M}\right)B.
\end{aligned} \tag{2.3}$$

All variables and parameters are as defined in [88]. This model was developed to investigate how carriers, immune individuals and infectious individuals affect the transmission dynamics of typhoid. The model stabilizes to the disease-free equilibrium whenever the basic reproduction number is less than one, and it stabilizes to the endemic equilibrium whenever the basic reproduction number is greater than one. Changes to the basic reproduction number were found to be highly sensitive to the salmonella ingestion rate. Hence, sanitation was key for the man-

agement of the disease. Optimal control was introduced through several control strategies. Prevention, treatment and screening of careers significantly diminished the prevalence of the disease. The most optimal control strategy was found to be a combination of all three controls, and this optimal control strategy led to the disease dying out within two months.

2.3 Mathematical Models on Seasonality

Posny and Wang [71] presented a cholera model for periodic environments. They formulated the following model,

$$\begin{aligned}
\frac{\mathrm{d}S}{\mathrm{d}t} &= bN - Sf(t,I,B) - bS,\\
\frac{\mathrm{d}I}{\mathrm{d}t} &= Sf(t,I,B) - (\gamma + b)I,\\
\frac{\mathrm{d}R}{\mathrm{d}t} &= \gamma I - bR,\\
\frac{\mathrm{d}B}{\mathrm{d}t} &= h(t,I,B).
\end{aligned}$$

All variables and parameters are as defined in [71]. Two major challenges arise in the mathematical modeling of cholera. Firstly, the disease has multiple transmission routes, and model accuracy is enhanced by considering the human-to-human transmission and the environment-to-human transmission pathways. Secondly, the disease has a strong seasonal component. The major drivers of seasonality are usually societal, environmental, climatic and ecological. In this paper, a general mathematical framework for developing and analyzing non-autonomous periodic cholera models was presented. Ordinarily, seasonal fluctuations are added in the incidence function and the pathogen function. However, these fluctuations could also be added to other functions and model parameters, depending on the question that is being modeled. The major finding of this investigation is that the cholera model stabilizes to the disease free equilibrium when the basic reproduction number is less than one, and the model shows uniform persistence whenever the basic reproduction number is greater than one. These findings were then verified on three specific cholera models.

A seasonal model on positive periodic solutions of an general epidemic model

was proposed by Sun *et al.* [80]. The model that they proposed was the following,

$$\begin{aligned}
\frac{\mathrm{d}S}{\mathrm{d}t} &= rN\left(1-\frac{N}{k}\right)-\frac{\beta(t)SI}{N}-mS,\\
\frac{\mathrm{d}E}{\mathrm{d}t} &= \frac{\beta(t)SI}{N}-\sigma E-mE,\\
\frac{\mathrm{d}I}{\mathrm{d}t} &= \sigma E-mI-\mu I.
\end{aligned}$$

All variables and parameters are as defined in [80]. The seasonal model that was developed in this paper contains logistic growth and density dependent transmission. Including these two factors improves the accuracy of the model. The global stability analysis for the disease-free-equilibrium was carried out, and the attractive regions for the fixed points were determined. Two thresholds were found to be key in deciding the dynamical behaviour of the model. The first threshold was the basic demographic reproduction number $\mathcal{R}_d$, and the second threshold was the basic reproduction number $\mathcal{R}_0$. A sufficient condition for the model to stabilise at the endemic equilibrium was $\mathcal{R}_0 > 1$ and $\mathcal{R}_d > \mathcal{R}_0$, and a sufficient condition for the model to stabilise to the disease free equilibrium was $\mathcal{R}_0 > 1$and $\mathcal{R}_d < \mathcal{R}_0$. Several numerical methods have been developed to compute the basic reproduction number of mathematical models with seasonality in the literature. These methods were used to compare the basic reproduction number and the average basic reproduction number in his paper. The investigation showed that the average basic reproduction number consistently overestimates the risk of disease. The model would be greatly improved by the inclusion of spatial effects.

Li *et al.* [41] studied a Schistosomiasis model with seasonality, such as

$$\begin{aligned}
\frac{\mathrm{d}S_H}{\mathrm{d}t} &= \Lambda_H-\lambda_H S_H P-\mu_H S_H+\gamma_H I_H,\\
\frac{\mathrm{d}I_H}{\mathrm{d}t} &= \lambda_H S_H P-(\mu_H+\lambda_M)I_H,\\
\frac{\mathrm{d}M}{\mathrm{d}t} &= \lambda_M I_H-\mu_M M,\\
\frac{\mathrm{d}S_V}{\mathrm{d}t} &= \Lambda_V-\lambda_V S_V M-\alpha_V I_V,\\
\frac{\mathrm{d}P}{\mathrm{d}t} &= \lambda_P I_V-\mu_P P.
\end{aligned}$$

All variables and parameters are as defined in [41]. In this model, the seasonal fluctuations are incorporated in the forces of infection. The basic reproduction

number is calculated, and the stability of the dynamical system is analyzed. The model was fitted to data to justify its applicability to this study. It is observed that the main drivers of seasonality are rainfall, temperature and the area of snails. Control of the disease can be achieved through educational campaigns, where these campaigns focus on educating the public about the transmission routes of the disease, and the prevention of contact with contaminated water. Treatment is also an important factor to consider in the management of the disease. The model shows that migration is the primary driver of resurgence of the disease in China. This is due to migrants importing different strains of the infection into the country. Contact tracing is one method that can be used to mitigate this resurgence. A limitation of the model is that it does not consider how the different strains of the infection interact with various animal hosts.

Bilal and Michael [11] studied the effects of complexity and seasonality on backward bifurcation in vector-host models by analysing the following model,

$$
\begin{aligned}
\frac{\mathrm{d}S_1}{\mathrm{d}t} &= \Pi_{\mathrm{H1}} - \lambda_{\mathrm{H1}} S_1 - \mu_{\mathrm{H1}} S_1 + \alpha_{\mathrm{H1}} R_1, \\
\frac{\mathrm{d}E_1}{\mathrm{d}t} &= \lambda_{\mathrm{H1}} S_1 - (\mu_{\mathrm{H1}} + \sigma_{\mathrm{H1}}) E_1, \\
\frac{\mathrm{d}I_1}{\mathrm{d}t} &= \sigma_{\mathrm{H1}} E_1 - (\tau_{\mathrm{H1}} + d_{\mathrm{H1}} + \mu_{\mathrm{H1}}) I_1, \\
\frac{\mathrm{d}R_1}{\mathrm{d}t} &= \tau_{\mathrm{H1}} I_1 - \mu_{\mathrm{H1}} R_1 - \alpha_{\mathrm{H1}} R_1, \\
\frac{\mathrm{d}S_2}{\mathrm{d}t} &= \Pi_{\mathrm{H2}} - \lambda_{\mathrm{H2}} S_2 - \mu_{\mathrm{H2}} S_2 + \alpha_{\mathrm{H2}} R_2, \\
\frac{\mathrm{d}E_2}{\mathrm{d}t} &= \lambda_{\mathrm{H2}} S_2 - (\mu_{\mathrm{H2}} + \sigma_{\mathrm{H2}}) E_2, \\
\frac{\mathrm{d}I_2}{\mathrm{d}t} &= \sigma_{\mathrm{H2}} E_2 - (\tau_{\mathrm{H2}} + d_{\mathrm{H2}} + \mu_{\mathrm{H2}}) I_2, \\
\frac{\mathrm{d}R_2}{\mathrm{d}t} &= \tau_{\mathrm{H2}} I_2 - \mu_{\mathrm{H2}} R_2 - \alpha_{\mathrm{H2}} R_2, \\
\frac{\mathrm{d}M_{\mathrm{S}}}{\mathrm{d}t} &= \Pi_{\mathrm{M}} - \lambda_{\mathrm{M}} M_{\mathrm{S}} - \mu_{\mathrm{M}} M_{\mathrm{S}}, \\
\frac{\mathrm{d}M_{\mathrm{E}}}{\mathrm{d}t} &= \lambda_{\mathrm{M}} M_{\mathrm{S}} - (\mu_{\mathrm{M}} + \sigma_{\mathrm{M}}) M_{\mathrm{E}}, \\
\frac{\mathrm{d}M_{\mathrm{I}}}{\mathrm{d}t} &= \sigma_{\mathrm{M}} M_{\mathrm{E}} - (d_{\mathrm{M}} + \mu_{\mathrm{M}}) M_{\mathrm{I}}.
\end{aligned}
$$

All variables and parameters are as defined in [11]. Most vector host models exhibit backward bifurcations. The effects of complexity, including seasonality, on backward bifurcations have not been investigated. In these models, delay classes are added and the effects on $\mathcal{R}_c$ are then documented. The models show that $\mathcal{R}_c$ is increased whenever the complexity of the model is increased through the addition of an exposed compartment or immune compartment. The results show how

complexity affects the bifurcation region of diseases. Culling of the host is the most effective control strategy for WNV since an increase in the natural death rate of hosts results in an increase in $\mathcal{R}_c$. Host vaccination is the most effective control strategy for malaria and dengue fever. This follows from the observation that increased immunity decreases the bifurcation regions. In cases where complexity is introduced through seasonality, it was discovered that highly seasonal vector host diseases are much easier to manage than weakly seasonal ones. This results follows from the observation that seasonality increases $\mathcal{R}_c$ whilst also decreasing $\mathcal{R}_0$. Nonlinear transmission rates and variable parameters are factors that also contribute to model complexity, yet these models have not accounted for these two factors. This could be considered to be the models' weaknesses.

A stochastic seasonal cholera model was formulated by Baracchini *et al.* [8]. The novelty of the model lies in the following two compartments: the water volume compartment and the pathogen concentration compartment. The model they formulated is as follows,

$$\begin{aligned}
\frac{\mathrm{d}S}{\mathrm{d}t} &= \kappa\epsilon R_3 + H + \frac{\mathrm{d}H}{\mathrm{d}t} - (\lambda(t) + \mu)S,\\
\frac{\mathrm{d}I}{\mathrm{d}t} &= \lambda(t)S - (\gamma + m + \mu)I,\\
\frac{\mathrm{d}R_1}{\mathrm{d}t} &= \gamma I - (\kappa\epsilon + \mu)R_1,\\
\frac{\mathrm{d}R_2}{\mathrm{d}t} &= \kappa\epsilon R_1 - (\kappa\epsilon + \mu)R_2,\\
\frac{\mathrm{d}R_3}{\mathrm{d}t} &= \kappa\epsilon R_2 - (\kappa\epsilon + \mu)R_3,\\
\frac{\mathrm{d}V}{\mathrm{d}t} &= J(t) - ET(T,V) - f(V)V,\\
\frac{\mathrm{d}B}{\mathrm{d}t} &= -\mu_B(T)B + p(t)[1 + \phi J(t)]I\xi(t) - f(V)B.
\end{aligned}$$

All variables and parameters are as defined in [8]. Mass migration and climate change remain a huge problem for policy makers. This model shows the strong link between the problem of mass migration and climate change, and the resurgence of cholera. In particular, it shows that water levels of a region are the main drivers of seasonality for the cholera disease. In dry regions, rainfall increases the prevalence of cholera; whilst, in wet regions, rainfall decreases the prevalence of cholera due to the dilution effect. For this reasons, understanding how water levels affect the transmission of cholera is vital to the management of this disease. Since migration and climate change have a direct impact on the water levels of a region, it follows that migration and climate change have a bearing on the resurgence of

a disease like cholera.

2.4 Mathematical Models on Coinfections

A coinfection model for Human Immunodeficiency Virus (HIV) and Hepatitis C Virus (HCV) was analyzed by Carvalho and Pinto [15]. The model that they presented in the paper was the following:

$$
\begin{aligned}
\frac{\mathrm{d}S}{\mathrm{d}t} &= \Lambda - \lambda_H S - \lambda_C S + r_1 I_c - \mu S,\\
\frac{\mathrm{d}I_a}{\mathrm{d}t} &= \lambda_H S - (\rho + \sigma\lambda_C + \mu) I_a + (1-\epsilon)\theta I_a + r_2 I_a I_c + \upsilon_1 A_a,\\
\frac{\mathrm{d}A_a}{\mathrm{d}t} &= \rho I_a - (\upsilon_1 + d_a + \mu) A_a + r_3 A_a I_c + \sigma\lambda_C A_a,\\
\frac{\mathrm{d}I_c}{\mathrm{d}t} &= \lambda_C S - (r_1 + \delta\lambda_H + \rho_1\sigma_C + \mu) I_c,\\
\frac{\mathrm{d}C_c}{\mathrm{d}t} &= \rho_1\sigma_C I_c - (\delta\lambda_H + d_c + \mu) I_C,\\
\frac{\mathrm{d}I_a I_c}{\mathrm{d}t} &= \delta\lambda_H I_c + \sigma\lambda_C I_a + \upsilon_2 A_a I_c - (r_2 + \rho + \rho_2\sigma_C + \mu) I_a I_c,\\
\frac{\mathrm{d}I_a C_c}{\mathrm{d}t} &= \rho_2\sigma_C I_a I_c + \delta\lambda_H C_c + \upsilon_3 A_a C_c - (\rho + d_c + \mu) I_a C_c,\\
\frac{\mathrm{d}A_a I_c}{\mathrm{d}t} &= \sigma\lambda_C A_a + \rho I_a I_c - (r_3 + \upsilon_2 + \rho_3\sigma_C + \mu + d_a) A_a I_c,\\
\frac{\mathrm{d}A_a C_c}{\mathrm{d}t} &= \rho_3\sigma_C A_a I_c + \rho I_a C_c - (\upsilon_3 + d_c + \mu + d_a) A_a A_c.
\end{aligned}
$$

All the variables and parameters are as defined in [15]. The model shows that treatment and educational campaigns are vital for the management of the HIV-HCV coinfection in humans. Campaigns aimed at reducing the number of sexual partners per person, and those that highlight the benefits of treatment amongst pregnant women, reduce the prevalence of HIV; whilst, campaigns aimed at educating people about the transmission routes of HCV, and those that highlight the benefits of treatment of HCV, reduce the number of carriers and infections by HCV. Additionally, HIV can be further controlled through the distribution of more condoms and enhancing research into AIDS.

Pinto and Carvalho [68] explained how treatment, awareness and condom use amongst homosexual men affects the HIV-HCV coinfection dynamics. The model

that they presented was the following:

$$\frac{\mathrm{d}S_{\bar{s}}}{\mathrm{d}t} = \Lambda_1 + \upsilon I_{\bar{c}} - \lambda_h S_{\bar{s}} - \lambda_c S_{\bar{s}} - kS_{\bar{s}} - \mu S_{\bar{s}},$$
$$\frac{\mathrm{d}S_s}{\mathrm{d}t} = \Lambda_2 + \upsilon I_c - (1-\psi)\lambda_h S_s - \lambda_c S_s + kS_{\bar{s}} - \mu S_s,$$
$$\frac{\mathrm{d}I_{\bar{a}}}{\mathrm{d}t} = (1-p)(1-\psi)\lambda_h S_s + \lambda_h S_{\bar{s}} - (\rho_1 + \sigma\lambda_c + \mu + k)I_{\bar{a}} + \upsilon_1 I_{\bar{a}} I_c,$$
$$\frac{\mathrm{d}I_a}{\mathrm{d}t} = p(1-\psi)\lambda_h S_s - (\rho_2 + \sigma\lambda_c + \mu)I_a + kI_{\bar{a}} + \upsilon_1 I_a I_c,$$
$$\frac{\mathrm{d}A_{\bar{a}}}{\mathrm{d}t} = \rho_1 I_{\bar{a}} - (\delta_2 + \mu)A_{\bar{a}},$$
$$\frac{\mathrm{d}A_a}{\mathrm{d}t} = \rho_2 I_a - (\delta_2 + \sigma\lambda_c + \mu)A_a + \upsilon_2 A I_c,$$
$$\frac{\mathrm{d}I_{\bar{c}}}{\mathrm{d}t} = \lambda_c S_{\bar{s}} - (k + \upsilon + \sigma_1 + \delta\lambda_h + \delta_1 + \mu)I_{\bar{c}},$$
$$\frac{\mathrm{d}I_c}{\mathrm{d}t} = \lambda_c S_s + kI_{\bar{c}} - (\upsilon + \sigma_1 + (1-\psi)\delta\lambda_h + \delta_1 + \mu)I_c,$$
$$\frac{\mathrm{d}C_{\bar{s}}}{\mathrm{d}t} = \sigma_1 I_{\bar{c}} - (k + \delta\lambda_h + \delta_1 + \mu)C_{\bar{s}},$$
$$\frac{\mathrm{d}C_s}{\mathrm{d}t} = \sigma_1 I_c + kC_{\bar{s}} - ((1-\psi)\delta\lambda_h + \delta_1 + \mu)C_s,$$
$$\frac{\mathrm{d}I_{\bar{a}}I_c}{\mathrm{d}t} = (1-p)(1-\psi)\delta\lambda_h I_c + \delta\lambda_h I_{\bar{c}} + \sigma\lambda_c I_{\bar{a}} - (k + \upsilon_1 + \rho_2 + \sigma_2 + \delta_1 + \mu)I_{\bar{a}} I_c,$$
$$\frac{\mathrm{d}CI_{\bar{a}}}{\mathrm{d}t} = (1-p)(1-\psi)\delta\lambda_h C_s + \delta\lambda_h C_{\bar{s}} + \sigma_2 I_c I_{\bar{a}} - (k + \rho_2 + \delta_1 + \mu)CI_{\bar{a}},$$
$$\frac{\mathrm{d}CI_a}{\mathrm{d}t} = p(1-\psi)\delta\lambda_h C_s + \sigma_2 I_c I_a + kCI_{\bar{a}} - (\rho_2 + \delta_1 + \mu)CI_a,$$
$$\frac{\mathrm{d}AI_c}{\mathrm{d}t} = \sigma\lambda_c A_a + \rho_2 I_{\bar{a}} I_c + \rho_2 I_a I_c - (\upsilon_2 + \sigma_2 + \delta_1 + \delta_2 + \mu)AI_c,$$
$$\frac{\mathrm{d}AC}{\mathrm{d}t} = \rho_2 CI_{\bar{a}} + \rho_2 CI_a + \sigma_2 I_c A - (\mu + \delta_1 + \delta_2)CA.$$

All the variables and parameters are as defined in [68]. The model incorporates classes for treatment, individuals that are aware and unaware of their diagnosis of HIV and condom use. The model is analyzed for stability, and bifurcation diagrams are drawn to determine the probability of a contact resulting in a successful transmission of HIV. The model shows that condom availability and educational awareness campaigns are crucial in reducing the prevalence of HIV. Educational campaigns should be focused on highlighting the importance of condom use during anal sex and the reduction of the number of sexual partners. HIV reduction is heavily dependent on the treatment of AIDS and the prevalence of new drugs to combat the infection. Treatment and information campaigns are also necessary to reduce the prevalence of HCV. The limitations of the model include the lack

of data to fit the model, as well as its failure to incorporate the effects of sharing needles on the dynamics of the coinfection.

Osman and Makinde [65] developed model (2.4) to study the transmission dynamics of a listeriosis and anthrax coinfection.

$$
\begin{aligned}
\frac{\mathrm{d}S}{\mathrm{d}t} &= \Omega_h + kR_a + \omega R_f + \psi R_{al} - \beta_h I_v S_h - \pi S_h - \mu_h S_h,\\
\frac{\mathrm{d}I_a}{\mathrm{d}t} &= \beta_h I_v S_h - \pi I_a - (\alpha + \mu_h + \phi) I_a,\\
\frac{\mathrm{d}I_t}{\mathrm{d}t} &= \pi S_h - \beta_l I_v I_t - (\delta + \mu_h + m + \rho) I_l,\\
\frac{\mathrm{d}I_{al}}{\mathrm{d}t} &= \beta_h I_v I_l + \pi I_a + (\sigma + \mu_h + \eta + \theta) I_{al},\\
\frac{\mathrm{d}R_a}{\mathrm{d}t} &= \alpha I_a - (k + \mu_h) R_a + (1-\tau)\gamma\sigma I_{al},\\
\frac{\mathrm{d}R_l}{\mathrm{d}t} &= \delta I_l - (\omega + \mu_h) R_l + (1-\tau)(1-\gamma)\sigma I_{al},\\
\frac{\mathrm{d}R_{al}}{\mathrm{d}t} &= \tau\sigma I_{al} - (\psi + \mu_h) R_{al},\\
\frac{\mathrm{d}C_p}{\mathrm{d}t} &= \rho I_l + \theta I_{al} - \mu_b C_p,\\
\frac{\mathrm{d}S_v}{\mathrm{d}t} &= \theta_v - \beta_v (I_a + I_{al}) S_v - \mu_v S_v,\\
\frac{\mathrm{d}I_v}{\mathrm{d}t} &= \beta_v (I_a + c I_{al}) S_v - \mu_v I_v.
\end{aligned}
\tag{2.4}
$$

All variables and parameters are as defined in [65]. The sub-models (anthrax only and listeriosis only models) show that a unique and endemic equilibrium exists whenever the basic reproduction number is greater than one, and they show that the model stabilizes to a disease free equilibrium whenever the basic reproduction number is less than one. For the coinfection model, the model exhibits backward bifurcation, and it follows from the backward bifurcation that the disease free equilibrium and the endemic equilibrium coexist whenever the basic reproduction number is less than one. Sensitivity analysis was carried out for both sub-models. For the anthrax sub-model, the basic reproduction number was most sensitive to the human transmission rate, vector transmission rate, human recruitment rate and the vector recruitment rate; for the listeriosis sub-model, the basic reproduction number was most sensitive to the bacteria ingestion rate, listeriosis related death rate, human recruitment rate and the listeriosis shedding rate. For the coinfection model, increases in the infected classes of anthrax listeriosis are caused by an

increase in the human contact rate.

The implications of HIV treatment on the HIV-malaria coinfection dynamics were studied from a modelling perspective by Nyabadza *et al.* [59]. The model they used to study the coinfection was the following,

$$
\begin{aligned}
\frac{\mathrm{d}S}{\mathrm{d}t} &= \Lambda_H + \phi E_M + \gamma I_M - (\lambda_M + \lambda_H + \mu)S,\\
\frac{\mathrm{d}E_M}{\mathrm{d}t} &= \Lambda_M S - (\phi + p + \mu)E_M,\\
\frac{\mathrm{d}I_M}{\mathrm{d}t} &= pE_M - (\gamma + \omega\lambda_H + \mu\delta_M)I_M,\\
\frac{\mathrm{d}I_H}{\mathrm{d}t} &= \lambda_H S + \epsilon_1\gamma I_{HM} - (\eta_1\lambda_M + \rho_1 + \alpha_1 + \mu + \delta_H)I_H,\\
\frac{\mathrm{d}T_H}{\mathrm{d}t} &= \rho_1 I_H + qT_{HM} - (\alpha_3 + \eta_3\lambda_M + \mu + \varphi\delta_H)T_H,\\
\frac{\mathrm{d}A_H}{\mathrm{d}t} &= \alpha_1 I_H + \epsilon_2\gamma A_{HM} - (\eta_2\lambda_M + \rho_2 + \mu + \delta_A)A_H,\\
\frac{\mathrm{d}T_A}{\mathrm{d}t} &= \rho_2 A_H + \alpha_3 T_H + \sigma qT_{AM} - (\eta_4\delta_M + \mu + \varphi\delta_A)T_A,\\
\frac{\mathrm{d}I_{HM}}{\mathrm{d}t} &= \eta_1\lambda_M I_H + \omega\lambda_M I_M - (\epsilon_1\gamma + \alpha_2 + \mu + \tau\delta_M)I_{HM},\\
\frac{\mathrm{d}A_{HM}}{\mathrm{d}t} &= \alpha_2 I_{HM} + \eta_2\lambda_M A_H - (\epsilon_2\gamma + \mu + \tau\delta_A)A_{HM},\\
\frac{\mathrm{d}T_{HM}}{\mathrm{d}t} &= \eta_3\lambda_M T_H - (q + \alpha_4 + \mu + \tau\delta_H)T_{HM},\\
\frac{\mathrm{d}T_{AM}}{\mathrm{d}t} &= \eta_4\lambda_M T_A + \alpha_4 T_{HM} - (\sigma q + \mu\tau\delta_A)T_{AM},\\
\frac{\mathrm{d}S_V}{\mathrm{d}t} &= \Lambda_V - (\lambda_V + \mu_V)S_V,\\
\frac{\mathrm{d}E_V}{\mathrm{d}t} &= \lambda_V S_V - (\theta_V + \mu_V)E_V,\\
\frac{\mathrm{d}I_V}{\mathrm{d}t} &= \theta_V E_V - \mu_V I_V.
\end{aligned}
$$

All variables and parameters are as defined in [59]. The model showed that understanding the dynamics of HIV in malaria endemic settings is vital to understanding the overall disease burden within Sub Saharan Africa. The model demonstrated that malaria exacerbates HIV prevalence, and it also showed that treatment remains one of the most crucial aspects of control for this disease. The authors advocate for a control strategy that is centered around treatment. However, the model displayed two major limitations: firstly, the number of parameters that were obtained from the literature was very low — only five of the forty three parameters were not estimated; secondly, the dynamics of those who are initially infected with malaria and subsequently infected with HIV are not shown by the model. This shows that only a partial understanding of the dynamics of the coin-

fection of HIV and malaria can be obtained through this model.
The following coinfection model of malaria and cholera diseases with optimal control was developed by Okosun and Makinde [63],

$$\begin{aligned}
\frac{\mathrm{d}S_h}{\mathrm{d}t} &= \Lambda_h + kR_m + \omega R_c + \psi R_{mc} - \beta_h I_v S_h - \lambda S_h - \mu_h S_h,\\
\frac{\mathrm{d}I_m}{\mathrm{d}t} &= \beta_h I_v S_h - \lambda I_m - (\alpha + \mu_h + \phi) I_m,\\
\frac{\mathrm{d}I_c}{\mathrm{d}t} &= \lambda S_h - \beta_h I_v I_c - (\delta + \mu_h + m) I_c,\\
\frac{\mathrm{d}G_{mc}}{\mathrm{d}t} &= \beta_h I_v I_c + \lambda I_m - (\sigma + \mu_h + \eta + q) G_{mc},\\
\frac{\mathrm{d}R_m}{\mathrm{d}t} &= \alpha I_m - (\kappa + \mu_h) R_m + \epsilon(1-\sigma) G_{mc},\\
\frac{\mathrm{d}R_c}{\mathrm{d}t} &= \delta I_c - (\omega + \mu_h) R_c + (1-\epsilon)(1-\sigma) G_{mc},\\
\frac{\mathrm{d}R_{mc}}{\mathrm{d}t} &= \sigma G_{mc} - (\psi + \mu_h) R_{mc},\\
\frac{\mathrm{d}B_c}{\mathrm{d}t} &= \rho(I_c + \theta G_{mc}) - \mu_b B_c,\\
\frac{\mathrm{d}S_v}{\mathrm{d}t} &= \Lambda_v - \beta_v (I_m + G_{mc}) S_v - \mu_v S_v,\\
\frac{\mathrm{d}I_v}{\mathrm{d}t} &= \beta_v S_v (I_m + G_{mc}) - \mu_v I_v.
\end{aligned}$$

All variables and parameters are as defined in [63]. The analysis of the confection model showed that the model attained local stability at the disease free equilibrium on condition the basic reproduction number was less than one. However, global asymptotic stability at the disease free equilibrium is not guaranteed if the basic reproduction number is less than one. This follows from the observation that the model exhibits backwards bifurcation, so the endemic equilibrium and the disease free equilibrium could coexist whenever the basically production number is less than one. Impact analysis revealed the malaria infection increases the risk of cholera, and that the converse was not true. It was discovered that a control strategy that exclusively targets each of the diseases yielded sub optimal results. Hence, optimal intervention was achieved when control of these two diseases was conducted in tandem.

Common limitations in the models mentioned above are the following. First, we observed that most of the models do not account for disease induced mortality. This implies that their populations are assumed to be constant. This is a restric-

tive assumption given that few societies meet this criterion. Models that factor in changes to population levels tend to be more realistic. Second, behavioural change induced by fear of infection and improvement of hygiene levels is seldom modelled for these two infections. It is reasonable to assume that when lethal infections like cholera and typhoid break out, people often change their behaviour to avoid getting infected. Third, models often disproportionately focus on one of the two transmission routes for these diseases. This is usually guided by the question that is being answered in that investigation. We seldom find investigations that quantify the impact of breaking the transmission in one of the routes has on the transmission of the other route.

The subsequent chapter includes the analysis of a cholera and typhoid coinfection mathematical model.

Chapter 3

Mathematical Analysis of Cholera Typhoid Coinfection Transmission Dynamics

3.1 Introduction

Cholera, an acute gastro-intestinal water-borne infection, is caused by the bacterium *Vibrio Cholerae*, V. *cholerae* O1 or O139. Some of the symptoms are vomiting and diarrhoea. If treatment is delayed, it can lead to severe dehydration and death within a few hours. The disease has two modes of transmission: direct and indirect transmission. Direct transmission (human-human) is very uncommon, whilst indirect transmission (environment-human), which occurs through the ingestion of contaminated food or water [13], is more frequent. A known estimate for the incubation period of cholera is 1.4 days [7]. On the other hand, the *Salmonella Typhi* bacteria is responsible for causing the life threatening typhoid fever disease. Cholera and typhoid fever have the same transmission modes. The recticuloendothelical system, the intestinal lymphoid, and the gall bladder are severely damaged by the typhoid fever disease. Once a susceptible individuals is

infected with typhoid fever, roughly 19 days are required for the disease to incubate within the host [81].

Mathematical models have been used for the past decades to give insights into the transmission dynamics of coinfections within the human population. Akinyi *et al.* [3], showed that whenever the basic reproduction number is lowered to below one, then the malaria and the pneumonia cases will be reduced in a model of malaria-pneumonia coinfection. Onyinge *et al.* [64] modelled the co-dynamics of pneumonia and HIV, and they showed that the model was mathematically and epidemiologically sound; Mushayabasa *et al.* [54] modelled malaria-typhoid coinfection and demonstrated that a typhoid outbreak will inevitably lead to a spike in the malaria cases. A number of mathematical models on typhoid have been proposed by a number of researchers. Mushayabasa [55], modelled how vaccines can help mitigate the spread of typhoid in Ghana. Pitzer *et al.* [69], extended the work in [55] by applying the model to South Asia. Khan *et al.* [36], studied the typhoid disease with a saturated incidence rate.

To the best of our knowledge, the coinfection dynamics of typhoid and cholera have not been investigated in the literature. A recent outbreak of these two infections in Zimbabwe prompted this theoretical inquiry into how these infections interact. Due to the complicated nature of the coinfection model, we begin our analysis by studying the underlying sub-models; namely, the cholera only and the typhoid only sub-models. For each of the models, a number of pertinent questions are investigated. The questions explored include: Which factors in the models are key to decreasing the prevalence of each disease and the coinfection? Within the population, are the infections in competition with each other, or are they symbiotic? The implications of the results to the public health are discussed.

The paper is arranged as follows; the development of the model and the properties of the basic reproduction number are established in Section 2. Section 3 contains the stability analysis of the model at the fixed points. Numerical simulations and parameter estimations are done in section 4. Section 5 concludes the chapter.

3.2 Methodology

3.2.1 Model Development

Our typhoid cholera coinfection model partitions the human population $N(t)$, at time t, into a susceptible class $S(t)$, a cholera infection class $I_c(t)$, a typhoid infection class $I_t(t)$, a coinfection class $I_{ct}(t)$, a cholera recovery class $R_c(t)$, a typhoid recovery class $R_c(t)$, and a coinfection recovery class $R_{ct}(t)$. Thus,

$$N(t) = S(t) + I_c(t) + R_c(t) + I_t(t) + R_t(t) + I_{ct}(t) + R_{ct}(t).$$

The bacterial concentration of *Salmonella Typhi*, $B_t(t)$, and *Vibrio Cholerae*, $B_c(t)$, in the environment are incorporated into the model as well. The formulation of this model is an extension to the work carried out by Matsebula *et al.* [45].

Since the incubation periods of the two infections are different, we assume that dually infected individuals can only transmit either cholera or typhoid but not both infections simultaneously. Transmission of cholera to susceptible individuals occurs in one of two routes—the direct transmission route (human-to-human) and the indirect transmission route (envirnment-to-human). The rates of the transmission routes, respectively, are given by

$$\lambda_{c_1} = \frac{\beta_{c_1}(I_c + \eta_c I_{ct})}{N}, \qquad \lambda_{c_2} = \frac{\beta_{c_2} B_c}{B_c + \kappa_c}.$$

The parameter β_{c_1} denotes the person-to-person cholera transmission. The effective contact rate for cholera multiplied by the probability of cholera transmission per contact gives the person to person cholera transmission. The modification parameter η_c, accounts for the relative infectiousness of individuals in class I_c relative to individuals in class I_{ct}. Since the contact rate of dually infected individuals is lower than the contact rate of individuals infected with a single disease (cholera or typhoid), it follows that $\eta_c \in (0, 1)$. The decreasing growth rate of bacteria and the saturation of bacteria are best modelled by a type II functional response. The

parameter β_{c_2} denotes the environment-to-humans per capita contact rate and the *Vibrio Cholerae* in the contaminated environment, whilst the parameter κ_c denotes the half saturation constant of the *Vibrio Cholerae*. The *half saturation constant* is the bacterial concentration that is required to support half of the maximum rate, β_{c_2}.

Similarly, the transmission of typhoid to susceptible individuals occurs in one of two routes—the direct transmission route (human-to-human) and the indirect transmission route (envirnment-to-human). The rates of the transmission routes, respectively, are given by

$$\lambda_{t_1} = \frac{\beta_{t_1}(I_t + \eta_t I_{ct})}{N}, \qquad \lambda_{t_2} = \frac{\beta_{t_2} B_t}{B_t + \kappa_t}.$$

The parameter β_{t_1} denotes the effective person-to-person typhoid transmission rate. The effective contact rate for typhoid multiplied by the probability of typhoid transmission per contact gives the person to person typhoid transmission. The modification parameter η_t, accounts for the relative infectiousness of individuals in class I_t relative to individuals in class I_{ct}. Analogously, the force of infection, λ_{t_2}, is modelled using a type II functional response, and it is assumed that $\eta_t \in (0, 1)$. The per capita contact rate between the susceptibles and *Salmonela typhi* is represented by β_{t_2}, and the half saturation constant for λ_{t_2} is κ_t.

Transmission of cholera to typhoid infected individuals occurs in one of two routes—the direct transmission route (human-to-human) and the indirect transmission route (environment-to-human). The rates of the transmission routes, respectively, are given by

$$\lambda_{c_3} = \frac{\beta_{c_3}(I_c + \eta_c I_{ct})}{N}, \qquad \lambda_{c_4} = \frac{\beta_{c_4} B_c}{B_c + \kappa_c}.$$

The parameter β_{c_3} denotes the effective person-to-person cholera transmission rate of individuals in class I_t. The parameter β_{c_4} denotes the environment-to-humans per capita contact rate for individuals in class I_t and the *Vibrio Cholerae* in the contaminated environment. Transmission of typhoid to cholera infected individuals occurs in one of two routes—the direct transmission route (human-to-human) and the indirect transmission route (environment-to-human). The rates of

the transmission routes, respectively, are given by

$$\lambda_{t_3} = \frac{\beta_{t_3}(I_t + \eta_t I_{ct})}{N}, \qquad \lambda_{t_4} = \frac{\beta_{t_4} B_t}{B_t + \kappa_t}.$$

The parameter β_{t_3} denotes the person-to-person typhoid transmission rate of individuals in class I_c. The parameter β_{t_4} denotes the environment-to-humans per capita contact rate for individuals in class I_c and the *Salmonella Typhi* in the contaminated environment.

Infected individuals in classes I_c, I_t and I_{ct} experience disease related death at rates given respectively by δ_c, δ_t and δ_{ct}. Individuals in the infectious states I_c and I_t respectively excrete *Vibrio Cholerae* bacteria and *Salmonella Typhi* bacteria into the environment at rates α_c and α_t. Coinfected individuals shed *Vibrio Cholerae* and *Salmonella Typhi* into the environments at rates θ_c and θ_t, respectively. Infection is assume to confer temporary immunity. The cholera and typhoid immunity wanes at rates ρ_c, ρ_t and ρ_{ct}.

The generation rate of *Vibrio Cholerae* is $g_c B_c \left(1 - \frac{B_c}{k_c}\right)$, and its growth is enhanced by cholera infected individuals and the coinfected individuals that are shedding into the environment. The generation rate of *Salmonella Typhi* is $g_t B_t \left(1 - \frac{B_t}{k_t}\right)$ and its growth is enhanced by typhoid infected individuals and the coinfected individuals that are shedding into the environment. We assume that the *Vibrio Cholerae* and the *Salmonella Typhi* bacteria in the environment are respectively removed by interventions such as improved sanitation and treatment of contaminated environments at rates μ_c and μ_t. The parameter Λ represents the recruitment into the susceptibles, while the parameter μ represents the natural death rate. It is assumes that individuals mix homogeneously and that they are indistinguishable in each of the classes. The model diagram is shown in Figure 3.1.

The dynamical system associated with the schematic diagram in Figure 3.1 is the following,

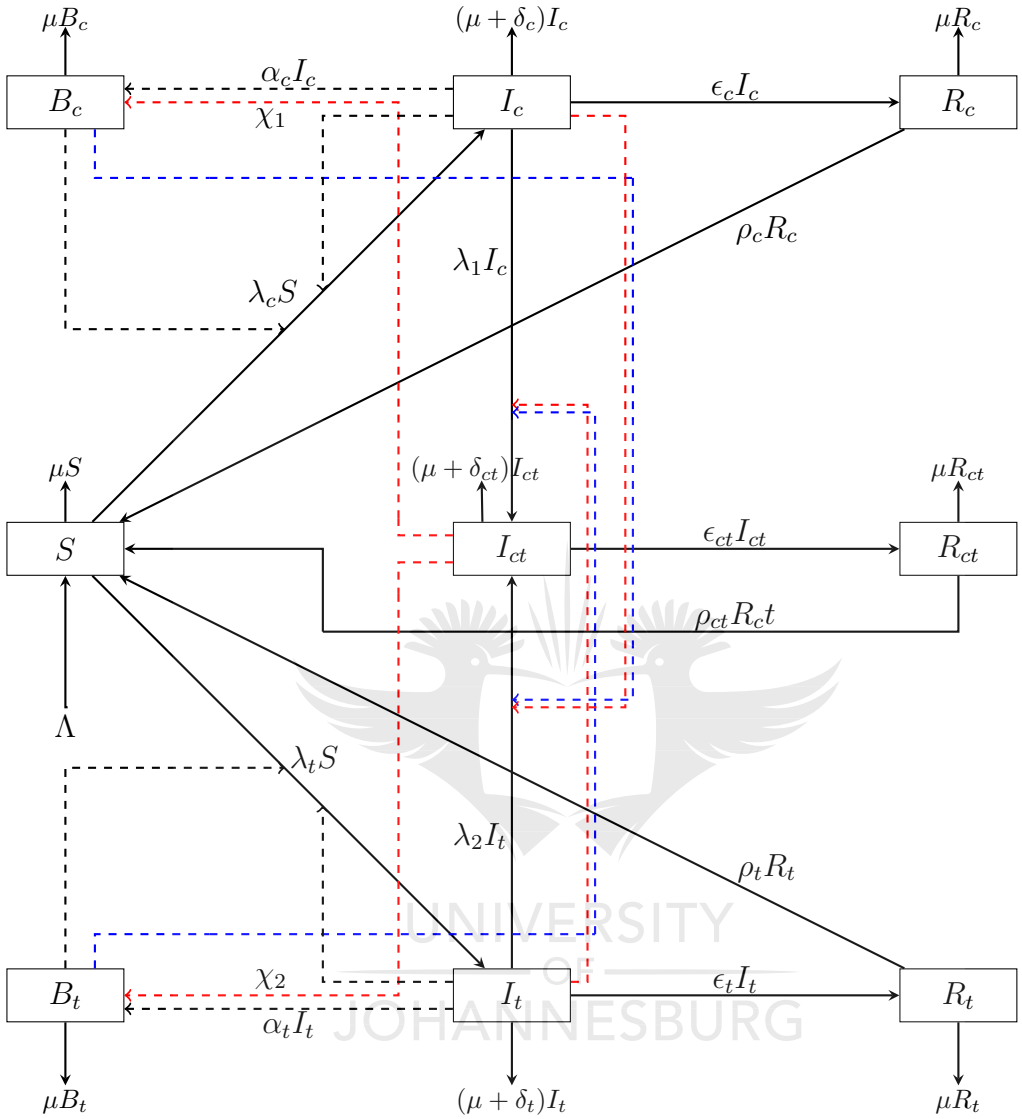

Figure 3.1: The cholera typhoid coinfection compartmental model. For the concise presentation of our model flow diagram, we make use of the following expressions:
$\chi_1 = g_c B_c \left(1 - \frac{B_c}{k_c}\right) + \theta_c I_{ct},\ \chi_2 = g_t B_t \left(1 - \frac{B_t}{k_t}\right) + \theta_t I_{ct},\ \lambda_c = \lambda_{c_1} + \lambda_{c_2},$
$\lambda_t = \lambda_{t_1} + \lambda_{t_2},\ \lambda_1 = \lambda_{t_3} + \lambda_{t_4},\ \lambda_2 = \lambda_{c_3} + \lambda_{c_4}.$

$$
\begin{aligned}
\frac{dS}{dt} =& \Lambda - (\lambda_{c_1} + \lambda_{c_2} + \lambda_{t_1} + \lambda_{t_2})S - \mu S + \rho_c R_c + \rho_t R_t + \rho_{ct} R_{ct}, \\
\frac{dI_c}{dt} =& (\lambda_{c_1} + \lambda_{c_2})S - (\lambda_{t_3} + \lambda_{t_4})I_c - (\mu + \delta_c + \epsilon_c)I_c, \\
\frac{dI_t}{dt} =& (\lambda_{t_1} + \lambda_{t_2})S - (\lambda_{c_3} + \lambda_{c_4})I_t - (\mu + \delta_t + \epsilon_t)I_t, \\
\frac{dI_{ct}}{dt} =& (\lambda_{t_3} + \lambda_{t_4})I_c + (\lambda_{c_3} + \lambda_{c_4})I_t - (\mu + \delta_{ct} + \epsilon_{ct})I_{ct}, \\
\frac{dR_c}{dt} =& \epsilon_c I_c - (\mu + \rho_c)R_c, \\
\frac{dR_t}{dt} =& \epsilon_t I_t - (\mu + \rho_t)R_t, \\
\frac{dR_{ct}}{dt} =& \epsilon_{ct} I_{ct} - (\mu + \rho_{ct})R_{ct}, \\
\frac{dB_c}{dt} =& g_c B_c \left(1 - \frac{B_c}{k_c}\right) + \alpha_c I_c + \theta_c I_{ct} - \mu_c B_c, \\
\frac{dB_t}{dt} =& g_t B_t \left(1 - \frac{B_t}{k_t}\right) + \alpha_t I_t + \theta_t I_{ct} - \mu_t B_t,
\end{aligned}
\tag{3.1}
$$

with initial conditions

$$
\begin{aligned}
S(0) =& S_0 > 0, \quad B_c(0) = B_{c0} \geq 0, \quad B_t(0) = B_{t0} \geq 0, \quad I_c(0) = I_{c0} \geq 0, \\
I_t(0) =& I_{t0} \geq 0, \quad I_{ct}(0) = I_{ct0} \geq 0, \; R_c(0) = R_{c0} \geq 0, \quad R_t(0) = R_{t0} \geq 0, \\
R_{ct}(0) =& R_{ct0} \geq 0.
\end{aligned}
$$

3.2.2 Cholera-only Model

We define the cholera only model as the model obtained from setting all the typhoid classes and its associated parameters to zero. We thus have the following

$$
\begin{aligned}
\frac{dS}{dt} &= \Lambda - (\tilde{\lambda}_{c_1} + \lambda_{c_2})S - \mu S + \rho_c R_c, \\
\frac{dI_c}{dt} &= (\tilde{\lambda}_{c_1} + \lambda_{c_2})S - q_c I_c, \\
\frac{dR_c}{dt} &= \epsilon_c I_c - (\mu + \rho_c)R_c, \\
\frac{dB_c}{dt} &= g_c B_c \left(1 - \frac{B_c}{k_c}\right) + \alpha_c I_c - \mu_c B_c,
\end{aligned}
\tag{3.2}
$$

where

$$\tilde{\lambda}_{c_1} = \frac{\beta_{c_1} I_c}{N_c}, \quad q_c = \mu + \delta_c + \epsilon_c, \quad N_c = S + I_c + R_c,$$

with initial conditions

$$S(0) = S_0 > 0, \quad B_c(0) = B_{c0} \geq 0, I_c(0) = I_{c0} \geq 0, \quad R_c(0) = R_{c0} \geq 0.$$

3.2.2.1 Boundedness and Non-negative Trajectories

We argue that model (3.2) yields non negative trajectories in this section. Within the feasible region, $\Omega \subseteq \Omega_c$, we summarize the results on the boundedness and positivity of the solutions to the cholera model, where

$$\Omega_c = \left\{ (S, I_c, R_c, B_c) \middle| 0 \leq N_c \leq \frac{\Lambda}{\mu} \right], B_c \in \left[0, \max \left\{ \frac{k_c(g_c - \mu_c + 1)}{g_c}, \alpha_c \frac{\Lambda}{\mu} \right\} \right] \right\}.$$

Theorem 1. *The set Ω_c is a positively invariant domain for dynamical system (3.2).*

Proof. Since $I_c \leq N_c$ and $B_c \leq B_c + \kappa_c$, it follows that

$$\frac{dS}{dt} \geq -(\tilde{\lambda}_{c_1} + \lambda_{c_2} + \mu)S \geq -(\beta_{c_1} + \beta_{c_2} + \mu)\, S. \tag{3.3}$$

If we integrate the separable differential inequality (3.3), we get a lower bound $S \geq S_0 \exp(-(\beta_{c_1} + \beta_{c_2} + \mu)\, t)$. Integrating the inequality

$$\frac{dI_c}{dt} \geq -q_c I_c$$

produces a lower bound $I_c \geq I_{c0} \exp(-q_c t)$. Similarly,
$R_c \geq R_{c0} \exp(-(\mu + \rho_c)t)$. The bacterial class, B_c, gives us the differential inequality

$$\frac{dB_c}{dt} \geq g_c B_c \left(1 - \frac{B_c}{k_c}\right) - \mu_c B_c.$$

This is a Bernoulli type differential inequality. The substitution, $y = B_c^{-1}$, produces a separable differential inequality

$$\frac{dy}{dt} + \Phi_c y \leq \eta_c, \tag{3.4}$$

where $\Phi_c = g_c - \mu_c$, $\eta_c = g_c/k_c$. Integrating (3.4) and substituting B_c back gives the lower bounds

$$B_c \geq \frac{\Phi_c}{\eta_c - M\exp(-\Phi_c t)} \geq \frac{-\Phi_c}{M\exp(-\Phi_c t)},$$

for some positive constant M. Note that $B_c \geq 0$ whenever $\mu_c \geq g_c$. □

Theorem 2. *All solutions of the cholera only sub-model (3.2) are bounded within* Ω *whenever* $\mu_c \geq g_c$.

Proof. The time derivative of the population for the cholera model (3.2) is bounded above by

$$\frac{dN_c}{dt} = \Lambda - \mu N_c - \delta_c I_c \leq \Lambda - \mu N_c,$$

Upper bounds for the human population, $N_c(t)$, are obtained by integrating the separable differential inequality as follows,

$$N_c \leq \frac{\Lambda - M\exp(-\mu t)}{\mu} \leq \frac{\Lambda}{\mu}.$$

By extension, Λ/μ is also the upper bound for each of the human classes. Whereas, owing to $I_c \leq N_c \leq \Lambda/\mu$, an upper bound for the bacterial classes can be obtained as follows,

$$\frac{dB_c}{dt} = g_c B_c\left(1 - \frac{B_c}{k_c}\right) + \alpha_c I_c - \mu_c B_c \leq g_c B_c\left(1 - \frac{B_c}{k_c}\right) + \alpha_c\frac{\Lambda}{\mu} - \mu_c B_c. \tag{3.5}$$

From inequality (3.5), if

$$B_c \geq \alpha_c\frac{\Lambda}{\mu}, \tag{3.6}$$

then

$$\frac{dB_c}{dt} \leq (g_c - \mu_c)B_c - \tfrac{g_c}{k_c}B_c^2 + B_c = (g_c - \mu_c + 1)B_c\left(1 - \frac{g_c B_c}{k_c(g_c - \mu_c + 1)}\right), \tag{3.7}$$

The constant

$$\frac{k_c(g_c - \mu_c + 1)}{g_c}, \tag{3.8}$$

is the upper bound for the differential inequality (3.7) since (3.7) is the logistic growth model with carrying capacity (3.8). For some $t \geq 0$, $(\alpha_c + \theta_c)\Lambda/\mu$ is an upper bound for B_c whenever (3.6) is false, whilst B_c is bounded above by (3.8) for the rest of the time points in the domain of B_c if (3.6) is true. Thus, in both cases, $B_c \leq \max\left\{\frac{k_c(g_c - \mu_c + 1)}{g_c}, \alpha_c\frac{\Lambda}{\mu}\right\}$. □

3.2.2.2 The Stability of the Disease Free Equilibrium and the Reproduction Number, $\mathcal{R}_C$.

The disease free equilibrium of system (3.2) is given by

$$\mathbf{x}_0 = (S, I_c, R_c, B_c) = \left(\frac{\Lambda}{\mu}, 0, 0, 0\right).$$

The Jacobian of dynamical system (3.2) is given by

$$J = \begin{pmatrix} -\mu & -\beta_{c_1} & \rho_c & -\frac{\Lambda\beta_{c_2}}{\mu\kappa_c} \\ 0 & \beta_{c_1} - q_c & 0 & \frac{\Lambda\beta_{c_2}}{\mu\kappa_c} \\ 0 & \epsilon & -(\mu + \rho_c) & 0 \\ 0 & \alpha_c & 0 & g_c - \mu_c \end{pmatrix}.$$

The dynamical system (3.2) is locally asymptotically stable if all four of its eigenvalues have negative real parts. Two of the eigenvalues for the Jacobian, J, are $\lambda_1 = -\mu$ and $\lambda_2 = -(\mu + \rho_c)$. The other two eigenvalues for J are the eigenvalues from the sub-matrix

$$\bar{J} = \begin{pmatrix} \beta_{c_1} - q_c & \frac{\Lambda\beta_{c_2}}{\mu\kappa_c} \\ \alpha_c & g_c - \mu_c \end{pmatrix}.$$

The characteristic equation for matrix $\bar{J}$ is $\lambda^2 + \nu_1\lambda + \nu_2$, where

$$\begin{aligned}\nu_1 =& -\left((g_c - \mu_c) + (\beta_{c_1} - q_c)\right),\\ \nu_2 =&(\beta_{c_1} - q_c)(g_c - \mu_c)\left(1 - \frac{\alpha_c\beta_{c_2}\Lambda}{(\beta_{c_1} - q_c)(g_c - \mu_c)\kappa_c\mu}\right)\\ =&(\beta_{c_1} - q_c)(g_c - \mu_c)\left(1 - \mathcal{R}_C\right),\end{aligned}$$

and

$$\mathcal{R}_C = \frac{\alpha_c\beta_{c_2}\Lambda}{\kappa_c\mu\mu_c q_c(1-\mathcal{R}_h)(1-\mathcal{R}_b)}, \quad \mathcal{R}_h = \frac{\beta_{c_1}}{q_c} \quad \mathcal{R}_b = \frac{g_c}{\mu_c}.$$

The constants $\mathcal{R}_b$ and $\mathcal{R}_h$ are *the bacterial regeneration threshold* and *the human-to-human sub reproduction number*, respectively. The constant $\mathcal{R}_C$ is the so-called *basic reproduction number* for the system (3.2). Clearly, $\mathcal{R}_h, \mathcal{R}_b < 1$ or $\mathcal{R}_h, \mathcal{R}_b > 1$ if and only if $\mathcal{R}_C > 0$.

It follows from the Routh Hurwitz criterion that the two eigenvalues of $\bar{J}$ have negative real parts if $\nu_1, \nu_2 > 0$. It is easy to see that $\nu_1, \nu_2 > 0$ if $\mathcal{R}_h < 1$, $\mathcal{R}_h < 1$ and $\mathcal{R}_C < 1$. Hence, a positive basic reproduction number for system (3.2) that is less than unity implies that the system is locally asymptotically stable at the disease free equilibrium.

3.2.2.3 Endemic Equilibrium

Setting the derivatives of the classes to zero gives the endemic equilibrium for the cholera only sub-model (3.2). Let $\lambda = \tilde{\lambda}_{c_1} + \lambda_{c_2}$.

$$\frac{\mathrm{d}S}{\mathrm{d}t} = \Lambda - (\lambda + \mu)S + \rho_c R_c, \tag{3.9}$$

$$\frac{\mathrm{d}I_c}{\mathrm{d}t} = \lambda S - q_c I_c, \tag{3.10}$$

$$\frac{\mathrm{d}R_c}{\mathrm{d}t} = \epsilon_c I_c - (\mu + \rho_c)R_c, \tag{3.11}$$

$$\frac{\mathrm{d}B_c}{\mathrm{d}t} = g_c B_c\left(1 - \frac{B_c}{k_c}\right) + \alpha_c I_c - \mu_c B_c. \tag{3.12}$$

From (3.10),

$$S^* = \frac{q_c}{\lambda^*} I_c^*.$$

From (3.9),

$$R_c^* = \frac{1}{\rho_c}\left[\frac{\mathcal{A}q_c I_c^*}{\lambda^*} - \Lambda\right].$$

Consider (3.11),

$$\epsilon I_c^* - \frac{(\mu+\rho_c)}{\rho_c}\left[\frac{\mathcal{A}q_c I_c^*}{\lambda^*} - \Lambda\right] = 0,$$

therefore

$$I_c^* = \frac{\lambda^*\Lambda\,(\mu+\rho_c)}{q_c\mathcal{A}\,(\mu+\rho_c) - \epsilon_c\rho_c\lambda^*}.$$

Given that

$$\lambda^* = \frac{\beta_{c_1} I_c^*}{S + I_c + R_c} + \frac{\beta_{c_2} B_c}{B_c + \kappa_c}.$$

Using (3.12), we have a quadratic equation in B_c of the form

$$\nu_2 B_c^2 + \nu_1 B_c + \nu_0 = 0,$$

where

$$\nu_2 = g_c\left[q_c\mathcal{A}\,(\mu+\rho_c) - \epsilon_c\rho_c\lambda^*\right], \quad \nu_1 = -\mu_c\kappa_c(\mathcal{R}_b - 1)\nu_2,$$
$$\nu_0 = -\lambda^*\Lambda\kappa_c\alpha_c\,(\mu+\rho_c),$$

with

$$\mathcal{R}_b = \frac{g_c}{\mu_c}.$$

Clearly, $\nu_0 < 0,\ \nu_1 < 0$ if $\mathcal{R}_b > 1$. Since

$$B_c = \frac{-\nu_1 \pm \sqrt{\nu_1^2 - 4\nu_2\nu_0}}{2\nu_2}, \tag{3.13}$$

it follows that if $\nu_2 < 0,\ \mathcal{R}_b > 1$, then B_c has negative roots, and if $\nu_2 > 0$, $\mathcal{R}_b > 1$, then B_c has only one positive root. We shall call the positive root B_c^+. Let

$$B = \frac{B_c^+}{B_c^+ + \kappa_c}.$$

Then

$$\lambda_{c_2}^* = \frac{\beta_{c_2} B_c^+}{B_c^+ + \kappa_c} = \beta_{c_2} B.$$

We have an expression for λ^* such that

$$a_2\lambda^{*2} + a_1\lambda^* + a_0 = 0 \tag{3.14}$$

where,

$$a_2 = \mu + \epsilon_c + \rho_c > 0,\ a_1 = q_c(\mu + \rho_c) - (\beta_{c_1}(\mu + \rho_c) + B\beta_{c_2}(\mu + \epsilon_c + \rho_c)),$$
$$a_0 = -Bq_c\beta_{c_2}(\mu + \rho_c) < 0.$$

Since

$$\lambda = \frac{-a_1 \pm \sqrt{a_1^2 - 4a_2a_0}}{2a_2},$$

it follows that if $a_1 > 0$, then the polynomial (3.14) has a positive root, and if $a_1 < 0$, then the polynomial (3.14) has a positive root. So the polynomial (3.14) will always have one positive root.
So system (3.2) has a unique endemic equilibrium if $\mathcal{R}_b > 1$.

Remark 1. Due to the symmetric structure of the cholera only and typhoid only sub-models, the typhoid only sub-model has similar structural results to those obtained for the cholera only sub-model. To avoid repetition, we have not shown the analysis of the typhoid only sub-model.

3.2.3 Cholera-Typhoid Coinfection Model

We study the full coinfection model (3.1) in this section.

3.2.3.1 Non-negative Trajectories and Boundedness

We prove in this subsection that model (3.1) has non-negative trajectories. Within the feasible region, $\Omega \subseteq \Omega_{co}$, we summarize the results on the boundedness and

positivity of the solutions to the coinfection model (3.1).

$$\Omega_{co} = \Bigg\{ (S, I_c, I_t, I_{ct}, R_c, R_t, R_{ct}, B_c, B_t) \Big| 0 \leq N \leq \frac{\Lambda}{\mu}, \\ B_c \in \left[0, \max\left\{\frac{k_c(g_c - \mu_c + 1)}{g_c}, (\alpha_c + \theta_c)\frac{\Lambda}{\mu}\right\}\right], \\ B_t \in \left[0, \max\left\{\frac{k_t(g_t - \mu_t + 1)}{g_t}, (\alpha_t + \theta_t)\frac{\Lambda}{\mu}\right\}\right]\Bigg\}.$$

Theorem 3. *All solutions of the coinfection model (3.1) are positively invariant within Ω whenever $\mu_c \geq g_c$ and $\mu_t \geq g_t$.*

Proof. Since $\Lambda + \rho_c R_c + \rho_t R_t + \rho_{ct} R_{ct} \geq 0$, it follows that

$$\begin{aligned} \frac{dS}{dt} &\geq -(\lambda_{c_1} + \lambda_{c_2} + \lambda_{t_1} + \lambda_{t_2} + \mu)S \\ &= -\left(\frac{\beta_{c_1}(I_c + \eta_c I_{ct})}{N} + \frac{\beta_{c_2} B_c}{B_c + k_c} + \frac{\beta_{t_1}(I_t + \eta_t I_{ct})}{N} + \frac{\beta_{t_2} B_t}{B_t + k_t} + \mu\right)S. \end{aligned} \tag{3.15}$$

From inequality (3.15), and since $\max\{1, \eta_c\} \geq \eta_c$, $\max\{1, \eta_c\} \geq 1$, $\max\{1, \eta_t\} \geq \eta_t$, $\max\{1, \eta_t\} \geq 1$, we have

$$\begin{aligned} &\frac{dS}{dt} \\ &\geq -\left(\frac{\beta_{c_1}(I_c + \max\{1, \eta_c\} I_{ct})}{N} + \frac{\beta_{c_2} B_c}{B_c + k_c} + \frac{\beta_{t_1}(I_t + \max\{1, \eta_t\} I_{ct})}{N} + \frac{\beta_{t_2} B_t}{B_t + k_t} + \mu\right)S, \\ &\geq -\left(\frac{\max\{1, \eta_c\}\beta_{c_1}(I_c + I_{ct})}{N} + \frac{\beta_{c_2} B_c}{B_c + k_c} + \frac{\max\{1, \eta_t\}\beta_{t_1}(I_t + I_{ct})}{N} + \frac{\beta_{t_2} B_t}{B_t + k_t} + \mu\right)S, \\ &\geq -\left(\max\{1, \eta_c\}\beta_{c_1} + \beta_{c_2} + \max\{1, \eta_t\}\beta_{t_1} + \beta_{t_2} + \mu\right)S. \end{aligned}$$

The last inequality follows from $I_c + I_{ct} \leq N$, $I_t + I_{ct} \leq N$, $B_c \leq B_c + \kappa_c$ and $B_t \leq B_t + \kappa_t$. If we integrate the separable differential inequality above, we get $S \geq S_0 \exp\left(-t\left(\max\{1, \eta_c\}\beta_{c_1} + \beta_{c_2} + \max\{1, \eta_t\}\beta_{t_1} + \beta_{t_2} + \mu\right)\right)$. Similarly,
$I_c \geq I_{c0} \exp\left(-\left(\max\{1, \eta_t\}\beta_{t_3} + \beta_{t_4} + q_c\right)t\right)$,
$I_t \geq I_{t0} \exp\left(-\left(\max\{1, \eta_c\}\beta_{c_3} + \beta_{c_4} + q_t\right)t\right)$,
$I_{ct} \geq I_{ct0} \exp(-q_{ct}t)$, $R_{ct} \geq R_{ct0} \exp(-(\mu + \rho_{ct})t)$, where $q_{ct} = \mu + \delta_{ct} + \epsilon_{ct}$.

Note that for both models — the cholera only model (3.2) and the coinfection model (3.1) — each of the trajectories above are bounded below by the product

of a non-negative constant and a non-negative function of t. This implies that all these products are also non-negative for all values of t. Hence, each of these trajectories are bounded below by zero.

The bacterial classes give us the differential inequality

$$\frac{dB_c}{dt} \geq g_c B_c \left(1 - \frac{B_c}{k_c}\right) - \mu_c B_c.$$

This is a Bernoulli type differential inequality. The substitution, $y = B_c^{-1}$, produces a separable differential inequality

$$\frac{dy}{dt} + \Phi_c y \leq \eta_c, \tag{3.16}$$

where $\Phi_c = g_c - \mu_c$, $\eta_c = g_c/k_c$. Integrating (3.16) and substituting B_c back gives the lower bounds

$$B_c \geq \frac{\Phi_c}{\eta_c - M\exp(-\Phi_c t)} \geq \frac{-\Phi_c}{M\exp(-\Phi_c t)},$$

for some positive constant M. Note that $B_c \geq 0$ whenever $\mu_c \geq g_c$. Similarly, $B_t \geq 0$ whenever $\mu_t \geq g_t$. □

Theorem 4. *All solutions of the coinfection model (3.1) are bounded within Ω whenever $\mu_c \geq g_c$ and $\mu_t \geq g_t$.*

Proof. Since $\delta_{ct}(I_c + I_{ct}) \geq 0$, it follows that the upper bound for the time derivative of the total human population, $N(t)$, is

$$\frac{dN}{dt} = \Lambda - \mu N - \delta_{ct}(I_c + I_{ct}) \leq \Lambda - \mu N.$$

Using separation of variables, we obtain the following upper bound for the human population,

$$N \leq \frac{\Lambda - M\exp(-\mu t)}{\mu} \leq \frac{\Lambda}{\mu}.$$

This upper bound for the population implies that each of the classes are also bounded above by the same constant Λ/μ. Since $I_c, I_{ct} \leq \Lambda/\mu$, it follows that

the upper bound for the bacterial concentration of *Vibros Cholerae* is bounded above by

$$\begin{aligned}\frac{dB_c}{dt} =& g_c B_c\left(1-\frac{B_c}{k_c}\right)+\alpha_c I_c+\theta_c I_{ct}-\mu_c B_c,\\ \leq& g_c B_c\left(1-\frac{B_c}{k_c}\right)+(\alpha_c+\theta_c)\frac{\Lambda}{\mu}-\mu_c B_c. \end{aligned} \tag{3.17}$$

From inequality (3.17), if

$$B_c \geq (\alpha_c+\theta_c)\frac{\Lambda}{\mu}, \tag{3.18}$$

then,

$$\begin{aligned}\frac{dB_c}{dt} &\leq (g_c-\mu_c)B_c-\frac{g_c}{k_c}B_c^2+B_c,\\ &= (g_c-\mu_c+1)B_c\left(1-\frac{g_c B_c}{k_c(g_c-\mu_c+1)}\right). \end{aligned} \tag{3.19}$$

The constant

$$\frac{k_c(g_c-\mu_c+1)}{g_c}, \tag{3.20}$$

is the upper bound for the differential inequality (3.19) since (3.19) is the logistic growth model with carrying capacity (3.20). For some $t \geq 0$, $(\alpha_c+\theta_c)\Lambda/\mu$ is an upper bound for B_c whenever (3.18) is false, whilst B_c is bounded above by (3.20) for the rest of the time points in the domain of B_c if (3.18) is true. Thus, in both cases,

$$B_c \leq \max\left\{\frac{k_c(g_c-\mu_c+1)}{g_c}, (\alpha_c+\theta_c)\frac{\Lambda}{\mu}\right\}.$$

□

3.2.3.2 Stability Analysis of the Disease Free Equilibrium and Reproduction Number, $\mathcal{R}_0$

We find the conditions required for the disease free equilibrium for dynamical system (3.1) to be locally asymptotically stable in this section. The disease free

equilibrium of dynamical system (3.1) is

$$(S, I_c, I_t, I_{ct}, R_c, R_t, R_{ct}, B_c, B_t) = \left(\frac{\Lambda}{\mu}, 0, 0, 0, 0, 0, 0, 0, 0\right) =: \mathbf{X_0}.$$

The Jacobian of the full system is

$$J = \tag{3.21}$$

$$\begin{pmatrix}
-\mu & -\beta_{c_1} & -\beta_{t_1} & -(\beta_{c_1}\eta_c + \beta_{t_1}\eta_t) & \rho_c & \rho_t & \rho_{ct} & -\frac{\Lambda\beta_{c_2}}{\mu\kappa_c} & -\frac{\Lambda\beta_{t_2}}{\mu\kappa_t} \\
0 & \beta_{c_1} - q_c & 0 & \eta_c\beta_{c_1} & 0 & 0 & 0 & \frac{\Lambda\beta_{c_2}}{\mu\kappa_c} & 0 \\
0 & 0 & \beta_{t_1} - q_t & \eta_t\beta_{t_1} & 0 & 0 & 0 & 0 & \frac{\Lambda\beta_{t_2}}{\mu\kappa_t} \\
0 & 0 & 0 & -(\mu + \delta_{ct} + \epsilon_{ct}) & 0 & 0 & 0 & 0 & 0 \\
0 & \epsilon_c & 0 & 0 & -(\mu + \rho_c) & 0 & 0 & 0 & 0 \\
0 & 0 & \epsilon_t & 0 & 0 & -(\mu + \rho_t) & 0 & 0 & 0 \\
0 & 0 & 0 & \epsilon_{ct} & 0 & 0 & -(\mu + \rho_{ct}) & 0 & 0 \\
0 & \alpha_c & 0 & \theta_c & 0 & 0 & 0 & g_c - \mu_c & 0 \\
0 & 0 & \alpha_t & \theta_t & 0 & 0 & 0 & 0 & g_t - \mu_t
\end{pmatrix}, \tag{3.22}$$

The dynamical system (3.1) is locally asymptotically stable if all nine of its eigenvalues have negative real parts. Five of the eigenvalues for the Jacobian, J, are $\lambda_1 = -\mu$, $\lambda_2 = -(\mu + \rho_c)$, $\lambda_3 = -(\mu + \rho_t)$, $\lambda_4 = -(\mu + \rho_{ct})$ and $\lambda_5 = -(\mu + \delta_{ct} + \epsilon_{ct})$. The other four eigenvalues for J are the eigenvalues from the sub-matrix

$$\bar{J} = \begin{pmatrix}
\beta_{c_1} - q_c & 0 & \frac{\Lambda\beta_{c_2}}{\mu\kappa_c} & 0 \\
0 & \beta_{t_1} - q_t & 0 & \frac{\Lambda\beta_{t_2}}{\mu\kappa_t} \\
\alpha_c & 0 & g_c - \mu_c & 0 \\
0 & \alpha_t & 0 & g_t - \mu_t
\end{pmatrix}.$$

The characteristic equation for matrix $\bar{J}$ is $(\lambda^2 + \nu_1\lambda + \nu_2)(\lambda^2 + \nu_3\lambda + \nu_4)$, where

$$\nu_1 = -\left((g_c - \mu_c) + (\beta_{c_1} - q_c)\right), \quad \nu_2 = (\beta_{c_1} - q_c)(g_c - \mu_c)\left(1 - \mathcal{R}_C\right),$$
$$\nu_3 = -\left((g_t - \mu_t) + (\beta_{t_1} - q_t)\right), \quad \nu_4 = (\beta_{t_1} - q_t)(g_t - \mu_t)\left(1 - \mathcal{R}_T\right),$$

and

$$\mathcal{R}_C = \frac{\alpha_c\beta_{c_2}\Lambda}{\kappa_c\mu\mu_c q_c(1 - \mathcal{R}_h^c)(1 - \mathcal{R}_b^c)}, \quad \mathcal{R}_T = \frac{\alpha_t\beta_{t_2}\Lambda}{\kappa_t\mu\mu_t q_t(1 - \mathcal{R}_h^t)(1 - \mathcal{R}_b^t)},$$
$$\mathcal{R}_h^c = \frac{\beta_{c_1}}{q_c} \quad \mathcal{R}_b^c = \frac{g_c}{\mu_c}, \quad \mathcal{R}_h^t = \frac{\beta_{t_1}}{q_t} \quad \mathcal{R}_b^t = \frac{g_t}{\mu_t}.$$

The constants $\mathcal{R}_b^c$ and $\mathcal{R}_h^c$ are *the bacterial regeneration threshold* and *the human-to-human sub reproduction number*, respectively, for the cholera only sub-model. The constants $\mathcal{R}_b^t$ and $\mathcal{R}_h^t$ are *the bacterial regeneration threshold* and *the human-to-human sub reproduction number*, respectively, for the typhoid only sub-model. The constants $\mathcal{R}_C$ and $\mathcal{R}_T$ are the so-called *basic reproduction numbers* for the cholera only sub-model and the typhoid only sub-model, respectively. Clearly, $\mathcal{R}_h^c, \mathcal{R}_b^c < 1$ or $\mathcal{R}_h^c, \mathcal{R}_b^c > 1$ if and only if $\mathcal{R}_C > 0$; Similarly, $\mathcal{R}_h^t, \mathcal{R}_b^t < 1$ or $\mathcal{R}_h^t, \mathcal{R}_b^t > 1$ if and only if $\mathcal{R}_T > 0$.
We note that

$$\begin{aligned}\nu_2 >&(\beta_{c_1} - q_c)(g_c - \mu_c)\left(1 - \max\left\{\mathcal{R}_C, \mathcal{R}_T\right\}\right),\\ \nu_4 >&(\beta_{t_1} - q_t)(g_t - \mu_t)\left(1 - \max\left\{\mathcal{R}_C, \mathcal{R}_T\right\}\right).\end{aligned}$$

Thus

$$\mathcal{R}_0 = \max\left\{\mathcal{R}_C, \mathcal{R}_T\right\}.$$

The constant $\mathcal{R}_0$ is the *basic reproduction number* for the systems (3.1). It follows from the Routh Hurwitz criterion that the four eigenvalues of $\bar{J}$ have negative real parts if $\nu_1, \nu_2, \nu_3, \nu_4 > 0$. It is easy to see that $\nu_1, \nu_2, \nu_3, \nu_4 > 0$ if $\mathcal{R}_h^t < 1, \mathcal{R}_b^t < 1$, $\mathcal{R}_h^t < 1, \mathcal{R}_b^t < 1$ and $\mathcal{R}_0 < 1$. Hence, a positive basic reproduction number for system (3.1) that is less than unity implies that the system is locally asymptotically stable at the disease free equilibrium.

3.2.3.3 Global Stability Analysis of the Disease Free Equilibrium

If we define the $\mathbf{M} = (S, R_c, R_t, R_{ct})$ and $\mathbf{N} = (I_c, I_t, I_{ct}, B_c, B_t)$, then we can cast the system (3.1) into the following form,

$$\frac{d\mathbf{M}}{dt} = \mathbf{F}(\mathbf{M}, \mathbf{N}), \quad \frac{d\mathbf{N}}{dt} = \mathbf{G}(\mathbf{M}, \mathbf{N}), \quad \mathbf{G}(\mathbf{M}, \mathbf{0}) = \mathbf{0},$$

whereas,

$$\mathbf{U}_0 = (\mathbf{M}^*, \mathbf{0}), \quad \mathbf{M}^* = \left(\frac{\Lambda}{\mu}, \mathbf{0}\right),$$

represents the disease free equilibrium. For global stability to be established, the following conditions must be met by any system.

(C1) $\dfrac{d\mathbf{M}}{dt} = \mathbf{F}(\mathbf{M}, \mathbf{0}), \quad \mathbf{M}^*$ is globally asymptotically stable,

(C2) $\mathbf{G}(\mathbf{M}, \mathbf{N}) = A\mathbf{N} - \hat{\mathbf{G}}(\mathbf{M}, \mathbf{N}), \quad \hat{\mathbf{G}}(\mathbf{M}, \mathbf{N}) = \mathbf{0} \quad$ for $(\mathbf{M}, \mathbf{N}) \in \Omega,$

where the region of biological significance is ω and the matrix $A = D_Y \mathbf{G}(\mathbf{M}^*, \mathbf{0})$ is a Metzler matrix.

Theorem 5. *The fixed point* $\mathbf{U}_0 = (\mathbf{M}^*, \mathbf{0})$ *is a globally asymptotically stable equilibrium of the system provided that* $R_0 < 1$*, and conditions* $(C1)$ *and* $(C2)$ *are satisfied.*

Applying condition $(C1)$ to the system gives

$$\frac{d\mathbf{M}}{dt} = \mathbf{F}(\mathbf{M}^*, \mathbf{0}) = \begin{pmatrix} \Lambda - \mu S + \rho_c R_c + \rho_t R_t + \rho_{ct} R_{ct} \\ -(\mu + \rho_c) R_c \\ -(\mu + \rho_t) R_t \\ -(\mu + \rho_{ct}) R_{ct} \end{pmatrix}. \tag{3.23}$$

The Jacobian of equation (3.23) is

$$D_X \mathbf{F}(\mathbf{M}^*, \mathbf{0}) = \begin{pmatrix} -\mu & \rho_c & \rho_t & \rho_{ct} \\ 0 & -(\mu + \rho_c) & 0 & 0 \\ 0 & 0 & -(\mu + \rho_t) & 0 \\ 0 & 0 & 0 & -(\mu + \rho_{ct}) \end{pmatrix}.$$

The solution for system (3.23) is

$$\begin{aligned} X =& c_1 \exp(-ut)\mathbf{e}_1 + c_2 \exp(-(u + \rho_c)t)(\mathbf{e}_1 - \mathbf{e}_2) + c_3 \exp(-(u + \rho_t)t)(\mathbf{e}_1 - \mathbf{e}_3) \\ &+ c_4 \exp(-(u + \rho_{ct})t)(\mathbf{e}_1 - \mathbf{e}_4) + \frac{\Lambda}{\mu}\mathbf{e}_1, \end{aligned}$$

where $\{\mathbf{e}_1, \mathbf{e}_2, \mathbf{e}_3, \mathbf{e}_4\}$ is the standard basis in $\mathbb{E}^4$. Thus, $\lim_{t\to\infty} \mathbf{M} = \mathbf{M}^*$.

Applying condition $(C2)$ to the system yields

$$A = \begin{pmatrix} \beta_{c_1} - q_c & 0 & \eta_c\beta_{c_1} & \frac{\beta_{c_2}\Lambda}{\kappa_c\mu} & 0 \\ 0 & \beta_{t_1} - q_t & \eta_t\beta_{t_1} & 0 & \frac{\beta_{t_2}\Lambda}{\kappa_t\mu} \\ 0 & 0 & -q_{ct} & 0 & 0 \\ \alpha_c & 0 & \theta_c & g_c - \mu_c & 0 \\ 0 & \alpha_t & \theta_t & 0 & g_t - \mu_t \end{pmatrix}$$

and

$$\hat{\mathbf{G}} = \begin{pmatrix} \beta_{c_1}\left(I_c + \eta_c I_{ct}\right)\left(1 - \frac{S}{N}\right) + \left(\lambda_{t_3} + \lambda_{t_4}\right) I_c + \beta_{c_2} B_c \left(\frac{\Lambda}{\kappa_c\mu} - \frac{S}{B_c + \kappa_c}\right) \\ \beta_{t_1}\left(I_t + \eta_t I_{ct}\right)\left(1 - \frac{S}{N}\right) + \left(\lambda_{c_3} + \lambda_{c_4}\right) I_t + \beta_{t_2} B_t \left(\frac{\Lambda}{\kappa_t\mu} - \frac{S}{B_t + \kappa_t}\right) \\ -\left(\lambda_{t_3} + \lambda_{t_4}\right) I_c - \left(\lambda_{c_3} + \lambda_{c_4}\right) I_t \\ \frac{g_c}{\kappa_c} B_c^2 \\ \frac{g_t}{\kappa_t} B_t^2 \end{pmatrix}.$$

Notably, $-\left(\lambda_{t_3} + \lambda_{t_4}\right) I_c - \left(\lambda_{c_3} + \lambda_{c_4}\right) I_t \ngeq 0$ for $(\mathbf{M}, \mathbf{N}) \in \Omega$, hence condition $(C2)$ is not satisfied. This implies that the disease free equilibrium $\mathbf{U}_0$ may not be globally asymptotically stable.

3.2.3.4 Impact Analysis

In this section, we show how cholera affects typhoid, and through symmetry, we show how typhoid affects cholera.

The reproduction numbers for cholera and typhoid are

$$\mathcal{R}_C = \frac{\alpha_c\beta_{c_2}\Lambda}{\kappa_c\mu\mu_c q_c(1 - \mathcal{R}_h^c)(1 - \mathcal{R}_b^c)}, \quad \mathcal{R}_T = \frac{\alpha_t\beta_{t_2}\Lambda}{\kappa_t\mu\mu_t q_t(1 - \mathcal{R}_h^t)(1 - \mathcal{R}_b^t)}, \tag{3.24}$$

respectively. These two reproduction numbers are dependent on each other. The constant, Λ/μ, allows for the expression of one reproduction number in terms of the other. From the second equation above, (3.24), isolating, Λ/μ, yields

$$\mathcal{R}_C = \mathcal{R}_T \frac{\alpha_c\beta_{c_2}\kappa_t\mu_t q_t(1 - \mathcal{R}_h^t)(1 - \mathcal{R}_b^t)}{\alpha_t\beta_{t_2}\kappa_c\mu_c q_c(1 - \mathcal{R}_h^c)(1 - \mathcal{R}_b^c)}. \tag{3.25}$$

Differentiating $\mathcal{R}_C$ with respect to $\mathcal{R}_T$ gives

$$\frac{\partial \mathcal{R}_C}{\partial \mathcal{R}_T} = \frac{\alpha_c \beta_{c_2} \kappa_t \mu_t q_t (1-\mathcal{R}_h^t)(1-\mathcal{R}_b^t)}{\alpha_t \beta_{t_2} \kappa_c \mu_c q_c (1-\mathcal{R}_h^c)(1-\mathcal{R}_b^c)}. \tag{3.26}$$

We conclude that an increase in cholera cases may be associated with an increase in typhoid cases, and an increase in typhoid cases may be associated with an increase in cholera cases. This conclusion is subject to the following conditions: firstly, the *the bacterial regeneration threshold* for both cholera and typhoid must be less than unity; secondly, *the human-to-human sub reproduction number* for both cholera and typhoid must also be less than unity. This result proves the symbiotic nature of the relationship between the typhoid disease and the Cholera disease.

3.3 Numerical Simulations

In this section, we give a brief outline of the numerical results obtained in the investigation. Table 3.1 shows the parameters of the cholera typhoid coinfection model (3.1). The basic reproduction number, $\mathcal{R}_0$, obtained from the Table 3.1 is 1.4. The initial conditions used to produce the figures in this section were: $S(0) = 99980,\ I_c(0) = 20,\ I_t(0) = 20,\ I_{ct}(0) = 20,\ R_c(0) = 0,$
$R_t(0) = 0,\ R_{ct}(0) = 0,\ B_c(0) = 40000,\ B_t(0) = 40000$. Note that all figures in this section are presented in the logarithmic scale since the range of some of the plots spanned several orders of magnitude.

Par.	Range	Point Value	Source	Par.	Range	Point Value	Source
β_{c_1}		1	Assumed	g_t		0.014	[56]
β_{t_1}		1	[55]	α_c		10	Assumed
β_{c_2}	(0.1—1)	1.97×10^{-11}	[19, 9, 44, 57]	α_t		10	[56]
β_{t_2}		1.97×10^{-11}	[52]	μ	(0.017—0.123)	0.02	[27, 50, 57]
β_{c_3}		0.5	Assumed	μ_t		0.0345	[56]
β_{t_3}		1	Assumed	Λ	(100—467)	449.32	[12]
β_{c_4}		10^{-1}	Assumed	μ_c		0.0345	Assumed
β_{t_4}		10^{-1}	Assumed	ϵ_c	(0.07—0.245)	0.07	[74, 57, 75, 28]
k_c	(10^6—10^9)	5×10^6	[19]	ϵ_t		0.1	[2, 53]
k_t		5×10^6	Assumed	ϵ_{ct}		0.1	Assumed
δ_c		6.58×10^{-1}	[57, 75, 77]	κ_c		0.62	Assumed
δ_t		0.6	[52]	κ_t		0.62	Assumed
ρ_c		8.12×10^{-3}	[37, 74]	θ_c		0.8	Assumed
ρ_t		1.3×10^{-3}	[62]	θ_t		0.8	Assumed
ρ_{ct}		1.3×10^{-3}	Assumed	η_c		7×10^{-4}	Assumed
g_c		0.014	Assumed	η_c		7×10^{-2}	Assumed

Table 3.1: Parameter values and their sources.

Coupled with the parameters from Table 3.1, the sensitivity indices of the variables above are shown on Figure 3.2. Latin Hypercube sampling was utilized to generate the plot above (Figure 3.2). This method returns the correlation between the state variable I_{ct} and each of the model parameters, and it also returns the ranks of all these correlations (PRCC). The simulation was carried out over 1000 runs. A parameter with a negative PRCC value means that parameter is negatively correlated with I_{ct}, whilst a parameter with a positive PRCC value represents a positive correlation between that parameter and I_{ct}. Relative to the current model parameters, we note that the coinfection class is most sensitive to changes to the person-to-person typhoid transmission rate, β_{t_1}, and the correlation is positive between this parameter and the state variable. The typhoid induced death rate is that second most sensitive parameter to the coinfection class, and it is negatively correlated to the coinfection class. Due to the large number of parameters in model 3.1, we have opted to split the PRCC values into 4 equal sets, see Figure 3.2.

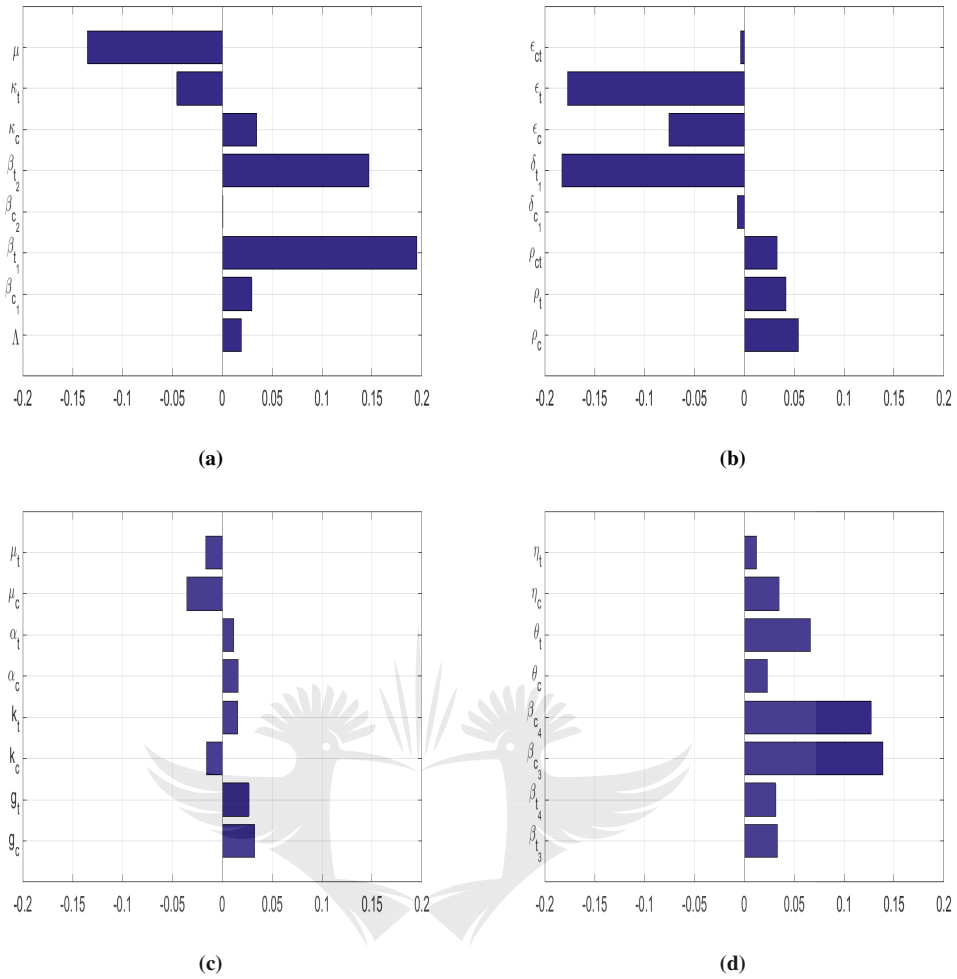

Figure 3.2: The correlation between the coinfected class and each of the model's parameter are shown in this bar graph (PRCC). (a) Shows the PRCC values for $\{\Lambda, \beta_{c_1}, \beta_{t_1}, \beta_{c_2}, \beta_{t_2}, \kappa_c, \kappa_t, \mu\}$. (b) Shows the PRCC values for $\{\rho_c, \rho_t, \rho_{ct}, \delta_c, \delta_t, \epsilon_c, \epsilon_t, \epsilon_{ct}\}$. (c) Shows the PRCC values for $\{g_c, g_t, k_c, k_t, \alpha_c, \alpha_t, \mu_c, \mu_t\}$. (d) Shows the PRCC values for $\{\beta_{t_3}, \beta_{t_4}, \beta_{c_3}, \beta_{c_4}, \theta_c, \theta_t, \eta_c, \eta_t\}$.

The contour map of $\mathcal{R}_0$ as a function of the typhoid recovery rate, ϵ_t, and the cholera recovery rate, ϵ_c is shown in Figure 3.3. Using the parameters from Table 3.1, the base case as well as the contour levels are also shown in Figure 3.3. The basic reproduction number $\mathcal{R}_0$ attains its global minimum if both the typhoid and cholera recovery rate are maximised. It is be observed that, locally, a reduction in the reproduction number, $\mathcal{R}_0$, is only achieved by increasing the cholera recovery

rate. Since the reproduction number, $\mathcal{R}_0$, is the maximum of the reproduction numbers of the individual diseases, it follows that a reduction in the reproduction number, $\mathcal{R}_0$, means a reduction in the reproduction numbers of each of the diseases. Hence, locally, an increase in the cholera recovery rate will not only reduce the cholera reproduction number, $\mathcal{R}_c$, but it has the added benefit of indirectly reducing the reproduction number for typhoid, $\mathcal{R}_t$, as well. It is also observed that increasing the typhoid recovery rate exclusively will have no immediate benefits locally. This finding is consistent with the previous findings of an optimal treatment plan being centred around the recovery rate of cholera.

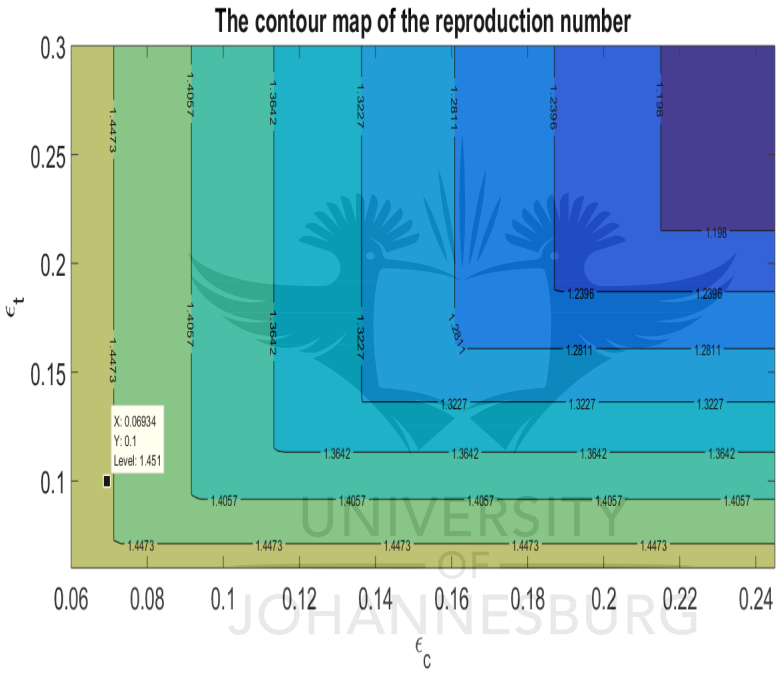

Figure 3.3: The contour map of the basic reproduction number, $\mathcal{R}_0$, as a function of the typhoid recovery rate, ϵ_t, and the cholera recovery rate, ϵ_c.

We show the trajectories of the three infectious classes of model (3.1). An initial surge in infections followed closely by an immediate recovery is shown in Figure 3.4. The phenomenon of waning immunity results in the smaller second wave of infections. The coinfected class is the only exception to this observation. We see

the coinfected class reach a local minimum before the first surge in cholera only or typhoid only infections is reached. A possible reason for this is that, unlike the cholera and typhoid classes, the coinfected class does not recruit directly from the susceptible class. This is due to the fact that the cholera disease has a shorter incubation period than the typhoid disease. The incubation periods are 1.4 days for cholera [7] and 19 days for typhoid [81]. What is then observed in the coinfected class is a case of people leaving the class either through death or recovery coupled with the delayed recruitment into the class. All the diseases reach stability after the second waves of infection.

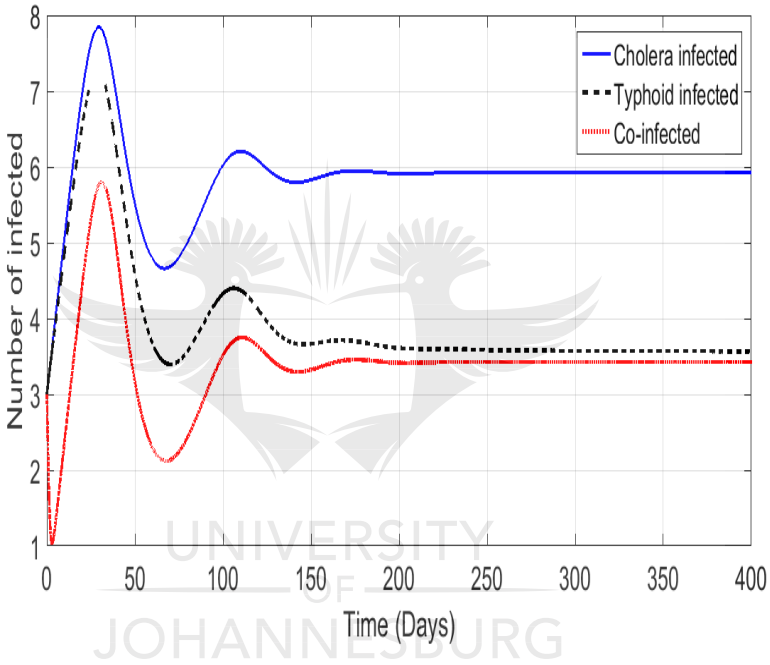

Figure 3.4: The trajectories of the infectious classes.

In order to understand how the diseases interact with each other, we vary the different recovery rates and observe how the prevalence of each of the infections change. In Figure 3.5, plot (a) and (b) show the impact of varying the recovery rate of the coinfected on the cholera and typhoid prevalence, whilst plot (c) and (d) show the impact of varying the recovery rates of cholera and typhoid on the prevalence of the coinfected individuals. Figure (c) shows a significant reduction

in the coinfected class' prevalence when the cholera recovery rate is increased, whilst Figure (d) shows that this reduction is negligible when the typhoid recovery rate was increased. Figures (a) and (b) show that an increase in the coinfected class' recovery rate reduces the typhoid prevalence more than the cholera prevalence. The net effect is that an increased cholera recovery rate may be associated with a decreased prevalence of the coinfected individuals and a higher coinfected recovery rate. This in turn, produces a reduced typhoid prevalence. Given the current model parameters, this finding suggests that an optimal treatment plan for the two infections should primarily focus on increasing the cholera recovery rate as opposed to the typhoid recovery rate. This also underscores the point made earlier about the symbiotic nature of the two diseases.

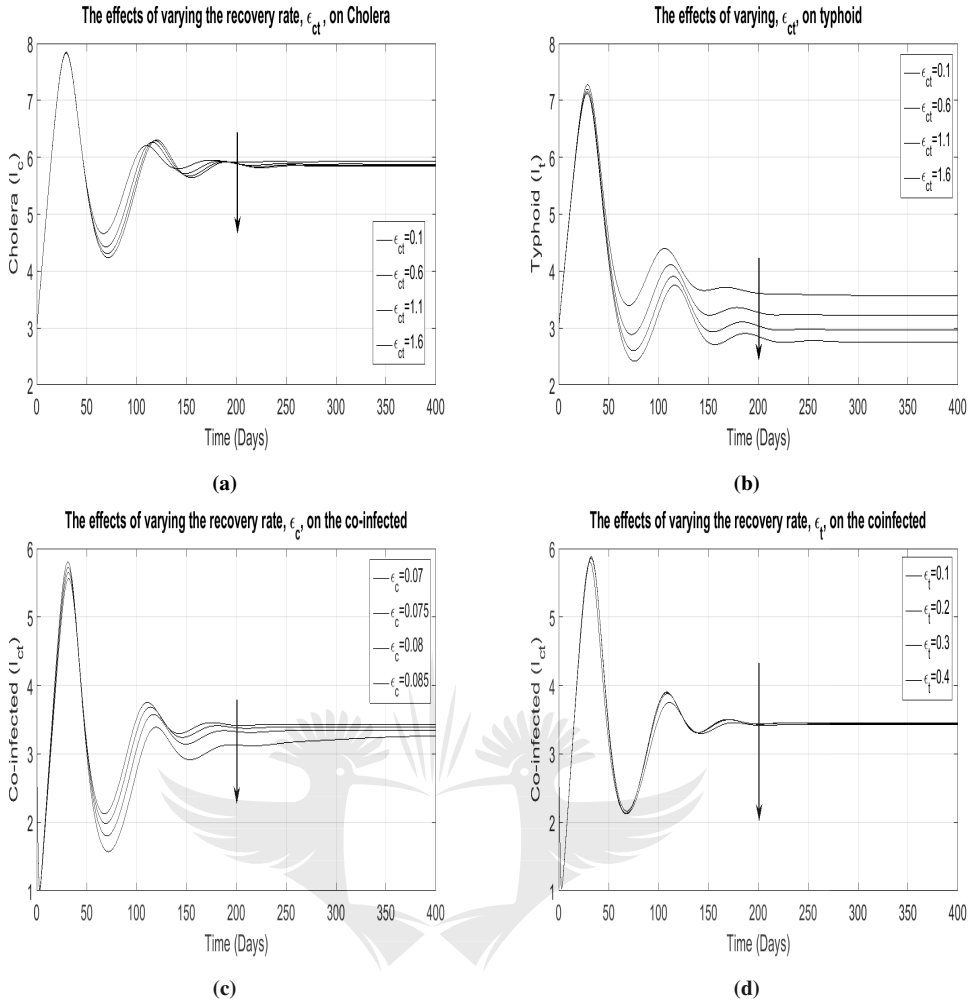

Figure 3.5: Plots (a) and (b) show the cholera and typhoid prevalence, respectively, as the coinfection recovery rate, ϵ_{ct}, runs through $\{0.1, 0.6, 1.1, 1.6\}$. Plots (c) and (d) show the prevalence of the coinfected as the cholera and typhoid recovery rates are varied through the sets $\{0.07, 0.075, 0.08, 0.085\}$ and $\{0.1, 0.2, 0.3, 0.4\}$, respectively.

3.4 Discussion and Conclusion

In this article, we formulated and analysed a theoretical model for the transmission dynamics of a cholera typhoid coinfection model. Through numerical simulations, we were able to verify a number of the results obtained analytically.

The birth and death rates of the bacteria are central to proving the boundedness and positivity of all three models—cholera only sub-model, typhoid only sub-model, and the full cholera typhoid coinfection model. For the cholera-only model, if the birth rate of the *Vibrio Cholerae* bacteria exceeds its death rate, then the cholera only model has non-negative and bounded trajectories. For the typhoid only model, if the birth rate of the *Salmonella Typhi* bacteria exceeds its death rate, then the typhoid only model has non-negative and bounded trajectories. For the full cholera typhoid coinfection model, if the birth rates of the *Vibrio Cholerae* bacteria and the *Salmonella Typhi* bacteria exceed their death rates, simultaneously, then the cholera-typhoid coinfection model has non-negative and bounded trajectories.

In analysing the equilibria of the coinfection models, several key sights were discovered. We showed the existence of the disease free equilibria, by finding them, for all three models. Sufficient conditions for the existence of the endemic equilibria for the cholera only sub-model and the typhoid only sub-model were documented. We showed that if the reproduction number is less than one for the all the models, then the disease free equilibria are locally asymptotically stable, otherwise they are unstable. Global stability could not be guaranteed, both at the disease free equilibria and the endemic equilibria, in any of the models. Sensitivity analysis revealed the parameters in the model were at the heart of the spread of the cholera typhoid coinfection. The prevalence of cholera is decreased whenever η_t, β_{t_3}, β_{t_4} are increased and/or β_{c_1}, β_{c_2}, ϵ_{ct}, η_c and θ_c are decreased. The prevalence of typhoid is decreased whenever η_c, β_{c_3}, β_{c_4} are increased and/or β_{t_1}, β_{t_2}, ϵ_{ct}, η_t and θ_t are decreased.

From the impact analysis section, we found that an increase in cholera cases may be associated with an increased risk of typhoid and that an increase in typhoid cases may be associated with an increased risk of cholera. This result proves the symbiotic nature of the relationship between the typhoid disease and the cholera disease.

The findings in this investigation come with some limitations. The most glaring

of all is the lack of data to fit the model to. Our model also fails to take into account the highly seasonal nature of each of the diseases. For the two infections, fear has a significant impact on the transmission dynamics. Future work should also be able to account for the effects of fear in the transmission dynamics of both infections. Notwithstanding these limitations, we believe that the findings of this investigation can still be useful to policy makers in containing an outbreak of these two diseases.

The following chapter includes the analysis of a typhoid fever mathematical model with a seasonal factor and a fear factor.

Chapter 4

Mathematical Analysis of Typhoid Fever Transmission Dynamics with Seasonality and Fear

4.1 Introduction

Typhoid fever is a life-threatening bacterial infection caused by *Salmonella Typhi* [84]. The transmission mode of typhoid is identical to that of cholera—that is, direct transmission (human-human) and indirect transmission (environment-human). This disease adversely affects the Recticuloendothelical system, the gall bladder and the intestinal lymphoid [52]. Known estimates of the incubation period for the typhoid fever disease range from ten to fourteen days [52]. The case fatality rate of typhoid fever was $10-20\%$ before the advent of treatment, whilst, with prompt treatment, the case fatality rate was reduced to less than 1% [29]. It was observed that the number of deaths caused by typhoid fever in the year 1990 was 181 000 [1]; in the year 2000, it was 217 000 [21]; and in the year 2013, it was 161 000 [1]. In the Democratic Republic of Congo, more than 42 000 people contracted the typhoid fever disease during the years 2004 and 2005 [94].

For a number of incurable communicable diseases, modellers typically make the assumption of homogeneous mixing of susceptible and infected individuals in a given population [24]. This assumption is reasonable for most non-lethal infections, such as influenza and chickenpox. However, for lethal infections such as COVID-19, typhoid, cholera and HIV/AIDS this assumption is debatable. In the case of HIV/AIDS, examples of partner preferences can be seen when individuals reduce the number of sexual partners they have, and through stigmatization of those who are already infected [76, 86]. During a cholera, typhoid or COVID-19 outbreak, fear drives individuals to self-isolate and improve personal hygiene in order to reduce the contact rate of these diseases [26, 72, 90]. Indeed, a reduced contact rate, due to fear, has a huge bearing on the dynamics of a lethal infection. The role of fear has been considered in mathematical models with interacting species, see [23, 24, 91]. Recently, the role of fear has been modelled for Ebola virus disease [34]. Very few mathematical models have considered fear as an essential component in human response to infection.

Mathematical models with seasonality have been considered by a number of authors. In [18], a malaria model with seasonality is considered in which a system of differential equations is analysed. A model for malaria was also considered in [85] in with climatic factors where considered to influence the biting rate. Other infections in which seasonality was considered include brucellosis [60], clostridium difficile [46], schistosomiasis [41], respiratory syncytial virus [48], buruli ulcer [6] and cholera [67]. In these models, seasonality is modelled by incorporating a trigonometric function in the force of infection. It is also common to come across mathematical models for diarrhoeal diseases such as cholera, typhoid and many others that assume a constant rate of infection. The primary reason of making such an assumption is that it makes for relatively easy analysis, in that, it produces models that contain systems of autonomous ordinary differential equations [71]. To this end, there are numerous tools for analysing systems of autonomous ordinary differential equations in the literature [31, 82]. The major drawback of assuming a constant infection rate for a seasonal disease is that the accuracy of the model might be compromised, thus compromising model predictions. Empir-

ically, it has been shown that typhoid fever is highly seasonal and it peaks during the rainy seasons [73], hence a seasonal mathematical model is befitting to study such a disease.
To the best of our knowledge, the dynamics of typhoid fever's seasonality coupled with a behavioural change in the population due to the fear of infection has not been investigated. A comparison of a seasonal mathematical model of typhoid fever and one where the assumption of seasonality is relaxed is carried out. We seek to understand the effects of seasonality on the basic reproduction number, the number of steady states, the stability of these steady states and to carry out the stability analysis of the steady states.

The paper is arranged as follows; in Section 2, we formulate and establish the basic properties of the model. The model is analysed for stability in Section 3. In Section 4, we carry out some numerical simulations. Parameter estimation and numerical results are also presented in this section. The paper is concluded in Section 5.

4.2 Methodology

4.2.1 Model Formulation

The typhoid infection model classifies the total human population at time t, denoted by $N(t)$, into susceptible individuals $S(t)$, typhoid infected individuals $I(t)$, individuals who recovered from typhoid $R(t)$. Thus, $N(t) = S(t) + I(t) + R(t)$. The model has an additional compartment $B(t)$ which represents the *Salmonella Typhi* concentration in the environment. The dynamics of the model developed in this paper follows from the model developed by Mushanyu *et al.* [51].
We assume that susceptible individuals acquire typhoid fever either through person-to-person transmission or by ingesting *Salmonella Typhi* from contaminated aquatic

reservoirs at the rates

$$\lambda_1 = \frac{\beta_{t_1} I}{1 + kI}, \quad \lambda_2 = \frac{\beta_{t_2} B}{\kappa_t + B}\left(1 + \theta \sin\left(\frac{2\pi t}{365}\right)\right),$$

respectively. The parameter β_{t_1} denotes the person-to-person typhoid transmission rate of susceptibles, and is defined as the product of the probability of typhoid transmission per contact and the effective contact rate for typhoid transmission to occur. The force of infection, λ_2, is modelled by a type II functional response and a trigonometric function. The type II functional response captures the decreasing growth rate of the bacteria and the saturation of the bacteria, whilst the trigonometric function introduces seasonality with a period of 365 days into the force of infection. The parameter β_{t_2} denotes the environment-to-humans per capita contact rate for susceptibles and the *Salmonella Typhi* in the contaminated environment and κ_t denotes the half saturation constant relative to the *Salmonella Typhi*. Here, we assume that individuals under treatment are infectious but cannot infect susceptible individuals since they will be confined to a certain place and separated from the general population where they will be released upon successful treatment or due to mortality (natural or disease related).

Infected individuals in class I experience disease related death at a rate given by δ. Individuals in the infectious state I excrete *Salmonella Typhi* bacteria into the environment at rate α. Individuals in the recovered class R are temporarily immune to typhoid infection, and immunity wanes at a rate given by ρ, leading to the individuals being susceptible again.

The *Salmonella Typhi* bacteria population is generated at a rate $g_b B$ and its growth is enhanced by individuals in the infectious state I. We assume that the *Salmonella Typhi* bacteria in the environment becomes non-infectious at a rate μ_b. The constant recruitment into the susceptible population is represented by Λ, while the natural death rate for the general population is represented by μ_h. We assume that individuals in each compartment are indistinguishable and there is homogeneous mixing. The schematic diagram for the typhoid model to be analysed in this work is given below.

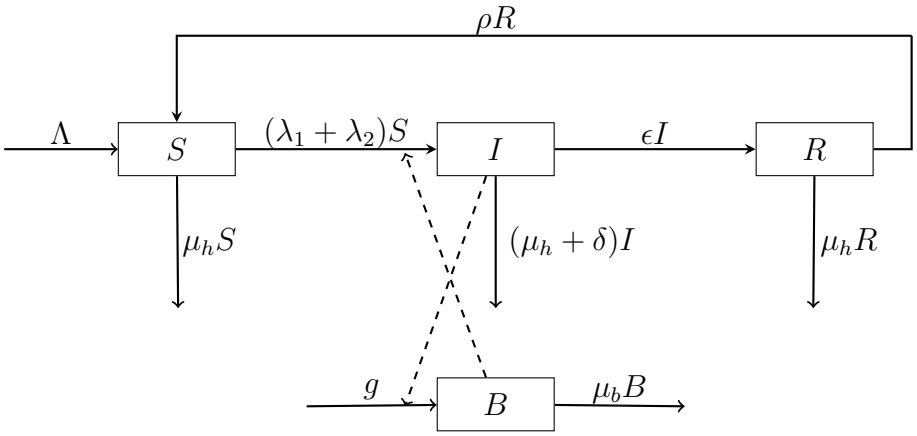

Figure 4.1: The model, with $g = g_b B\left(1-\frac{B}{k_t}\right)\left(1+\xi\sin\left(\frac{2\pi t}{365}\right)\right)+\alpha I$.

Given the schematic diagram in Fig 4.1 and the given model assumptions, we formulate the typhoid fever model as follows

$$\begin{aligned}
\frac{\mathrm{d}S}{\mathrm{d}t} &= \Lambda-(\lambda_1+\lambda_2)S-\mu_h S+\rho R,\\
\frac{\mathrm{d}I}{\mathrm{d}t} &= (\lambda_1+\lambda_2)S-qI,\\
\frac{\mathrm{d}R}{\mathrm{d}t} &= \epsilon I-(\mu_h+\rho)R,\\
\frac{\mathrm{d}B}{\mathrm{d}t} &= g_b B\left(1-\frac{B}{k_t}\right)\left(1+\xi\sin\left(\frac{2\pi t}{365}\right)\right)+\alpha I-\mu_b B,
\end{aligned} \tag{4.1}$$

where $q=\mu_h+\delta+\epsilon$, with initial conditions

$$S(0)=S_0>0,\quad B(0)=B_0\geq 0,\quad I(0)=I_0\geq 0,\quad R(0)=R_0\geq 0.$$

4.2.2 Non-seasonal Typhoid Model

Applying the time-average function, $[f(t)]=\frac{1}{\omega}\int_0^{\omega} f(t)\,\mathrm{d}t$, to each component of the typhoid model (4.1) gives the following auxiliary system

$$\begin{aligned}
\frac{\mathrm{d}S}{\mathrm{d}t} &= \Lambda - (\lambda_1 + [\lambda_2])S - \mu_h S + \rho R, \\
\frac{\mathrm{d}I}{\mathrm{d}t} &= (\lambda_1 + [\lambda_2])S - qI, \\
\frac{\mathrm{d}R}{\mathrm{d}t} &= \epsilon I - (\mu_h + \rho)R, \\
\frac{\mathrm{d}B}{\mathrm{d}t} &= g_b B\left(1 - \frac{B}{k_t}\right) + \alpha I - \mu_b B,
\end{aligned} \tag{4.2}$$

with initial conditions

$$S(0) = S_0 > 0, \quad B(0) = B_0 \geq 0, \quad I(0) = I_0 \geq 0, \quad R(0) = R_0 \geq 0.$$

Here $[\lambda_2] = \frac{\beta_{t_2} B}{\kappa_t + B}$.

4.2.2.1 Non-negative Trajectories and Boundedness

We show that all the trajectories of the dynamical system are non-negative. The approach outlined in Yang *et al.* [95] to show that all the solutions are bounded below by zeros is used in this case.

It is clear that

$$\left.\frac{\mathrm{d}S}{\mathrm{d}t}\right|_{S=0} = \Lambda + \rho R > 0, \quad \left.\frac{\mathrm{d}I}{\mathrm{d}t}\right|_{I=0} = [\lambda_2]S \geq 0, \quad \left.\frac{\mathrm{d}R}{\mathrm{d}t}\right|_{R=0} = \epsilon I \geq 0,$$
$$\left.\frac{\mathrm{d}B}{\mathrm{d}t}\right|_{B=0} = \alpha I \geq 0.$$

Using Lemma 2 of Yang *et al.* [95], it follows that the trajectories of model (4.2) are all non-negative. The time derivative of the human population is given by

$$\frac{\mathrm{d}N}{\mathrm{d}t} = \Lambda - \mu_h N - \delta I \leq \Lambda - \mu_h N,$$

This separable differential inequality can be integrated to get the following upper bound for $N(t)$

$$N \leq \frac{\Lambda - M\exp(-\mu_h t)}{\mu_h} \leq \frac{\Lambda}{\mu_h}.$$

This implies that each class containing humans is also bounded above by Λ/μ_h. Since $I \leq N \leq \Lambda/\mu_h$, the bacterial class produces the following differential inequality

$$\frac{\mathrm{d}B}{\mathrm{d}t} = g_b B\left(1 - \frac{B}{k_t}\right) + \alpha I - \mu_b B \leq g_b B\left(1 - \frac{B}{k_t}\right) + \alpha\frac{\Lambda}{\mu_h} - \mu_b B. \tag{4.3}$$

From inequality (4.3), if

$$B \geq \alpha\frac{\Lambda}{\mu_h}, \tag{4.4}$$

then

$$\frac{\mathrm{d}B}{\mathrm{d}t} \leq (g_b - \mu_b)B - \frac{g_b}{k_t}B^2 + B = (g_b - \mu_b + 1)B\left(1 - \frac{g_b B}{k_t(g_b - \mu_b + 1)}\right). \tag{4.5}$$

Note that the differential inequality (4.5) is a derivative of the logistic growth model with carrying capacity

$$\frac{k_t(g_b - \mu_b + 1)}{g_b}. \tag{4.6}$$

On the other hand, if condition (4.4) is false, then B is bounded above by the constant $\alpha\Lambda/\mu_h$ for some $t \geq 0$. For the rest of the time points in the domain of B, condition (4.4) is true, and hence the upper bound for B is (4.6). Thus, in both cases,

$$B \leq \max\left\{\frac{k_t(g_b - \mu_b + 1)}{g_b}, \alpha\frac{\Lambda}{\mu_h}\right\}.$$

The results on positivity and boundedness of the solutions to the typhoid model (4.2) can be summarized within the feasible region $\Omega \subseteq \Omega_c$, where

$$\Omega_c = \left\{(S, I, R, B) \in \mathbb{R}^4 \middle| \, 0 \leq S, I, R \leq \frac{\Lambda}{\mu_h},\ 0 \leq B \leq \max\left\{\frac{k_t(g_b - \mu_b + 1)}{g_b}, \alpha\frac{\Lambda}{\mu_h}\right\}\right\}.$$

Theorem 6. *All solutions of the typhoid model (4.2) are positively invariant and bounded within* Ω.

4.2.2.2 Disease Free Equilibrium and Time Average Reproduction Number, ($[\mathcal{R}]_0$)

The disease free equilibrium for system (4.2) is

$$\mathbf{x}_0 = (S, I, R, B) = \left(\frac{\Lambda}{\mu_h}, 0, 0, 0\right). \tag{4.7}$$

The basic reproduction number, $[\mathcal{R}_0]$, is defined as the spectral radius of the next generation matrix [87] or given a completely susceptible population, an alternative definition of the basic reproduction number is the average number of secondary infections that arise out of an average primary case [35].

The new infections vector $[\mathcal{F}]$, transmission vector $[\mathcal{V}]$, and their respective Jacobians $[F]$ and $[V]$ are

$$[\mathcal{F}] = \begin{pmatrix} (\lambda_1 + \lambda_2)S \\ 0 \end{pmatrix}, \; [\mathcal{V}] = \begin{pmatrix} qI \\ \mu_b B - g_b B\left(1 - \frac{B}{k_t}\right) - \alpha I \end{pmatrix}, \; [F] = \begin{pmatrix} \frac{\Lambda\beta_{t_1}}{\mu_h} & \frac{\Lambda\beta_{t_2}}{\mu_h \kappa_t} \\ 0 & 0 \end{pmatrix},$$

$$[V] = \begin{pmatrix} q & 0 \\ -\alpha & \mu_b - g_b \end{pmatrix},$$

since the time average of $\left(1 + \theta \sin\left(\frac{2\pi t}{365}\right)\right)$ is one. Thus the spectral radius of the matrix

$$[F][V]^{-1} = \begin{pmatrix} \dfrac{\Lambda\beta_{t_1}}{q\mu_h} + \dfrac{\beta_{t_2}\alpha\Lambda}{q\kappa_t\mu_h(\mu_b - g_b)} & \dfrac{\beta_{t_2}\Lambda}{\kappa_t\mu_h(\mu_b - g_b)} \\ 0 & 0 \end{pmatrix}$$

is

$$[\mathcal{R}_0] = \frac{\Lambda\beta_{t_1}}{q\mu_h} + \frac{\beta_{t_2}\alpha\Lambda}{q\kappa_t\mu_h(\mu_b - g_b)},$$

where $[\mathcal{R}_0]$ is the so-called *time-averaged basic reproduction number* for the typhoid model (4.2). It follows that $\mu_b > g_b$ implies $[\mathcal{R}_0] > 0$.

4.2.2.3 Local Stability Analysis of the Disease Free Equilibrium

We begin by analysing the stability of the solutions of model (4.2) at the disease free equilibrium $\mathbf{x}_0$. We apply the Routh-Hurwitz criterion [30] in order to find the nature of the eigenvalues.

Theorem 7. *The disease free equilibrium, $\mathbf{x}_0$, for system (4.2) is locally asymptotically stable whenever $\mu_b > g_b$ and $[\mathcal{R}_0] < 1$. It is unstable otherwise.*

Proof. The Jacobian of system (4.2) at the disease free equilibrium is

$$J(\mathbf{x}_0) = \begin{pmatrix} -\mu_h & -\frac{\Lambda\beta_{t_1}}{\mu_h} & \rho & -\frac{\Lambda\beta_{t_2}}{\mu_h\kappa_t} \\ 0 & \frac{\Lambda\beta_{t_1}}{\mu_h} - q & 0 & \frac{\Lambda\beta_{t_2}}{\mu_h\kappa_t} \\ 0 & \epsilon & -(\mu_h + \rho) & 0 \\ 0 & \alpha & 0 & g_b - \mu_b \end{pmatrix}.$$

By inspection, it is clear that the two eigenvalues, $-\mu_h$ and $-(\mu_h + \rho)$, of $J(\mathbf{x}_0)$ lie in the left open half plane. The properties of the remaining two eigenvalues will be obtained from the following sub-matrix

$$\bar{J}(\mathbf{x}_0) = \begin{pmatrix} \frac{\Lambda\beta_{t_1}}{\mu_h} - q & \frac{\Lambda\beta_{t_2}}{\mu_h\kappa_t} \\ \alpha & g_b - \mu_b \end{pmatrix}.$$

The characteristic polynomial associated with matrix $\bar{J}(\mathbf{x}_0)$ is $\lambda^2 - tr(\bar{J}(\mathbf{x}_0))\lambda + \det(\bar{J}(\mathbf{x}_0))$. The Routh-Hurwitz criterion states that the roots of $\bar{J}(\mathbf{x}_0)$ lie in the left open half plane if and only if $tr(\bar{J}(\mathbf{x}_0)) < 0$ and $\det(\bar{J}(\mathbf{x}_0)) > 0$. Indeed,

$$tr(\bar{J}(\mathbf{x}_0)) = \frac{\Lambda\beta_{t_1}}{\mu_h} - q + g_b - \mu_b = q\left(\frac{\Lambda\beta_{t_1}}{\mu_h q} - 1 + \frac{g_b - \mu_b}{q}\right),$$

$$\det(\bar{J}(\mathbf{x}_0)) = q(g_b - \mu_b)\left(\frac{\Lambda\beta_{t_1}}{\mu_h q} - 1 + \frac{\alpha\Lambda\beta_{t_2}}{\mu_h\kappa_t q(\mu_b - g_b)}\right) = q(\mu_b - g_b)(1 - [\mathcal{R}_0]).$$

We observe that $tr(\bar{J}(\mathbf{x}_0)) < 0$ if $\mu_b > g_b$ and $\frac{\Lambda\beta_{t_1}}{\mu_h q} < 1$, whilst $\det(\bar{J}(\mathbf{x}_0)) > 0$ if $\mu_b > g_b$ and $[\mathcal{R}_0] < 1$. It is also worth noting that $[\mathcal{R}_0] < 1$ implies $\frac{\Lambda\beta_{t_1}}{\mu_h q} < 1$. Thus $tr(\bar{J}(\mathbf{x}_0)) < 0$ and $\det(\bar{J}(\mathbf{x}_0)) > 0$ whenever $\mu_b > g_b$ and $[\mathcal{R}_0] < 1$. Therefore, it follows from the Routh-Hurwitz criterion that $\mu_b > g_b$ and $[\mathcal{R}_0] < 1$ implies that all four eigenvalues of $J(\mathbf{x}_0)$ lie in the left open half plane. □

4.2.2.4 Global Stability Analysis of the Disease Free Equilibrium

Following Bhunu *et al.* [10], we study the global stability of the system by casting the system into the following form

$$\frac{\mathrm{d}\mathbf{X}}{\mathrm{d}t} = \mathbf{F}(\mathbf{X}, \mathbf{Y}), \quad \frac{\mathrm{d}\mathbf{Y}}{\mathrm{d}t} = \mathbf{G}(\mathbf{X}, \mathbf{Y}), \quad \mathbf{G}(\mathbf{X}^*, \mathbf{0}) = \mathbf{0},$$

where $\mathbf{X} = (S, R)$ and $\mathbf{Y} = (I, B)$. The disease free equilibrium is then written in the form

$$\mathbf{U}_0 = (\mathbf{X}^*, \mathbf{0}), \quad \mathbf{X}^* = \left(\frac{\Lambda}{\mu_h}, \mathbf{0}\right).$$

The conditions that must be met in order for the system to be globally asymptotically stable are:

(H1) $\dfrac{\mathrm{d}\mathbf{X}}{\mathrm{d}t} = \mathbf{F}(\mathbf{X}^*, \mathbf{0}), \quad \mathbf{X}^*$ is globally asympototically stable,

(H2) $\mathbf{G}(\mathbf{X}, \mathbf{Y}) = A\mathbf{Y} - \hat{\mathbf{G}}(\mathbf{X}, \mathbf{Y}), \quad \hat{\mathbf{G}}(\mathbf{X}, \mathbf{Y}) \geq \mathbf{0}$ for $(\mathbf{X}, \mathbf{Y}) \in \Omega$,

where $A = \mathrm{D}_Y\, \mathbf{G}(\mathbf{X}^*, \mathbf{0})$ is a Metzler matrix, and Ω is the region of biological significance.

Theorem 8. ([16], p. 19) *The fixed point* $\mathbf{U}_0 = (\mathbf{X}^*, \mathbf{0})$ *is a globally asymptotically stable equilibrium of a system provided that* $[\mathcal{R}_0] < 1$*, and conditions* $(H1)$ *and* $(H2)$ *are satisfied.*

We establish the global stability of system (4.2) following Theorem (8).

Theorem 9. *The disease free equilibrium of the typhoid model (4.2) is globally asymptotically stable if* $[\mathcal{R}_0] < 1$.

Proof. Applying condition $(H1)$ to the system gives

$$\frac{\mathrm{d}\mathbf{X}}{\mathrm{d}t} = \mathbf{F}(\mathbf{X}^*, \mathbf{0}) = \begin{pmatrix} \Lambda - \mu_h S + \rho R \\ -(\mu_h + \rho) R \end{pmatrix}. \tag{4.8}$$

The Jacobian of equation (4.8) is

$$\mathrm{D}_X\,\mathbf{F}(\mathbf{X}^*,\mathbf{0}) = \begin{pmatrix} -\mu_h & \rho \\ 0 & -(\mu_h+\rho) \end{pmatrix}.$$

We conclude that the fixed point $\mathbf{X}^*$ is a globally asymptotically stable equilibrium point of system (4.8) since the system is linear, and all the eigenvalues of the Jacobian are negative and real. Alternatively, the solution for system (4.8) is

$$\mathbf{X} = c_1\exp(-ut)\mathbf{e}_1 + c_2\exp(-(u+\rho)t)(\mathbf{e}_1-\mathbf{e}_2) + \frac{\Lambda}{\mu_h}\mathbf{e}_1,$$

where $\{\mathbf{e}_1,\mathbf{e}_2\}$ is the standard basis in $\mathbb{E}^2$. Thus, $\lim_{t\to\infty}\mathbf{X} = \mathbf{X}^*$.
Applying condition $(H2)$ to the system yields

$$[A] = \begin{pmatrix} \frac{\Lambda}{\mu_h}\beta_{t_1} - q & \frac{\beta_{t_2}\Lambda}{\kappa_t\mu_h} \\ \alpha & g_b-\mu_b \end{pmatrix},$$

$$[\hat{\mathbf{G}}] = \begin{pmatrix} \beta_{t_1} I\left(\frac{\Lambda}{\mu_h} - \frac{S}{1+kI}\right) + \beta_{t_2}B\left(\frac{\Lambda}{\kappa_t\mu_h} - \frac{S}{B+\kappa_t}\right) \\ \frac{g_b}{\kappa_t}B^2 \end{pmatrix}.$$

Since $\frac{1}{(1+kI)} \leq 1$ and $S \leq \frac{\Lambda}{\mu_h}$, it follows that $\frac{S}{(1+kI)} \leq \frac{\Lambda}{\mu_h}$ or $\frac{\Lambda}{\mu_h} - \frac{S}{(1+kI)} \geq 0$. Also, since $\frac{B}{(B+\kappa_t)} \leq \frac{B}{\kappa_t}$, and $S \leq \frac{\Lambda}{\mu_h}$, it follows that $\frac{SB}{(B+\kappa_t)} \leq \frac{\Lambda B}{\mu_h\kappa_t}$ or $\frac{\Lambda}{\mu_h\kappa_t} - \frac{S}{(B+\kappa_t)} \geq 0$. We conclude that $\hat{\mathbf{G}}(\mathbf{X},\mathbf{Y}) \geq \mathbf{0}$ in the biologically feasible region Ω. Since system (4.2) satisfies conditions $(H1)$ and $(H2)$, it follows from Theorem (8) that $[\mathcal{R}_0] < 1$ implies that the disease free equilibrium for system (4.2) is globally asymptotically stable. □

4.2.2.5 Endemic Equilibrium

The endemic equilibrium for the typhoid model (4.2) is given by setting the time derivative for each class to zero.

$$\Lambda - (\lambda_1^* + \lambda_2^*)S^* - \mu_h S^* + \rho R^* = 0, \quad (\lambda_1^* + \lambda_2^*)S^* - qI^* = 0,$$
$$\epsilon I^* - (\mu_h+\rho)R^* = 0, \quad g_b B^*\left(1 - \frac{B^*}{k_t}\right) + \alpha I^* - \mu_b B^* = 0.$$

We isolate R^* and S^* from $\epsilon I^* - (\mu_h + \rho)R^* = 0$ and $(\lambda_1^* + \lambda_2^*)S^* - qI^* = 0$, respectively. We then substitute those expressions for $R^* = \epsilon I^*/(\mu_h + \rho)$ and $S^* = qI^*/(\lambda_1^* + \lambda_2^*)$ into $\Lambda - (\lambda_1^* + \lambda_2^*)S^* - \mu_h S^* + \rho R^* = 0$ to produce

$$\Lambda - qI^* - \frac{\mu_h q I^*}{\lambda_1^* + \lambda_2^*} + \frac{\rho\epsilon I^*}{\mu_h + \rho} =$$
$$\Lambda + \left(\frac{(\lambda_1^* + \lambda_2^*)\rho\epsilon - q(\mu_h + \rho)(\lambda_1^* + \lambda_2^* + \mu_h)}{(\mu_h + \rho)(\lambda_1^* + \lambda_2^*)} \right) I^* = 0.$$

Isolation of I^* gives

$$I^* = \frac{\Lambda(\mu_h + \rho)(\lambda_1^* + \lambda_2^*)}{(\lambda_1^* + \lambda_2^*)\left(\rho\left(\mu_h + \delta\right) + \mu_h q\right) + \mu_h q\left(\mu_h + \rho\right)}. \tag{4.9}$$

Back substituting equation (4.9) into $R^* = \epsilon I^*/(\mu_h + \rho)$ and $S^* = qI^*/(\lambda_1^* + \lambda_2^*)$, respectively, gives

$$R^* = \frac{\epsilon\Lambda(\lambda_1^* + \lambda_2^*)}{(\lambda_1^* + \lambda_2^*)\left(\rho\left(\mu_h + \delta\right) + \mu_h q\right) + \mu_h q\left(\mu_h + \rho\right)},$$
$$S^* = \frac{q\Lambda(\mu_h + \rho)}{(\lambda_1^* + \lambda_2^*)\left(\rho\left(\mu_h + \delta\right) + \mu_h q\right) + \mu_h q\left(\mu_h + \rho\right)}.$$

In order to show the existence of the endemic equilibrium for the typhoid model (4.2), we complete the square on the equation: $g_b B^*\left(1 - \frac{B^*}{k_t}\right) + \alpha I^* - \mu_b B^* = 0$, to obtain

$$\left(B^* + \frac{k_t(\mu_b - g_b)}{2g_b}\right)^2 = \frac{k^2(\mu_b - g_b)^2 + 4g_b k_t \alpha I^*}{4g_b^2}. \tag{4.10}$$

The two roots for the equation (4.10) are

$$B_1 = \frac{-k_t(\mu_b - g_b) + \sqrt{k_t^2(\mu_b - g_b)^2 + 4g_b k_t \alpha I^*}}{2g_b},$$
$$B_2 = \frac{-k_t(\mu_b - g_b) - \sqrt{k_t^2(\mu_b - g_b)^2 + 4g_b k_t \alpha I^*}}{2g_b}.$$

Since $k_t^2(\mu_b - g_b)^2 \leq k_t^2(\mu_b - g_b)^2 + 4g_b k_t \alpha I^*$, it follows from taking the square root function on both sides of the inequality that

$$k_t|\mu_b - g_b| \leq \sqrt{k_t^2(\mu_b - g_b)^2 + 4g_b k_t \alpha I^*}.$$

Therefore

$$-\sqrt{k_t^2(\mu_b - g_b)^2 + 4g_b k_t \alpha I^*} \leq k_t(\mu_b - g_b) \leq \sqrt{k_t^2(\mu_b - g_b)^2 + 4g_b k_t \alpha I^*}.$$

Hence subtracting $k_t(\mu_b - g_b)$ from the inequalities and then dividing by $2g_b$ yields $B_2 \leq 0 \leq B_1$. Clearly, B_2 must be discarded since it is negative, thus $B^* = B_1$.

4.2.3 The Seasonal Typhoid Model

We study the full effects of seasonality on the typhoid model by removing the time-average function, $[f(t)] = \frac{1}{\omega}\int^{\omega} f(t)\,\mathrm{d}t$, from our analysis. We apply our analysis on model (4.1) for the rest of this section. The model with seasonality thus becomes non-autonomous.

4.2.3.1 Properties of the Non-autonomous Model

We show that model (4.1) is well posed, it has non-negative trajectories, a unique disease free equilibrium, among others. Setting all the derivatives of dynamical system (4.1) to zeros, and setting $(I, B) = (0, 0)$, gives a unique disease free equilibrium $(S^*, I^*, R^*, B^*) = \big(\Lambda/\mu_h, 0, 0, 0\big)$.

Since $\lambda_1, \lambda_2 \geq 0$, it follows that $\lambda_1 + \lambda_2 \geq 0$. We conclude that the force of infection for model (4.1) is non-negative.

The partial derivatives of the force of infection are

$$\frac{\partial}{\partial I}\Big(\lambda_1 + \lambda_2\Big) = \frac{\beta_{t_1}}{(1 + kI)^2} \geq 0,$$
$$\frac{\partial}{\partial B}\Big(\lambda_1 + \lambda_2\Big) = \frac{\beta_{t_2}\kappa_t}{(B + \kappa_t)^2}\left(1 + \theta \sin\left(\frac{2\pi t}{365}\right)\right) \geq 0.$$

It is clear that the force of infection increases with the number of infected people and the concentration of bacteria. The bacterial growth rates are bounded as

follows:

$$\frac{\partial}{\partial B}\left(\frac{\mathrm{d}B}{\mathrm{d}t}\right) = g_b\left(1-2\frac{B}{k_t}\right)\left(1+\xi\sin\left(\frac{2\pi t}{365}\right)\right) - \mu_b \leq 0,\ \frac{\partial}{\partial I}\left(\frac{\mathrm{d}B}{\mathrm{d}t}\right) = \alpha \geq 0,$$

whenever $B \geq k_t/2$. The first inequality shows that the bacterial growth rate increases with the number of infected individuals; the second inequality shows that in the absence of infected people, there exists a threshold, $k_t/2$, such that if the bacteria exceeds this threshold, then the bacterial growth rate decreases with the concentration of the bacteria.

We show, geometrically, that the surface that represents the force of infection, $\lambda_1 + \lambda_2$, lies below its associated tangent plane at the origin. This means that the remainder term, R_1, from the truncated Taylor expansion of $\lambda_1 + \lambda_2$ when the degree equals one is non-positive. The second partial derivatives of the force of infection are

$$\frac{\partial^2}{\partial I^2}\left(\lambda_1+\lambda_2\right) = \frac{-2\beta_{t_1}k}{(1+kI)^3} \leq 0, \quad \frac{\partial^2}{\partial B\partial I}\left(\lambda_1+\lambda_2\right) = 0,$$
$$\frac{\partial^2}{\partial B^2}\left(\lambda_1+\lambda_2\right) = \frac{-2\beta_{t_2}\kappa_t}{(B+\kappa_t)^3}\left(1+\theta\sin\left(\frac{2\pi t}{365}\right)\right) \leq 0.$$

Consider the matrix

$$A = \begin{bmatrix} \frac{\partial^2}{\partial I^2}\left(\lambda_1+\lambda_2\right) & \frac{\partial^2}{\partial B\partial I}\left(\lambda_1+\lambda_2\right) \\ \frac{\partial^2}{\partial B\partial I}\left(\lambda_1+\lambda_2\right) & \frac{\partial^2}{\partial B^2}\left(\lambda_1+\lambda_2\right) \end{bmatrix}$$
$$= \begin{bmatrix} \frac{-2\beta_{t_1}k}{(1+kI)^3} & 0 \\ 0 & \frac{-2\beta_{t_2}\kappa_t}{(B+\kappa_t)^3}\left(1+\theta\sin\left(\frac{2\pi t}{365}\right)\right) \end{bmatrix}.$$

Since

$$\begin{bmatrix} I \\ B \end{bmatrix}^T \begin{bmatrix} \frac{-2\beta_{t_1}k}{(1+kI)^3} & 0 \\ 0 & \frac{-2\beta_{t_2}\kappa_t}{(B+\kappa_t)^3}\left(1+\theta\sin\left(\frac{2\pi t}{365}\right)\right) \end{bmatrix} \begin{bmatrix} I \\ B \end{bmatrix} =$$

$$-2\left(\frac{\beta_{t_1}kI^2}{(1+kI)^3}+\frac{\beta_{t_2}\kappa_t B^2}{(B+\kappa_t)^3}\left(1+\theta\sin\left(\frac{2\pi t}{365}\right)\right)\right)\leq 0,$$

$$R_1 = -\left(\frac{\beta_{t_1}k\zeta^2}{(1+k\zeta)^3}+\frac{\beta_{t_2}\kappa_t\eta^2}{(\eta+\kappa_t)^3}\left(1+\theta\sin\left(\frac{2\pi t}{365}\right)\right)\right),$$

where $\zeta \in (0, I)$ and $\eta \in (0, B)$, it follows that $R_1 \leq -\left(\frac{\beta_{t_1}kI^2}{(1+kI)^3}+\frac{\beta_{t_2}\kappa_t B^2}{(B+\kappa_t)^3}\left(1+\theta\sin\left(\frac{2\pi t}{365}\right)\right)\right) \leq 0$, and that matrix A is negative semi-definite.

It is clear to see that $I > 0$ implies $\lambda_1 + \lambda_2 > 0$ and $B > 0$ implies $\lambda_1 + \lambda_2 > 0$. The model shows that in the absence of bacteria, a single infected individual is sufficient for a positive infection rate; and in the absence of infected individuals, the presence of bacteria is sufficient for a positive infection rate.

4.2.3.2 Basic Reproduction Number

We apply the methods outlined in [80, 89] to determine basic reproduction number.

We show that the system (4.1) meets the seven assumptions in the article by Wang and Zhao [89]. Let $\mathbf{x} = (S, I, R, B)^T$. The disease free equilibrium is $\mathbf{x}_0 = (\Lambda/\mu_h, 0, 0, 0)^T$ and the new infections vector and transfer vectors are as

follows

$$\mathcal{F} = \begin{pmatrix} (\lambda_1 + \lambda_2)S \\ 0 \\ 0 \\ 0 \end{pmatrix}, \quad \mathcal{V}^- = \begin{pmatrix} qI \\ \mu_b B \\ (\lambda_1 + \lambda_2)S + \mu_h S \\ (\mu_h + \rho)R \end{pmatrix},$$

$$\mathcal{V}^+ = \begin{pmatrix} 0 \\ g_b B\left(1 - \frac{B}{\kappa_t}\right)\left(1 + \xi \sin\left(\frac{2\pi t}{365}\right)\right) + \alpha I \\ \Lambda + \rho R \\ \epsilon I \end{pmatrix}.$$

The Jacobians of the input rate of new infections and the transfer rate of infections are

$$F(t) = \begin{pmatrix} \frac{\Lambda}{\mu_h}\beta_{t_1} & \frac{\Lambda\beta_{t_2}}{\mu_h k_t}\left(1 + \theta \sin\left(\frac{2\pi t}{365}\right)\right) \\ 0 & 0 \end{pmatrix}, \quad V(t) = \begin{pmatrix} q & 0 \\ -\alpha & \mu_b - g_b\left(1 + \xi \sin\left(\frac{2\pi t}{365}\right)\right) \end{pmatrix}.$$

Define $f = \mathcal{F} - \mathcal{V}$, $\mathcal{V} = \mathcal{V}^- - \mathcal{V}^+$, and $\rho(J)$ as the spectral radius of matrix J.

Lemma 1. ([96], Lemma 2.1.) *Let $A(t)$ be a continuous, cooperative, irreducible, and ω-periodic $k \times k$ matrix function and let $p = \frac{1}{\omega}\ln(\rho(\Phi_A(\omega)))$. Then*

$$\frac{\mathrm{d}\mathbf{x}(t)}{\mathrm{d}t} = A(t)\mathbf{x}(t), \tag{4.11}$$

gives a solution $\mathbf{x}(t) = e^{pt}\mathbf{v}(t)$ for some ω-periodic function $\mathbf{v}(t)$. $\Phi_A(\omega)$ denotes the monodromy matrix of system (4.11).

The next infection operator is defined by [89] as follows

$$(L\phi) = \int_0^\infty Y(t, t-s)F(t-s)\phi(t-s)ds, \tag{4.12}$$

where $Y(t,s)$ is the evolution operator for the system $dy/dt = -V(t)y$ and $\phi(t)$ is the initial distribution function of the infected. The spectral radius of L gives the basic reproduction number

$$\mathcal{R}_0 = \rho(L).$$

In most nonlinear systems, the integral in equation (4.12) is intractable, thus numerical methods are used to compute $\mathcal{R}_0$. Since the basic reproduction number is the maximum eigenvalue of the operator eigenvalue problem $(L\phi)t = \lambda\phi(t)$, the authors of [70] constructed an eigenvalue-preserving transformation of the above operator eigenvalue problem into a matrix eigenvalue problem. The spectral radius of the eigenvalue problem is an accurate estimator for the true basic reproduction number.

Theorem 10. ([89], Theorem 2.2) *The following statements are valid for model (4.1):*

1. $\mathcal{R}_0 = 1 \iff \rho(\Phi_f(365)) = 1$,
2. $\mathcal{R}_0 < 1 \iff \rho(\Phi_f(365)) < 1$,
3. $\mathcal{R}_0 > 1 \iff \rho(\Phi_f(365)) > 1$,
4. $\mathcal{R}_0 < 1$ *(*$\mathcal{R}_0 > 1$*)* $\implies \mathbf{x}_0$ *is locally asymptotically stable (unstable),*

whenever,

(B1) *The functions* $\mathcal{F}(t, \mathbf{x}) \geq 0$, $\mathcal{V}^+(t, \mathbf{x}) \geq 0$, *and* $\mathcal{V}^-(t, \mathbf{x}) \geq 0$ *are continuous, continuously differentiable with respect to* x *on* $\mathbb{R} \times \mathbb{R}^4_+$, *and each have a period of 365 with respect to* t.

(B2) $\mathbf{x}_i = 0 \implies \mathcal{V}_i^-$ *for* $i = 1, 2$.

(B3) $i > 2 \implies \mathcal{F}_i = 0$.

(B4) $\mathcal{F}_i(\mathbf{x}_0) = 0 \wedge \mathcal{V}_i^+(\mathbf{x}_0) = 0$ *for* $i = 1, 2$.

(B5) $\rho(\Phi_f(365)) < 1$, *where* $\rho(\Phi_f(365))$ *is the spectral radius of* $\Phi_f(365)$.

(B6) $\rho(\Phi_{-V}(365)) < 1$

We claim that, for model (4.1), f conditionally satisfies $(B1)$ to $(B6)$. By inspection, we can see that for each $i = 1, \ldots, 4$, the functions $\mathcal{F}_i(t, \mathbf{x})$, $\mathcal{V}_i^+(t, \mathbf{x})$, and $\mathcal{V}_i^-(t, \mathbf{x})$ are non-negative, continuous on $\mathbb{R} \times \mathbb{R}_+^4$, continuously differentiable with respect to $\mathbf{x}$, and 365-periodic in t. If $I = 0$ $(B = 0)$, then $\mathcal{V}_1^-(t, \mathbf{x}) = 0$ $(\mathcal{V}_2^-(t, \mathbf{x}) = 0)$. $\mathcal{F}_3(t, \mathbf{x}) = \mathcal{F}_4(t, \mathbf{x}) = 0$. At the disease free state, $\mathbf{x}_0$, for each $i = 1, 2$, $\mathcal{F}_i(t, \mathbf{x}) = \mathcal{V}_i^+(t, \mathbf{x}) = 0$. We define the matrix

$$M(t) = \left[\frac{\partial}{\partial x_j} \Big(f_i(t, \mathbf{x}_0) \Big) \right]_{3 \le i,j \le 4} = \begin{bmatrix} -\mu_h & \rho \\ 0 & -(\mu_h + \rho) \end{bmatrix},$$

where $f_i(t, \mathbf{x}_0) = \mathcal{F}_i(t, \mathbf{x}) - (\mathcal{V}_i^-(t, \mathbf{x}) - \mathcal{V}_i^+(t, \mathbf{x}))$. The initial value problem, $\mathbf{z}' = M\mathbf{z}$, $\mathbf{z}(s, s) = I_{2\times 2}$, can be written component wise to produce the system

$$\begin{aligned} \frac{\mathrm{d}z_1}{\mathrm{d}t} &= -\mu_h z_1 + \rho z_3, \quad \frac{\mathrm{d}z_2}{\mathrm{d}t} = -\mu_h z_2 + \rho z_4, \quad \frac{\mathrm{d}z_3}{\mathrm{d}t} = -(\mu_h + \rho) z_3, \\ \frac{\mathrm{d}z_4}{\mathrm{d}t} &= -(\mu_h + \rho) z_4. \end{aligned}$$

The solution and the monodromy matrices to the initial value problem above are, respectively,

$$\begin{aligned} z(t, s) &= \begin{bmatrix} \exp(\mu_h(s-t)) & \exp(\mu_h(s-t)) - \exp((\mu_h + \rho)(s-t)) \\ 0 & \exp((\mu_h + \rho)(s-t)) \end{bmatrix}, \\ z(t, 0) = \Phi_M(t) &= \begin{bmatrix} \exp(-\mu_h t) & \exp(-ut) - \exp(-(\mu_h + \rho)t) \\ 0 & \exp(-(\mu_h + \rho)t) \end{bmatrix}. \end{aligned} \tag{4.13}$$

The spectral radius of the monodromy matrix (4.13) at $t = 365$ is

$$\rho(\Phi_M(365)) = \max\{\exp(-365\mu_h),\ \exp(-365(\mu_h + \rho))\} < 1.$$

The initial value problem $\mathbf{Y}' = -V(t)\mathbf{Y}$, $\mathbf{Y}(s, s) = I_{2\times 2}$, can be written compo-

nent wise as follows

$$\frac{\mathrm{d}}{\mathrm{d}t}\Big(Y_1(t,s)\Big) = -qY_1(t,s), \quad \frac{\mathrm{d}}{\mathrm{d}t}\Big(Y_2(t,s)\Big) = -qY_2(t,s),$$
$$\frac{\mathrm{d}}{\mathrm{d}t}\Big(Y_3(t,s)\Big) = \alpha Y_1(t,s) + \left(\left(1+\xi\sin\left(\frac{2\pi t}{365}\right)\right)g_b - \mu_b\right)Y_3(t,s),$$
$$\frac{\mathrm{d}}{\mathrm{d}t}\Big(Y_4(t,s)\Big) = \alpha Y_2(t,s) + \left(\left(1+\xi\sin\left(\frac{2\pi t}{365}\right)\right)g_b - \mu_b\right)Y_4(t,s).$$

Thus a solution to the differential equation

$$\frac{\mathrm{d}}{\mathrm{d}t}\Big(Y(t,s)\Big) = -V(t)Y(t,s), \quad \forall t \geq s, \quad Y(s,s) = I_{2\times 2}, \tag{4.14}$$

is

$$Y(t,s) = \begin{bmatrix} Y_1(t,s) & Y_2(t,s) \\ Y_3(t,s) & Y_4(t,s) \end{bmatrix}$$
$$= \begin{bmatrix} \exp(q(s-t)) & 0 \\ Y_3(t,s) & \exp\left((g_b-\mu_b)(t-s) + \xi g_b\frac{365}{2\pi}\left(\cos\left(\frac{2\pi s}{365}\right) - \cos\left(\frac{2\pi t}{365}\right)\right)\right) \end{bmatrix},$$

where

$$Y_3(t,s) = \alpha\exp\left(qs + (g_b-\mu_b)t - \frac{365}{2\pi}\xi g_b\cos\left(\frac{2\pi t}{365}\right)\right)$$
$$\times\int_s^t \exp\left((\mu_b - g_b - q)\tau + \frac{365}{2\pi}\xi g_b\cos\left(\frac{2\pi\tau}{365}\right)\right)d\tau.$$

The monodromy matrix of differential equation (4.14)) is

$$\Phi_{-V}(t) = Y(t,0) = \begin{bmatrix} \exp(-qt) & 0 \\ Y_3(t,0) & \exp\left((g_b-\mu_b)t + \xi g_b\frac{365}{2\pi}\left(1-\cos\left(\frac{2\pi t}{365}\right)\right)\right) \end{bmatrix}.$$

Thus, the spectral radius is

$$\rho(\Phi_{-V}(365)) = \max\{\exp(-365q), \exp(365(g_b-\mu_b))\}.$$

It is clear to see that $\rho(\Phi_{-V}(365)) < 1$ whenever $g_b < \mu_b$. We have proven that assumptions $(A1)$—$(A7)$ of Wang [89] hold for model (4.1) if $g_b < \mu_b$.

Corollary 10.1. *The following statements are valid for model (4.1) if* $g_b < \mu_b$*:*

(I) $\mathcal{R}_0 = 1 \iff \rho(\Phi_f(365)) = 1.$

(II) $\mathcal{R}_0 < 1 \iff \rho(\Phi_f(365)) < 1.$

(III) $\mathcal{R}_0 > 1 \iff \rho(\Phi_f(365)) > 1.$

(IV) *The disease free equilibrium,* $\mathbf{x}_0$*, is locally asymptotically stable if* $\mathcal{R}_0 < 1$*, and unstable if* $\mathcal{R}_0 > 1$*.*

Proof. Since model (4.1) satisfies conditions $(A1)$—$(A7)$ of Wang [89] whenever $g_b < \mu_b$, it follows from Theorem 2.2 of [89] that $g_b < \mu_b$ implies that conditions $(I) - (IV)$ hold. □

4.2.3.3 Global Stability of the Disease Free Equilibrium

In this subsection, we prove that the disease free equilibrium of model (4.1) is globally asymptotically stable. We begin with the following Theorem.

Theorem 11. *([78], Theorem B.1.) Let* $D \subseteq \mathbb{R}^n$ *be open in* $\mathbb{R}^n$*. Let* $f : \mathbb{R} \times D \to \mathbb{R}^n$ *be continuous on* $\mathbb{R} \times D$ *such that. Let* $x(t)$ *be a solution of* $(B.1)$ *defined on* $[a, b]$*. If* $z(t)$ *is a continuous function on* $[a, b]$ *satisfying* $(B.2)$ *on* (a, b) *with* $z(a) \leq x(a)$*, then* $z(t) \leq x(t)$ *for all* t *in* $[a, b]$*. If* $y(t)$ *is continuous on* $[a, b]$ *satisfying* $(B.3)$ *on* (a, b) *with* $y(a) \geq x(a)$*, then* $y(t) \geq x(t)$ *for all* t *in* $[a, b]$*.*

Limiting our focus to the two infected classes, I and B, the Jacobian of system (4.1) is

$$[F(t) - V(t)] = \begin{bmatrix} \frac{\Lambda}{\mu_h}\beta_{t_1} - q & \frac{\Lambda\beta_{t_2}}{\mu_h k_t}\left(1 + \theta \sin\left(\frac{2\pi t}{365}\right)\right) \\ \alpha & g_b\left(1 + \xi \sin\left(\frac{2\pi t}{365}\right)\right) - \mu_b \end{bmatrix}.$$

Applying Lemma (1) to $\mathbf{z} = [\tilde{I}_t,\ \tilde{B}_t]^T$ gives

$$\frac{\mathrm{d}}{\mathrm{d}t}\begin{bmatrix}\tilde{I}_t\\ \tilde{B}_t\end{bmatrix} = \begin{bmatrix}\frac{\Lambda}{\mu_h}\beta_{t_1} - q & \frac{\Lambda\beta_{t_2}}{\mu_h k_t}\left(1+\theta\sin\left(\frac{2\pi t}{365}\right)\right)\\ \alpha & g_b\left(1+\xi\sin\left(\frac{2\pi t}{365}\right)\right) - \mu_b\end{bmatrix}\begin{bmatrix}\tilde{I}_t\\ \tilde{B}_t\end{bmatrix} \implies \begin{bmatrix}\tilde{I}_t\\ \tilde{B}_t\end{bmatrix} = e^{bt}\mathbf{v}(t).$$

Since $\mathcal{R}_0 < 1 \iff \rho(\Phi_f(365)) < 1 \iff b < 0$, it follows that $\mathcal{R}_0 < 1$ implies

$$\lim_{t\to\infty} e^{bt}\mathbf{v}(t) = [0,\ 0]^T.$$

From applying the Taylor expansion to first order and using the $R_1 \leq 0$, we obtain the following differential inequality

$$\begin{aligned}\frac{\mathrm{d}}{\mathrm{d}t}\begin{bmatrix}I\\ B\end{bmatrix} &= \begin{bmatrix}(\lambda_1+\lambda_2)S - qI\\ g_b B\left(1-\frac{B}{k_t}\right)\left(1+\xi\sin\left(\frac{2\pi t}{365}\right)\right) + \alpha I - \mu_b B\end{bmatrix},\\ &= \begin{bmatrix}\frac{\Lambda}{\mu_h}\beta_{t_1} - q & \frac{\Lambda\beta_{t_2}}{\mu_h k_t}\left(1+\theta\sin\left(\frac{2\pi t}{365}\right)\right)\\ \alpha & g_b\left(1+\xi\sin\left(\frac{2\pi t}{365}\right)\right) - \mu_b\end{bmatrix}\begin{bmatrix}I\\ B\end{bmatrix}\\ &\quad + \begin{bmatrix}R_1\\ -g_b\frac{B^2}{k_t}\left(1+\xi\sin\left(\frac{2\pi t}{365}\right)\right)\end{bmatrix},\\ &\leq \begin{bmatrix}\frac{\Lambda}{\mu_h}\beta_{t_1} - q & \frac{\Lambda\beta_{t_2}}{\mu_h k_t}\left(1+\theta\sin\left(\frac{2\pi t}{365}\right)\right)\\ \alpha & g_b\left(1+\xi\sin\left(\frac{2\pi t}{365}\right)\right) - \mu_b\end{bmatrix}\begin{bmatrix}I\\ B\end{bmatrix}.\end{aligned}$$

It follows from Theorem (11) that

$$\lim_{t\to\infty}[I,\ B]^T \leq \lim_{t\to\infty}[\tilde{I}_t,\ \tilde{B}_t]^T = [0,\ 0]^T,$$

thus

$$\lim_{t\to\infty}[I,\ B]^T = [0,\ 0]^T.$$

Theorem 12. *If $\mathcal{R}_0 < 1$, the following statements are valid for model (4.1):*

a) $\lim_{t\to\infty} R = 0$.

b) $\lim_{t\to\infty} S = \Lambda/\mu_h$.

Proof.

a) We want to show that for any $\upsilon > 0$, there exists $\gamma \in \mathbb{R}^+$, such that if $t > \gamma$, then $R < \upsilon$. Assume $\mathcal{R}_0 < 1$. Since $\lim_{t\to\infty} I = 0$, it follows that for any $\upsilon > 0$, there exists $\gamma_1 \in \mathbb{R}^+$, such that

$$t > \gamma_1 \implies I(t) < \frac{(\mu_h + \rho)}{\epsilon}\upsilon. \tag{4.15}$$

Choose $\gamma \geq \gamma_1$. Since $\dot{R} = \epsilon I - (\mu_h + \rho)R$, it follows from (4.15) that $t > \gamma$ implies $\dot{R} < (\mu_h + \rho)(\upsilon - R)$. The solution to the differential inequality, $\dot{R} < (\mu_h + \rho)(\upsilon - R)$, is $R < \upsilon - M\exp(-t(\mu_h + \rho))$ for some positive constant M. Indeed $R < \upsilon$.

b) Since $N = S + I + R$, it follows from $\lim_{t\to\infty} R = 0$ and $\lim_{t\to\infty} I = 0$ that $\mathcal{R}_0 < 1$ implies $\lim_{t\to\infty} N = \lim_{t\to\infty} S = \Lambda/\mu_h$.

□

We thus have the following result.

Theorem 13. *The disease free equilibrium, $\mathbf{x}_0$, of system (4.1) is globally asymptotically stable whenever $\mathcal{R}_0 < 1$.*

4.3 Numerical Simulation

In this section, simulation results are carried out through MATLAB. We hypothetically choose the following initial conditions and the parameter values in Table

(4.1). The initial conditions used were $S(0) = 99980,\ I(0) = 20,$
$R(0) = 0,\ B(0) = 40000.$

Table (4.1) shows the parameters of the typhoid model. On the same table, we include a column that shows the most sensitive parameters in the model. The human birth rate, Λ, has the highest sensitivity with sensitivity index equal to one. It is followed by the human natural death rate, μ_h, with a sensitivity index of -0.9901.

Parameter	Range	Point Value	Source
β_{t_1}	$0-1$	7.5×10^{-5}	Assumed
β_{t_2}	$0-1$	1.97×10^{-11}	[52, 56]
δ	$0.001-1$	0.06	[52]
ρ	$0-1$	1.3×10^{-3}	[62]
g_b	$0-1$	0.014	[56]
α	$0-20$	10	[56]
μ_b	$0-1$	0.0345	[56]
Λ	$100-467$	449.31	[12]
μ_h	$0.019-0.021$	0.02	[32]
ϵ	$0-1$	0.1	[2, 53]
κ_t	$0-1$	0.62	Assumed
k		0.2	Assumed
k_t		500000	Assumed

Table 4.1: Parameter values and their sources.

4.3.1 Sensitivity Analysis

We begin by considering the sensitivity analysis of the model parameters to the model output. The Latin Hypercube sampling method was used. This method

produced a set of partial rank correlation coefficients (PRCC) between each of the model parameters and the state variable I. The simulation was carried out over 1000 runs. The human birth rate, Λ, is the most sensitive parameter relative to the infectious class, and it is positively correlated to the infectious class. The natural human death rate, μ_h, is the second most sensitive parameter relative to the infectious class, and it is negatively correlated to the infectious class.

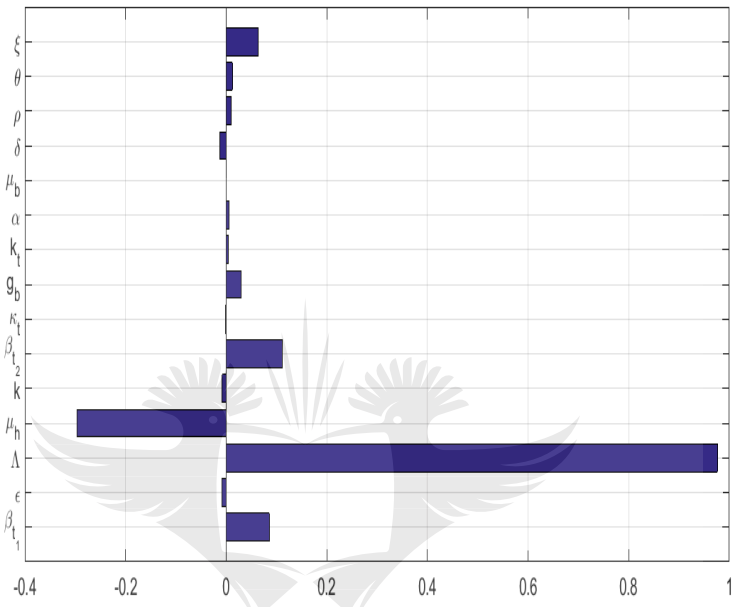

Figure 4.2: The partial rank correlation coefficients (PRCC). The correlation coefficients between the each of the parameters on Table 4.1 and the state variable I are shown. Parameters with negative PRCC values are negatively correlated to I, whilst those with positive PRCC values are positively correlated to I.

4.3.2 Plots of the Reproduction Numbers and Time Series

The graph of the basic reproduction number, $\mathcal{R}_0$, superimposed on the graph of the time average basic reproduction number, $[\mathcal{R}_0]$, is shown in Fig 4.3. The time average basic reproduction number was computed by setting the the direct transmission rate $\beta_{t_1} = 7.5 \times 10^{(-6)}$. Using the same direct transmission rate and the

method outlined in [70], we numerically computed the basic reproduction number when $\xi = 0$. Since the seasonal period of the disease in 365 days, the rate of exponential decay in all expressions containing the period will be fast. This then means that iterations exceeding five in such terms will achieve minimal improvement in the accuracy. It is for this reason that we have set $M = 10$ and $n = 100$ as defined in [70].

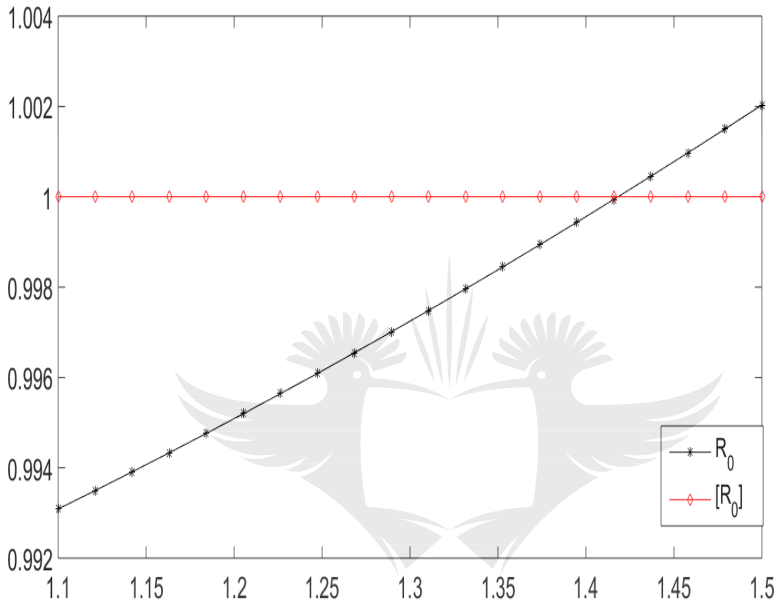

Figure 4.3: A comparison of the basic reproduction number, $\mathcal{R}_0$, and the time average basic reproduction number $[\mathcal{R}_0]$ as a function of the seasonal parameter θ.

We consider the seasonal plots for our models (with and without) seasonality. The trajectories of all the state variables are shown in Figure 4.4. This figure shows the trajectories of the: (a), the susceptible class; (b), the infectious class; (c), the recovered class; and (d) the bacterial class. In each of the four figures in Figure 4.4, the trajectories of the seasonal model (4.1) are superimposed onto the trajectories of the non-seasonal model (4.2).

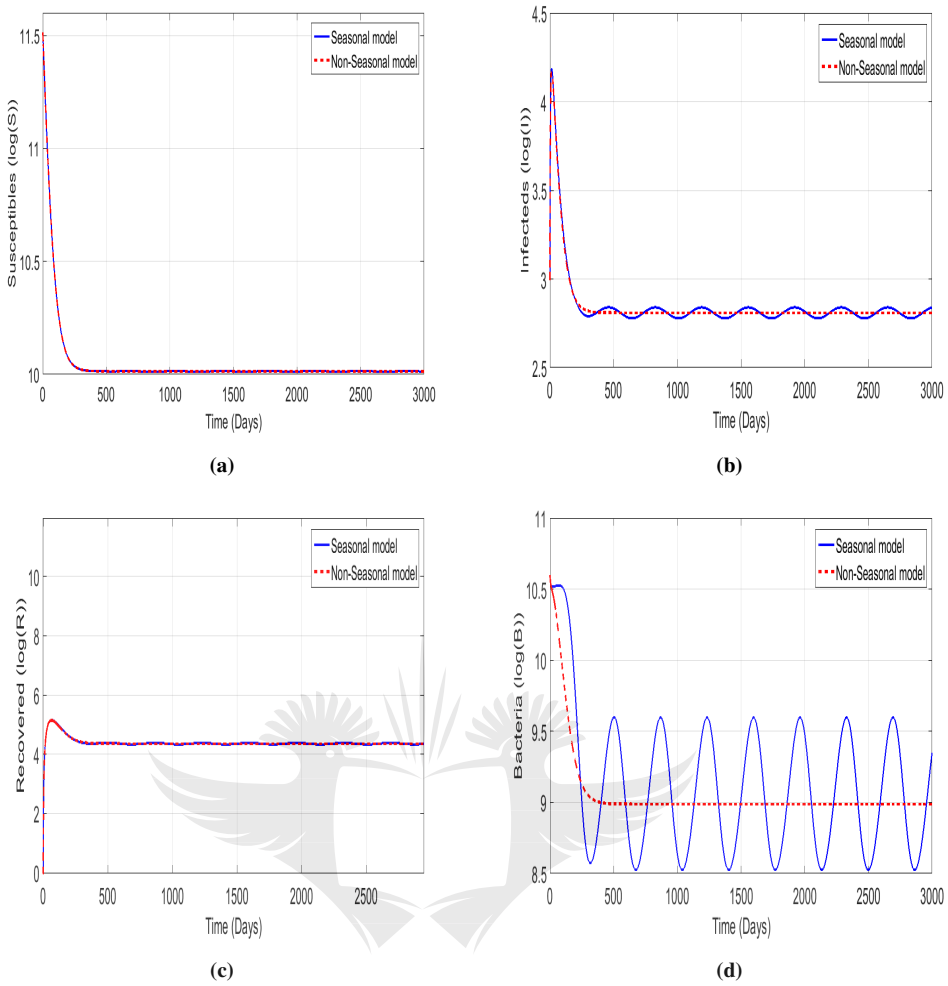

Figure 4.4: The trajectories of the models. The dotted lines depict the trajectories of the non-seasonal model (4.2), whilst the solid lines depict the trajectories of the seasonal model (4.1). The trajectories of the susceptibles, (a), the infected, (b), the recovered, (c), and the typhoid bacteria, (d) are shown.

4.3.3 Simulating the Role of Fear

We now consider the potential impact of fear on the model with and without seasonality. We use the logarithmic scale for clarity of presentation of results. The manner in which fear affects the prevalence of typhoid is shown in Figure 4.5.

Figure 4.5(a) shows this effect on the non-seasonal model (4.2), whilst Figure 4.5(b) shows the same effect on the seasonal model (4.1). In both cases, the fear constant k is allowed to run through the set $\{0.2, 0.3, 0.4, 0.5\}$.

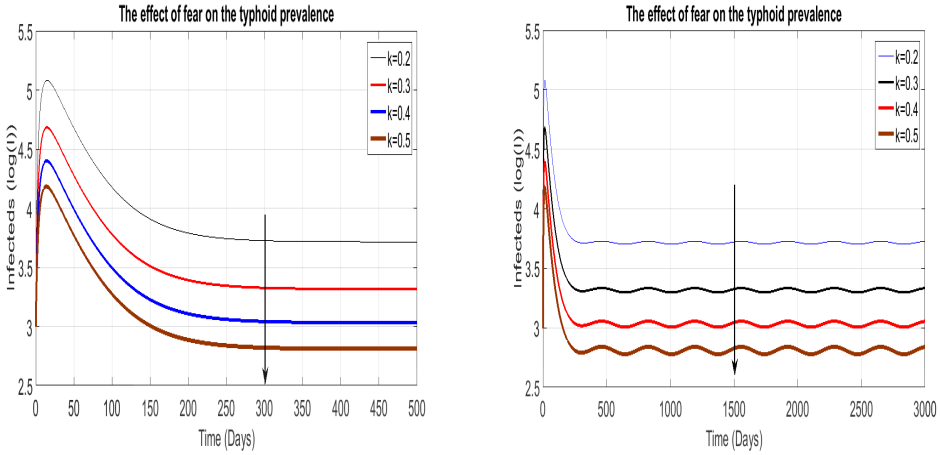

Figure 4.5: Typhoid prevalence as a function of fear. The fear constant, k, runs through $\{0.2, 0.3, 0.4, 0.5\}$. The effects of fear on the typhoid prevalence of the non-seasonal model (4.2) are shown in (a). The effects of fear on the typhoid prevalence of the seasonal model (4.1) are shown in (b).

4.4 Discussion and Conclusion

Seasonality is a common phenomenon in bacterial infections such as cholera and typhoid in which the diseases are more prevalent in summer than in winter. The spread of these diseases is further compounded by poor hygiene and maintenance of sewage disposal infrastructure. The mechanisms that drive seasonality in typhoid fever are mainly driven by rainfall patterns and poor sewage disposals system especially during summer. While some work has recently been done in [73], the role of fear, which impacts the rate of infection was not considered. Fear of infection has the propensity to reduce the infection rate, and in this paper, our interest was on investigating how the seasonality dynamics of typhoid fever are impacted by fear. In this paper, we propose and analyze a model of typhoid fever

that follows the work presented in [51] in the presence of fear. The model is motivated by the fact that in the presence of poor health infrastructure, behaviour changes become critical in the reducing the rate of typhoid fever infection in seasonally fluctuating environments. In addition, we are also motivated by scenarios in many countries in Sub-Saharan Africa, such as Zimbabwe, where typhoid fever remains a problem especially in Summer.

The seasonal fluctuations are modelled by the inclusion of a trigonometric function in the transmission rate driven by the bacterial population. The model is considered in cases where there is no seasonality and in the presence of seasonal fluctuations. In both cases, the basic reproduction numbers $\mathcal{R}_0$ and $[\mathcal{R}_0]$ are determined.

The stability of the steady states is carried out and we noted that the disease free equilibrium is globally stable when the basic reproduction number is less than unit. The existence of the endemic equilibrium is also discussed.

Numerical simulations are carried out following some hypothetical initial conditions and some chosen parameter values from the literature. Sensitivity analysis is also carried out using the Latin hyper cube sampling technique and the model is sensitive to the addition of susceptible individuals and the natural mortality rate of the human population.

It is important to note that the model presented in this paper has a number of limitations, as is the case with all mathematics models in which various assumptions are used in the construction of the models. The model is not validated by data. In the presence of data (which was not readily available in this case) the model would have been more robust, and in this case remains a theoretical model. This forms the basis of our future work. Despite this short coming, the model remains of great interest in the investigation of the role of human behaviour, such as fear in bacterial infections.

The subsequent chapter includes the analysis of a cholera and typhoid coinfection mathematical model with hygiene driven contact.

Chapter 5

A Mathematical Model of Hygiene Driven Contact in Cholera Typhoid Coinfection Transmission Dynamics

5.1 Introduction

Cholera is a water borne infection that is associated with vomiting and diarrhoea. The bacteria causing cholera, *V. cholerae*, is part of the estuary and coastal ecosystem [20]. The African continent has seen a sharp rise (31%) in cholera infections since 2004. In some developing countries, outbreaks occur as much as twice in a single year [33]. Malnutrition is one of the major drivers of cholera infections. In the world's poorest countries, cholera is often endemic. Zinc and vitamin A deficiency increase the susceptibility of children to the disease, and sub-Saharan Africa and South Asia have a vitamin A deficiency [79]. Child malnutrition in Zimbabwe led to an increase in cholera in 2008.

Typhoid fever is a waterborne infection that is associated with fever, vomiting, diarrhoea, weight loss, anaemia, and weakness. The infection is caused by salmonella

typhi bacteria. It is acquired through human-to-human transmission and through the ingestion of salmonella contaminated food. Twenty one million cases and half a million deaths per year have been caused by typhoid fever. Most of these deaths occur within the African continent.

Several models have been created to study the various aspects of typhoid fever and cholera in the literature. Mushayabasa *et al.* developed and analysed a typhoid malaria coinfection model [54]. They discovered that the two infections led to an increase in the prevalence of the coinfected individuals. Tilahun *et al.* proposed a pneumonia typhoid coinfection model with optimal control, and they discovered that prevention was the most effective control strategy and it was closely followed by treatment as the second best control strategy [84]. A malaria typhoid coinfection model was studied by Mutua *et al.* [56]. They concluded that the two infections must be managed in tandem for the most optimal results. Matsebula *et al.* developed and analysed a seasonal model for typhoid with fear [45]. One of the results was that the average basic reproduction number was an inaccurate estimator for the basic reproduction number in fluctuation environments. Baracchini *et al.* proposed a cholera a model with seasonality [8]. In that model, they showed that the phase of the model and whether the disease is unimodal or bimodal is decided by the level of water in the environment. Nyabadza *et al.* modelled the effects of limited resources on the dynamics of cholera, and they discovered that the model had multiple equilibria [51]. To the best of our knowledge, the effects of behavioural changes such as hygiene on the co-dynamics of typhoid and cholera have not been established in the literature.

5.2 Model Formulation

The cholera typhoid coinfection model classifies the total human population at time t, denoted by $N(t)$, into susceptible individuals $S(t)$, cholera infected individuals $I_c(t)$, individuals who recovered from cholera $R_c(t)$, typhoid infected individuals $I_t(t)$, individuals who recovered from typhoid $R_t(t)$, individuals in-

fected with both cholera and typhoid $I_{ct}(t)$, and individuals who recovered from both cholera and typhoid $R_{ct}(t)$. Thus,

$$N(t) = S(t) + I_c(t) + R_c(t) + I_t(t) + R_t(t) + I_{ct}(t) + R_{ct}(t).$$

Additional compartments $B_c(t)$ and $B_t(t)$, representing respectively the concentration of *Vibrio Cholerae* and *Salmonella Typhi* in the environment have also been incorporated in the model.

We construct a contact rate function

$$f(x, H) = \frac{x}{1 + Ae^{\zeta H}},$$

where x is the maximum contact rate and H is the proportion of the population that is hygienic. In this function, A is the scale parameter and ζ is the shape parameter. For this function to be well posed, it needs to exhibit the following characteristics. First, A must be between zero and one such that $(0 \leq A \ll 1)$. This is to allow the contact rate function to approach the maximum contact rate whenever the levels of hygiene are poor. Second, if $H = 1,\ f(x, H) \to 0$ iff $\zeta \to \infty$. This characteristic suggests that when the population is hygienic, the contact rate function approaches 0 whenever zeta approaches infinity. This means that zeta controls the speed at which improved hygiene translates to a break in transmission, or that a break in transmission is characterised by zeta approaching infinity. It is clear that zeta must be chosen to be high enough so that the correlation between the contact rate function approaching 0 and the hygiene levels approaching one is strong. Although shedding is also a function of hygiene, incorporating it into a functional response turns out to be cumbersome exercise, so this exercise is omitted from this work.

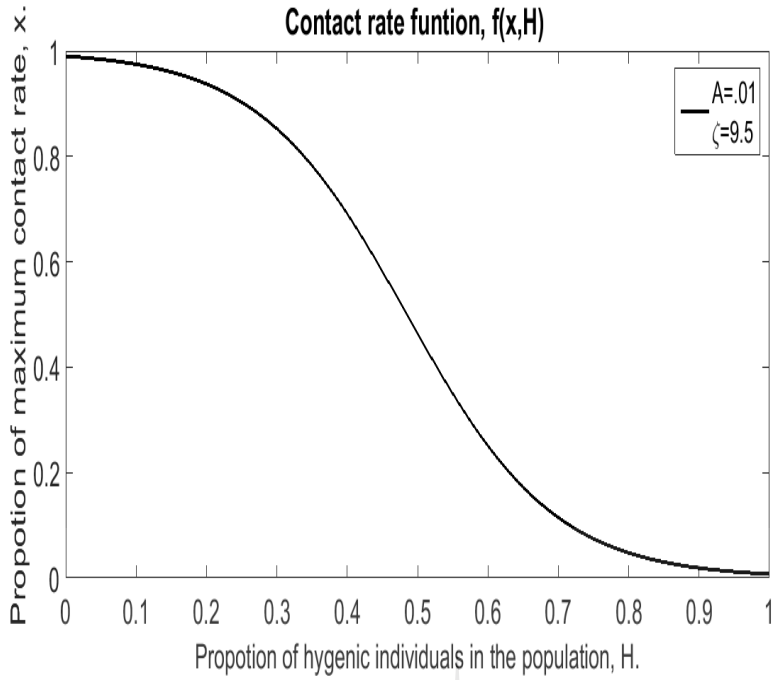

Figure 5.1: The proportion of the maximum contact rate, x, as a function of hygiene, H. The shape and scale parameters are as follows, $A = 0.01$ and $\zeta = 9.5$.

Since the incubation periods of the two infections are different, we assume that dually infected individuals can only transmit either cholera or typhoid but not both infections simultaneously. Susceptible individuals acquire cholera infection either through person-to-person transmission or by ingesting *Vibrio Cholerae* from contaminated aquatic reservoirs at the rates

$$\lambda_{c_1} = \frac{f(\beta_{c_1}^{\max}, H)(I_c + \eta_c I_{ct})}{N}, \qquad \lambda_{c_2} = \frac{\beta_{c_2} B_c}{B_c + \kappa_c},$$

respectively. The parameter $\beta_{c_1}^{\max}$ denotes the maximum person-to-person cholera transmission and is defined as the product of the probability of cholera transmission per contact and the effective contact rate for cholera transmission to occur. The modification parameter η_c, accounts for the relative infectiousness of individuals in class I_c relative to individuals in class I_{ct}. We assume that $\eta_c \in (0, 1)$. This assumption is motivated by the fewer numbers of coinfected individuals as compared to those infected with cholera only. The parameter β_{c_2} denotes the

environment-to-humans per capita contact rate and the *Vibrio Cholerae* in the contaminated environment and κ_c denotes the half saturation constant of the *Vibrio Cholerae*. The *half saturation constant* is the bacterial concentration that is required to support half of the maximum rate, β_{c_2}.

Similarly, susceptible individuals acquire typhoid infection at rates given by

$$\lambda_{t_1} = \frac{f(\beta_{t_1}^{\max}, H)(I_t + \eta_t I_{ct})}{N}, \qquad \lambda_{t_2} = \frac{\beta_{t_2} B_t}{B_t + \kappa_t},$$

respectively. The parameter $\beta_{t_1}^{\max}$ denotes the maximum effective person-to-person typhoid transmission rate and the modification parameter η_t, accounts for the relative infectiousness of individuals in class I_t relative to individuals in class I_{ct}. We also assume that $\eta_t \in (0, 1)$ following the assumptions given in the cholera infection dynamics. The parameter β_{t_2} denotes the environment-to-humans per capita contact rate for susceptibles and the *Salmonella Typhi* in the contaminated environment and κ_t denotes the half saturation constant relative to the *Salmonella Typhi*.

Individuals infected with typhoid acquire cholera infection either through person-to-person transmission or by ingesting *Vibrio Cholerae* from the contaminated environment at the rates

$$\lambda_{c_3} = \frac{f(\beta_{c_3}^{\max}, H)(I_c + \eta_c I_{ct})}{N}, \quad \lambda_{c_4} = \frac{\beta_{c_4} B_c}{B_c + \kappa_c},$$

respectively. The parameter $\beta_{c_3}^{\max}$ denotes the maximum effective person-to-person cholera transmission rate of individuals in class I_t. The parameter β_{c_4} denotes the environment-to-humans per capita contact rate for individuals in class I_t and the *Vibrio Cholerae* in the contaminated environment. Individuals infected with cholera acquire typhoid infection either through person-to-person transmission or by ingesting *Salmonella Typhi* from the contaminated environment at the rates

$$\lambda_{t_3} = \frac{f(\beta_{t_3}^{\max}, H)(I_t + \eta_t I_{ct})}{N}, \qquad \lambda_{t_4} = \frac{\beta_{t_4} B_t}{B_t + \kappa_t},$$

respectively. The parameter $\beta_{t_3}^{\max}$ denotes the maximum effective person-to-person typhoid transmission rate of individuals in class I_c. The parameter β_{t_4} denotes the

environment-to-humans per capita contact rate for individuals in class I_c and the *Salmonella Typhi* in the contaminated environment.

Infected individuals in classes I_c, I_t and I_{ct} experience disease related death at rates given respectively by δ_c, δ_t and δ_{ct}. Individuals in the infectious states I_c and I_t respectively excrete *Vibrio Cholerae* bacteria and *Salmonella Typhi* bacteria into the environment at rates α_c and α_t. Individuals in the infectious state I_{ct} excrete *Vibrio Cholerae* bacteria into the environment at a rate given by θ_c and also excrete *Salmonella Typhi* bacteria into the environment at a rate given by θ_t. Individuals in the recovered classes R_c, R_t and R_{ct} are temporarily immune to cholera/typhoid infection and immunity wanes out at rates given respectively by ρ_c, ρ_t and ρ_{ct}, leading to the individuals being susceptible again.

The *Vibrio Cholerae* bacteria population is generated at a rate $g_c B_c \left(1 - \frac{B_c}{k_c}\right)$ and its growth is enhanced by individuals in the infectious states I_c and I_{ct} at rates α_c and θ_c respectively. The *Salmonella Typhi* bacteria population is generated at a rate $g_t B_t \left(1 - \frac{B_t}{k_t}\right)$ and its growth is enhanced by individuals in the infectious states I_t and I_{ct} at rates α_t and θ_t respectively. We assume that the *Vibrio Cholerae* and the *Salmonella Typhi* bacteria in the environment are respectively removed by interventions such as improved sanitation and treatment of contaminated environments at rates μ_c and μ_t. The constant recruitment into the susceptible population is represented by Λ, while the natural death rate for the general population is represented by μ. We assume that individuals in each compartment are indistinguishable and there is homogeneous mixing.

The dynamical system associated with the schematic diagram in Figure 3.1 is;

$$
\begin{aligned}
\frac{dS}{dt} =& \Lambda - (\lambda_{c_1} + \lambda_{c_2} + \lambda_{t_1} + \lambda_{t_2})S - \mu S + \rho_c R_c + \rho_t R_t + \rho_{ct} R_{ct}, \\
\frac{dI_c}{dt} =& (\lambda_{c_1} + \lambda_{c_2})S - (\lambda_{t_3} + \lambda_{t_4})I_c - (\mu + \delta_c + \epsilon_c)I_c, \\
\frac{dI_t}{dt} =& (\lambda_{t_1} + \lambda_{t_2})S - (\lambda_{c_3} + \lambda_{c_4})I_t - (\mu + \delta_t + \epsilon_t)I_t, \\
\frac{dI_{ct}}{dt} =& (\lambda_{t_3} + \lambda_{t_4})I_c + (\lambda_{c_3} + \lambda_{c_4})I_t - (\mu + \delta_{ct} + \epsilon_{ct})I_{ct}, \\
\frac{dR_c}{dt} =& \epsilon_c I_c - (\mu + \rho_c)R_c, \\
\frac{dR_t}{dt} =& \epsilon_t I_t - (\mu + \rho_t)R_t, \\
\frac{dR_{ct}}{dt} =& \epsilon_{ct} I_{ct} - (\mu + \rho_{ct})R_{ct}, \\
\frac{dB_c}{dt} =& g_c B_c \left(1 - \frac{B_c}{k_c}\right) + \alpha_c I_c + \theta_c I_{ct} - \mu_c B_c, \\
\frac{dB_t}{dt} =& g_t B_t \left(1 - \frac{B_t}{k_t}\right) + \alpha_t I_t + \theta_t I_{ct} - \mu_t B_t,
\end{aligned}
\tag{5.1}
$$

with initial conditions

$$
\begin{aligned}
S(0) =& S_0 > 0, \quad B_c(0) = B_{c0} \geq 0, \quad B_t(0) = B_{t0} \geq 0, \quad I_c(0) = I_{c0} \geq 0, \\
I_t(0) =& I_{t0} \geq 0, \quad I_{ct}(0) = I_{ct0} \geq 0, \; R_c(0) = R_{c0} \geq 0, \quad R_t(0) = R_{t0} \geq 0, \\
R_{ct}(0) =& R_{ct0} \geq 0.
\end{aligned}
$$

The Jacobian of the full system is

$$
J = \left[\begin{array}{c|c} A & C \\ \hline B & D \end{array}\right], \tag{5.2}
$$

where

$$A = \begin{pmatrix} -\mu & -f(\beta_{c_1}^{\max}, H) & -f(\beta_{t_1}^{\max}, H) & -(f(\beta_{c_1}^{\max}, H)\eta_c + f(\beta_{t_1}^{\max}, H)\eta_t) & \rho_c \\ 0 & f(\beta_{c_1}^{\max}, H) - q_c & 0 & \eta_c f(\beta_{c_1}^{\max}, H) & 0 \\ 0 & 0 & f(\beta_{t_1}^{\max}, H) - q_t & \eta_t f(\beta_{t_1}^{\max}, H) & 0 \\ 0 & 0 & 0 & -(\mu + \delta_{ct} + \epsilon_{ct}) & 0 \\ 0 & \epsilon_c & 0 & 0 & -(\mu + \rho_c) \end{pmatrix},$$

$$B = \begin{pmatrix} 0 & 0 & \epsilon_t & 0 & 0 \\ 0 & 0 & 0 & \epsilon_{ct} & 0 \\ 0 & \alpha_c & 0 & \theta_c & 0 \\ 0 & 0 & \alpha_t & \theta_t & 0 \end{pmatrix}, \quad C = \begin{pmatrix} \rho_t & \rho_{ct} & -\frac{\Lambda\beta_{c_2}}{\mu\kappa_c} & -\frac{\Lambda\beta_{t_2}}{\mu\kappa_t} \\ 0 & 0 & \frac{\Lambda\beta_{c_2}}{\mu\kappa_c} & 0 \\ 0 & 0 & 0 & \frac{\Lambda\beta_{t_2}}{\mu\kappa_t} \\ 0 & 0 & 0 & 0 \\ 0 & 0 & 0 & 0 \end{pmatrix},$$

$$D = \begin{pmatrix} -(\mu + \rho_t) & 0 & 0 & 0 \\ 0 & -(\mu + \rho_{ct}) & 0 & 0 \\ 0 & 0 & g_c - \mu_c & 0 \\ 0 & 0 & 0 & g_t - \mu_t \end{pmatrix}.$$

The dynamical system (5.1) is locally asymptotically stable if all nine of its eigenvalues have negative real parts. Five of the eigenvalues for the Jacobian, J, are $\lambda_1 = -\mu$, $\lambda_2 = -(\mu + \rho_c)$, $\lambda_3 = -(\mu + \rho_t)$, $\lambda_4 = -(\mu + \rho_{ct})$ and $\lambda_5 = -(\mu + \delta_{ct} + \epsilon_{ct})$. The other four eigenvalues for J are the eigenvalues from the sub-matrix

$$\bar{J} = \begin{pmatrix} f(\beta_{c_1}^{\max}, H) - q_c & 0 & \frac{\Lambda\beta_{c_2}}{\mu\kappa_c} & 0 \\ 0 & f(\beta_{t_1}^{\max}, H) - q_t & 0 & \frac{\Lambda\beta_{t_2}}{\mu\kappa_t} \\ \alpha_c & 0 & g_c - \mu_c & 0 \\ 0 & \alpha_t & 0 & g_t - \mu_t \end{pmatrix}.$$

The characteristic equation for matrix $\bar{J}$ is $(\lambda^2 + \nu_1\lambda + \nu_2)(\lambda^2 + \nu_3\lambda + \nu_4)$, where

$$\begin{aligned} \nu_1 &= -\left((g_c - \mu_c) + (f(\beta_{c_1}^{\max}, H) - q_c)\right), \\ \nu_2 &= (f(\beta_{c_1}^{\max}, H) - q_c)(g_c - \mu_c)\,(1 - \mathcal{R}_C), \\ \nu_3 &= -\left((g_t - \mu_t) + (f(\beta_{t_1}^{\max}, H) - q_t)\right), \\ \nu_4 &= (f(\beta_{t_1}^{\max}, H) - q_t)(g_t - \mu_t)\,(1 - \mathcal{R}_T), \end{aligned}$$

and

$$\mathcal{R}_C = \frac{\alpha_c \beta_{c_2} \Lambda}{\kappa_c \mu \mu_c q_c (1-\mathcal{R}_h^c)(1-\mathcal{R}_b^c)}, \quad \mathcal{R}_T = \frac{\alpha_t \beta_{t_2} \Lambda}{\kappa_t \mu \mu_t q_t (1-\mathcal{R}_h^t)(1-\mathcal{R}_b^t)},$$
$$\mathcal{R}_h^c = \frac{f(\beta_{c_1}^{\max}, H)}{q_c}, \quad \mathcal{R}_b^c = \frac{g_c}{\mu_c}, \quad \mathcal{R}_h^t = \frac{f(\beta_{t_1}^{\max}, H)}{q_t}, \quad \mathcal{R}_b^t = \frac{g_t}{\mu_t}.$$

The constants $\mathcal{R}_b^c$ and $\mathcal{R}_h^c$ are *the bacterial regeneration threshold* and *the human-to-human sub reproduction number*, respectively, for the cholera only sub-model. The constants $\mathcal{R}_b^t$ and $\mathcal{R}_h^t$ are *the bacterial regeneration threshold* and *the human-to-human sub reproduction number*, respectively, for the typhoid only sub-model. The constants $\mathcal{R}_C$ and $\mathcal{R}_T$ are the so-called *basic reproduction numbers* for the cholera only sub-model and the typhoid only sub-model, respectively. Clearly, $\mathcal{R}_h^c, \mathcal{R}_b^c < 1$ or $\mathcal{R}_h^c, \mathcal{R}_b^c > 1$ if and only if $\mathcal{R}_C > 0$; Similarly, $\mathcal{R}_h^t, \mathcal{R}_b^t < 1$ or $\mathcal{R}_h^t, \mathcal{R}_b^t > 1$ if and only if $\mathcal{R}_T > 0$.

We note that

$$\nu_2 > (f(\beta_{c_1}^{\max}, H) - q_c)(g_c - \mu_c)\left(1 - \max\left\{\mathcal{R}_C, \mathcal{R}_T\right\}\right),$$
$$\nu_4 > (f(\beta_{t_1}^{\max}, H) - q_t)(g_t - \mu_t)\left(1 - \max\left\{\mathcal{R}_C, \mathcal{R}_T\right\}\right).$$

Thus

$$\mathcal{R}_0 = \max\left\{\mathcal{R}_C, \mathcal{R}_T\right\}.$$

The constant $\mathcal{R}_0$ is the *basic reproduction number* for the systems (5.1). It follows from the Routh Hurwitz criterion that the four eigenvalues of $\bar{J}$ have negative real parts if $\nu_1, \nu_2, \nu_3, \nu_4 > 0$. It is easy to see that $\nu_1, \nu_2, \nu_3, \nu_4 > 0$ if $\mathcal{R}_h^t < 1, \mathcal{R}_b^t < 1$, $\mathcal{R}_h^t < 1, \mathcal{R}_b^t < 1$ and $\mathcal{R}_0 < 1$. Hence, a positive basic reproduction number for system (5.1) that is less than unity implies that the system is locally asymptotically stable at the disease free equilibrium.

5.3 Numerical Simulation

In this section, we present the numerical results obtained in this investigation. Graphs depicting the cumulative differences arising from the improvement of hygiene in each of the states variables are shown. For all the graphs, the basic

reproduction number was 1.4 whenever the level of hygiene was 0%, whereas the basic reproduction number reduced to 1.3 whenever the level of hygiene was 25%. The initial conditions used for the state variables are as follows: $S(0) = 99980,\ I_c(0) = 20,\ I_t(0) = 20,$
$I_{ct}(0) = 20,\ R_c(0) = 0,\ R_t(0) = 0,\ R_{ct}(0) = 0,\ B_c(0) = 40000,$
$B_t(0) = 40000$. The parameters of the models are found in Table 5.1.

Par.	Range	Point Value	Source	Par.	Range	Point Value	Source
$\beta_{c_1}^{\max}$		1	Assumed	g_t		0.014	[56]
$\beta_{t_1}^{\max}$		1	[55]	α_c		10	Assumed
β_{c_2}	(0.1—1)	1.97×10^{-11}	[19, 9, 44, 57]	α_t		10	[56]
β_{t_2}		1.97×10^{-11}	[52]	μ	(0.017—0.123)	0.02	[27, 50, 57]
$\beta_{c_3}^{\max}$		0.5	Assumed	μ_t		0.0345	[56]
$\beta_{t_3}^{\max}$		1	Assumed	Λ	(100—467)	449.32	[12]
β_{c_4}		10^{-1}	Assumed	μ_c		0.0345	Assumed
β_{t_4}		10^{-1}	Assumed	ϵ_c	(0.07—0.245)	0.07	[74, 57, 75, 28]
k_c	(10^6—10^9)	5×10^6	[19]	ϵ_t		0.1	[2, 53]
k_t		5×10^6	Assumed	ϵ_{ct}		0.1	Assumed
δ_c		6.58×10^{-1}	[57, 75, 77]	κ_c		0.62	Assumed
δ_t		0.6	[52]	κ_t		0.62	Assumed
ρ_c		8.12×10^{-3}	[37, 74]	θ_c		0.8	Assumed
ρ_t		1.3×10^{-3}	[62]	θ_t		0.8	Assumed
ρ_{ct}		1.3×10^{-3}	Assumed	η_c		7×10^{-4}	Assumed
g_c		0.014	Assumed	η_c		7×10^{-2}	Assumed

Table 5.1: Parameter values and their sources.

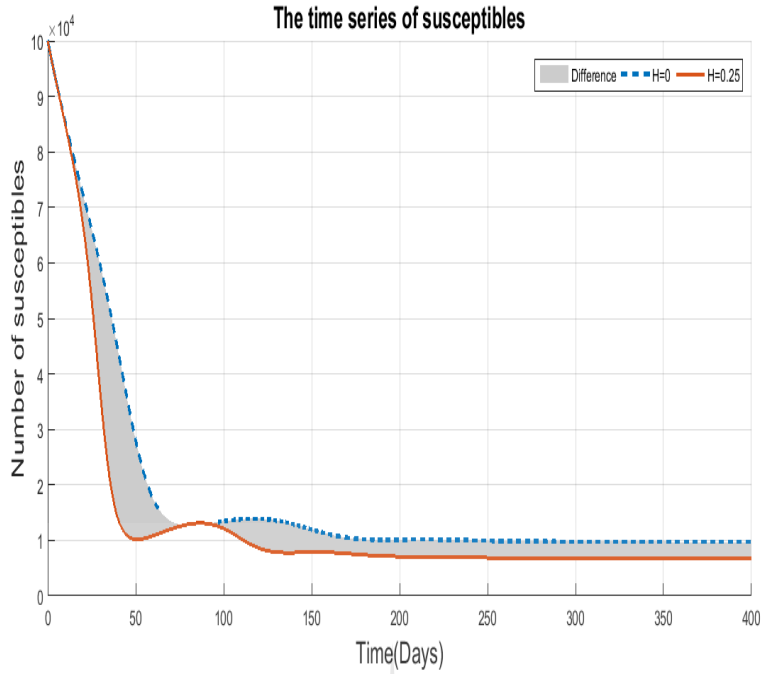

Figure 5.2: The trajectories of the susceptible classes are shown. The dotted curve shows the hygiene levels at zero, whilst the solid curve shows a 25% improvement of the hygiene levels. The total shaded region represents the cumulative number of susceptibles that avoid infection owing an improvement of hygiene.

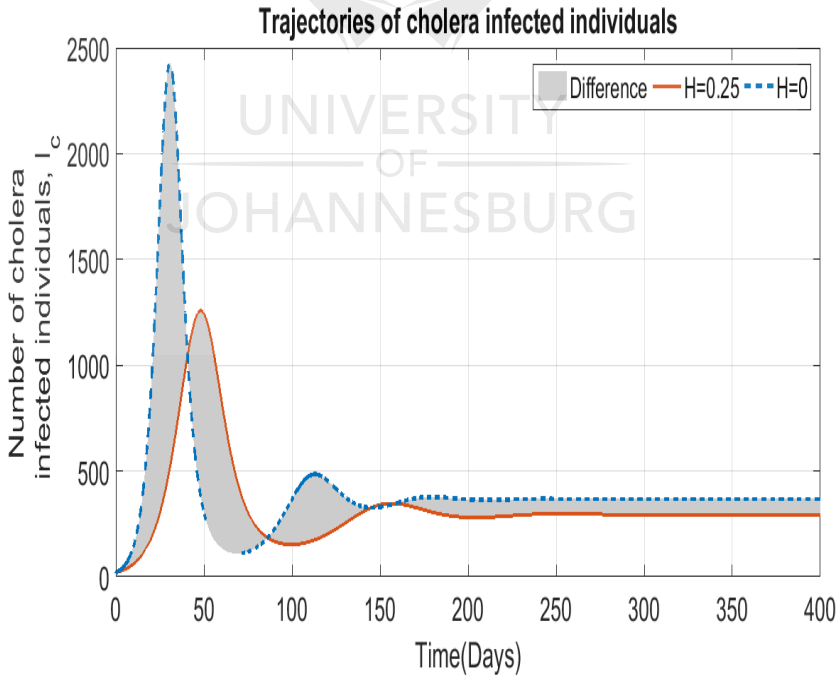

Figure 5.3: The trajectories of individuals infected with cholera are shown. The dotted curve shows the hygiene levels at zero, whilst the solid curve shows a 25% improvement of the hygiene levels. The total shaded region represents the cumulative number of cholera infections avoided by the improvement of hygiene.

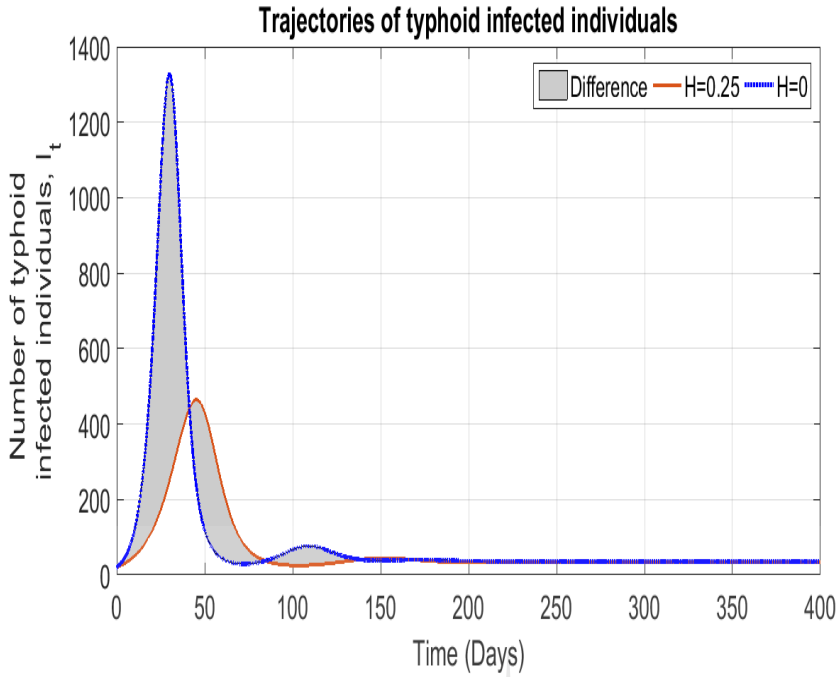

Figure 5.4: The trajectories of individuals infected with typhoid are shown. The dotted curve shows the hygiene levels at zero, whilst the solid curve shows a 25% improvement of the hygiene levels. The total shaded region represents the cumulative number of typhoid infections avoided by the improvement of hygiene.

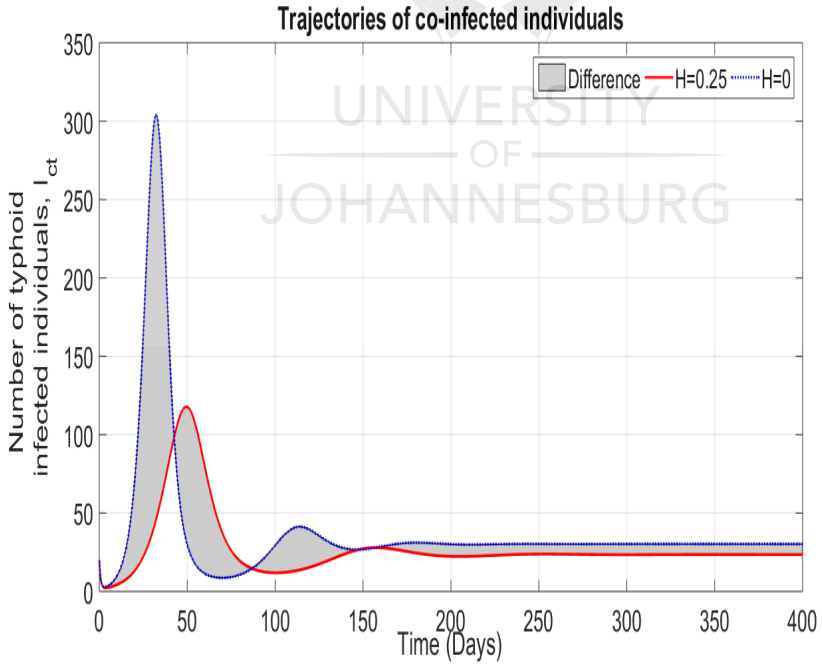

Figure 5.5: The trajectories of individuals infected with both cholera and typhoid are shown. The dotted curve shows the hygiene levels at zero, whilst the solid curve shows a 25% improvement of the hygiene levels. The total shaded region represents the cumulative number of coinfections avoided by the improvement of hygiene.

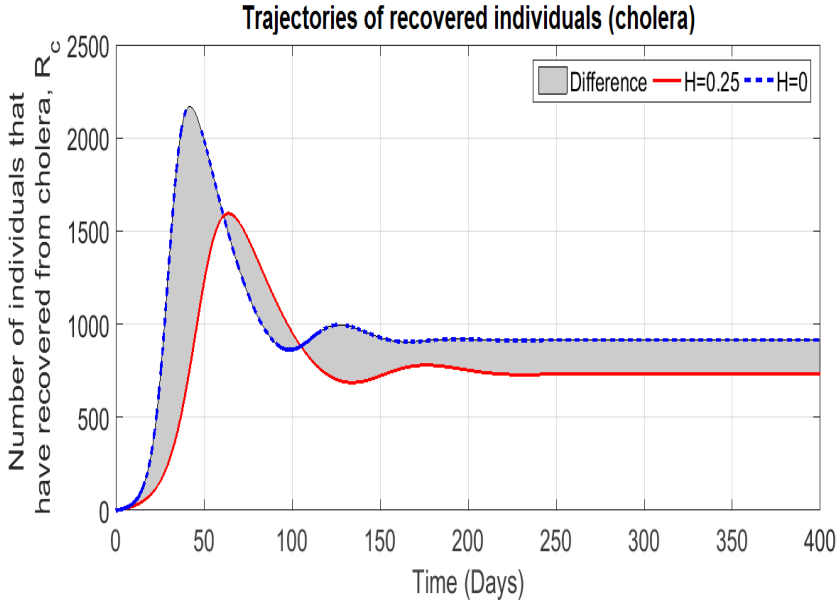

Figure 5.6: The trajectories of individuals that have recovered from cholera are shown. The dotted curve shows the hygiene levels at zero, whilst the solid curve shows a 25% improvement of the hygiene levels. The total shaded region represents the cumulative number of individuals that avoided the cholera infection because of the improvement of hygiene.

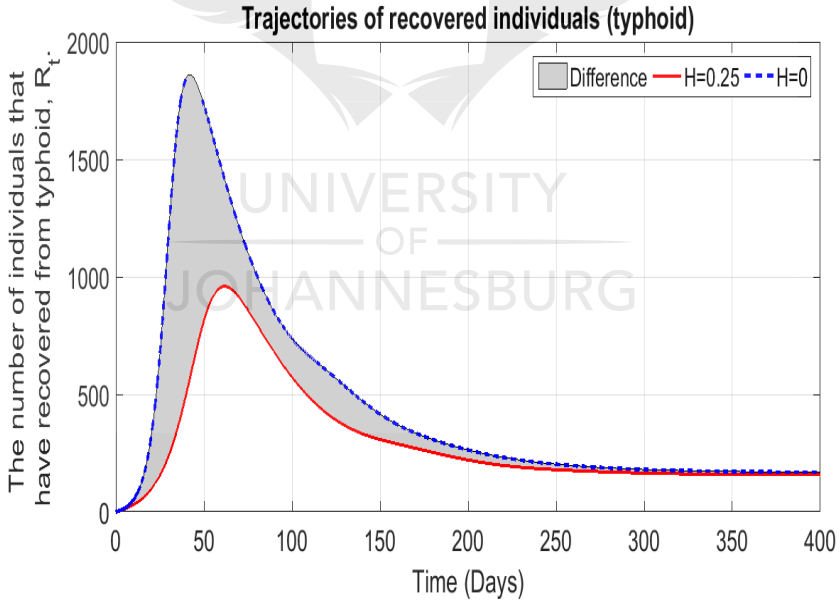

Figure 5.7: The trajectories of individuals that have recovered from typhoid are shown. The dotted curve shows the hygiene levels at zero, whilst the solid curve shows a 25% improvement of the hygiene levels. The total shaded region represents the cumulative number of individuals that avoided the typhoid infection because of the improvement of hygiene.

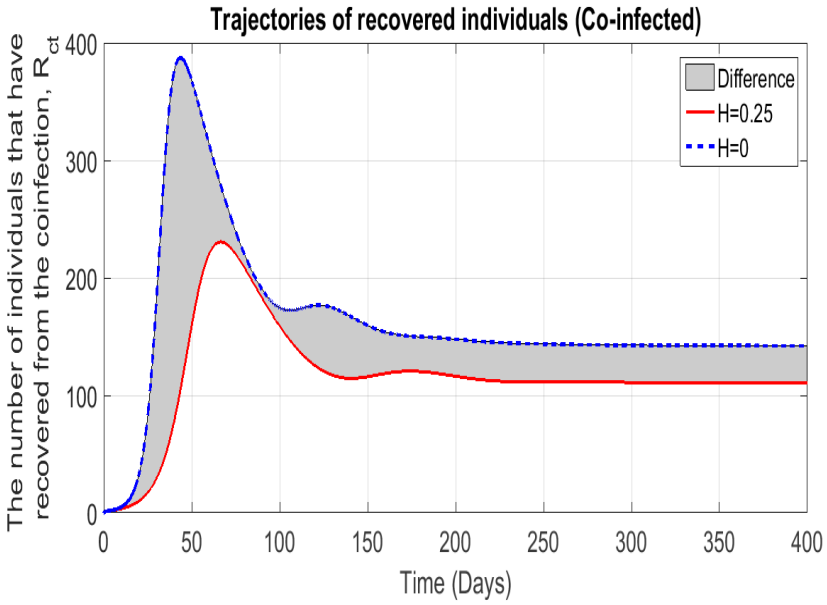

Figure 5.8: The trajectories of individuals that have recovered from the coinfection are shown. The dotted curve shows the hygiene levels at zero, whilst the solid curve shows a 25% improvement of the hygiene levels. The total shaded region represents the cumulative number of individuals that avoided the coinfection because of the improvement of hygiene.

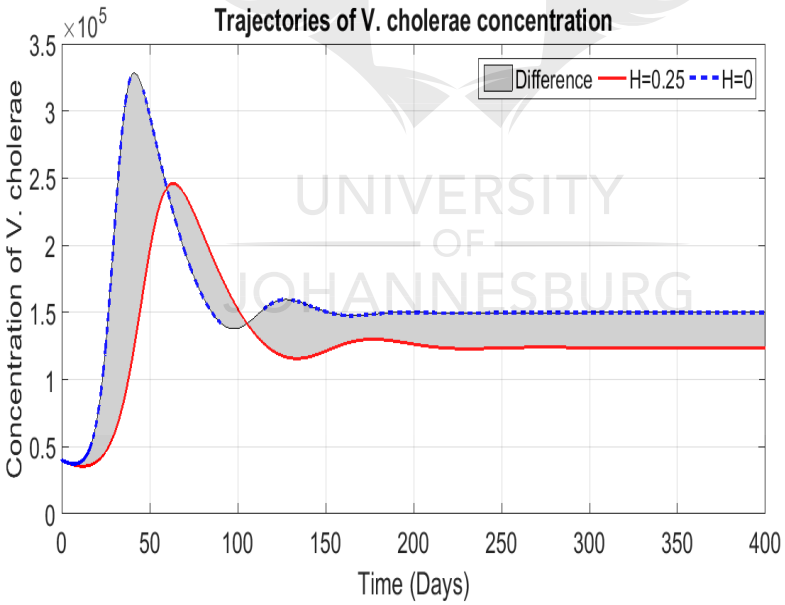

Figure 5.9: The trajectories of *V. cholerae* concentration, measured in vibros per litre, are shown. The dotted curve shows the hygiene levels at zero, whilst the solid curve shows a 25% improvement of the hygiene levels. The total shaded region represents the cumulative vibros per liter that were avoided because of the improvement of hygiene.

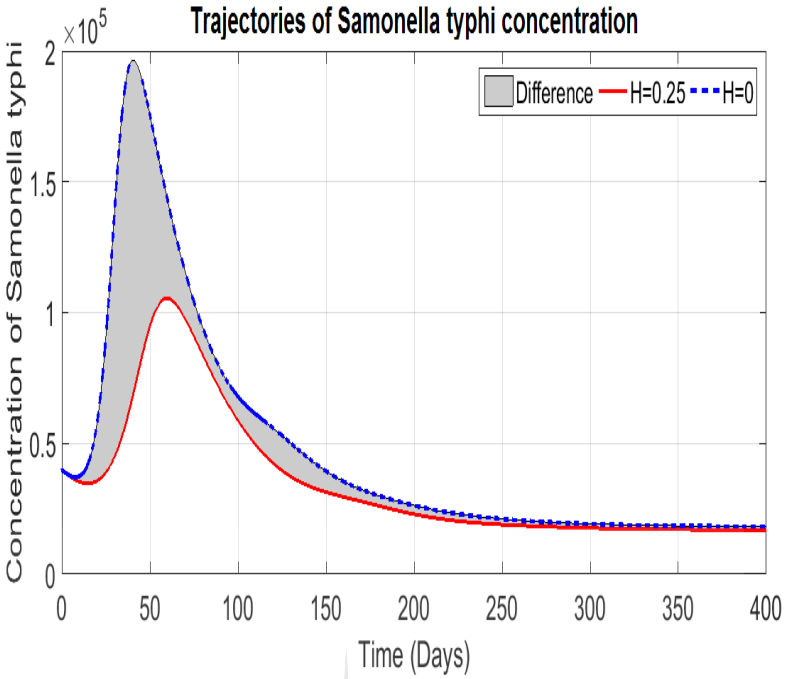

Figure 5.10: The trajectories of *S. typhi* concentration, measured in bacterial cell per litre, are shown. The dotted curve shows the hygiene levels at zero, whilst the solid curve shows a 25% improvement of the hygiene levels. The total shaded region represents the cumulative amount of bacteria per liter that were avoided because of the improvement of hygiene. $\mathcal{R}_0 = 1.4$ when $H = 0$, and $\mathcal{R}_0 = 1.3$ when $H = 0.25$.

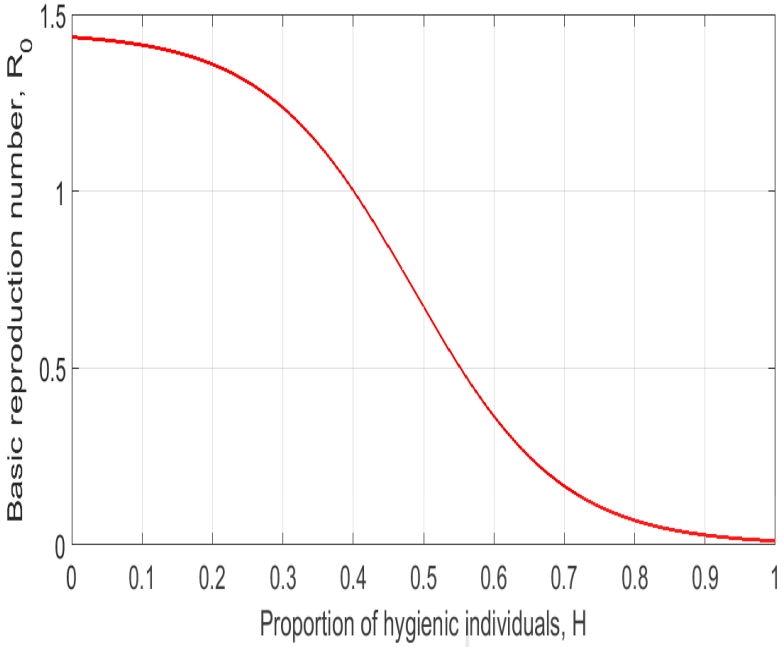

Figure 5.11: The basic reproduction number, R_0, as a function of hygiene, H, is shown.

We observe that the disease free equilibrium is locally asymptotically stable whenever the basic reproduction number is less than one. Increasing the hygiene by 25% does not yield a significant change in the reproduction number. However, the same increase of 25% in hygiene levels produces a significant change in the shape of the trajectories of the infected classes. We observe that the peak is delayed in each of the infectious classes, and the severity of the infection, that is the height of the peaks, are greatly diminished. These delayed peaks result in a negative difference in the short term, but the net difference is always positive in the long term. A significant difference in the concentration of the pathogen is also observed from a change in hygiene.

5.4 Conclusion

In this article, we present a hygiene dependent model for typhoid and cholera coinfection transmission dynamics. For the purposes of this model, the impact of hygiene on the direct transmission route is analysed. A sigmoidal decay curve is used to model the contact rate function. The effects of hygiene on the reproduction number are documented, as well as the effects of hygiene on the trajectories of each of the state variables are also documented.

The management of hygiene, even if it is limited to the direct transmission route, is sufficient to produce a significant drop in the prevalence levels of both infections. Despite the reproduction number changing minimally, significant changes in the disease peaks and delays in the peaks support this fact. This means that during an outbreak of these two infections, policymakers are afforded the necessary time to put together intervention strategies before the peak is reached, and it also means that hospitals will not be overwhelmed by number of infected individuals presenting with the diseases. Although the indirect transmission routes were not curtailed directly, managing the direct transmission routes through hygiene proved to have a positive effect on the indirect transmission route. This can be seen in how a significant difference in the concentration of pathogens was observed from a change in hygiene. The reason for this is that with fewer people getting infected, bacterial concentration will also be minimized since the number of individuals that are shedding are reduced.

The following chapter concludes the thesis.

Chapter 6

Discussion and Conclusion

This chapter gives a summary of the findings of the research. Recommendations for policy makers, limitations of the study, and the possibilities for future research are also discussed in this chapter.

A cholera typhoid coinfection model was analysed in this thesis. The analysis was carried out by first analysing the associated sub-models. Numerical simulations were carried out, and the conditions required for the model to be well posed were established. The equilibria and the stability of the model at the fixed points are determined. Through impact analysis, we were able to determine whether the two diseases were in conflict, or whether they were symbiotic. We then proposed and analysed a typhoid model with seasonality. A trigonometric function was inserted into the transmission rate to model the seasonality. To understand the effects of seasonality on the basic reproduction number, a comparison of the basic reproduction numbers of models with and without seasonality was done. The Latin Hypercube sampling technique was used to carry out the sensitivity analysis for this model. Lastly, we constructed a coinfection model for typhoid and cholera that is hygiene dependant. A sigmoidal decay curve was used to model the contact rate as a decreasing function of hygiene. We further showed how the reproduction number changes as the hygiene levels change.

Several results were discovered form the cholera typhoid coinfection model. Numerical simulations revealed the following properties about this model. First, it showed that increases in the coinfected recovery rate yields maximum impact in the presence of typhoid, yet it yields minimal impact in the presence of cholera. Second, the simulations also showed that the prevalence of the coinfected class is mostly impacted by an increase in cholera recovery rates, as opposed to typhoid recovery rates. For the model to be well posed, the death rates of the bacteria must exceed the birth rate of the bacteria. When this condition was not met, we observed that negative trajectories for the state variables could not be ruled out. We proved that the disease-free equilibrium locally was locally stable whenever the basic reproduction number was less than one, and that the endemic equilibrium was locally stable whenever the basic reproduction number was greater than one. A mathematical justification for why the two infections are symbiotic was provided.

Some key insights that were obtained from the typhoid model with seasonality where the following. First, the time average production number tends to be an unreliable estimator for the basic reproduction number for diseases with seasonal fluctuations. The recruitment rates and the natural mortality rate turned out to be the most sensitive parameters for this model.

The addition of hygiene dependence to the cholera typhoid coinfection model also produced several new insights. We observed that the decay sigmoidal curve used in this model, by design, reduced the force of infection in the direct transmission route. Unexpectedly, we also observed a substantial drop in the transmission along the indirect transmission route. It was also observed that the basic reproduction number was a decreasing function of hygiene.

Several limitations were present throughout the modelling in this thesis. The most consistent of all these limitations was the lack of data. For the typhoid cholera

coinfection model, the highly seasonal nature of the two infections was not considered, and fear was also a glaring omission in the modelling of these infections. This then formed the basis of the subsequent model on typhoid seasonality with fear. This typhoid model also had a problem of data, and the consideration of other behavioural factors such as hygiene was not done. To address these issues, we developed and analysed a hygiene dependant coinfection model for typhoid and cholera. This theoretical hygiene dependent coinfection model also had a data challenge. A possibility for future extensions to this model would be the introduction of hygiene dependency on both transmission routes, given that we understand how hygiene dependence affects the direct transmission routes. Despite these shortcomings, the results of these models can still be of great use to policymakers.

Bibliography

[1] I.I. Abubakar, T. Tillmann, and A. Banerjee. Global, regional, and national age–sex specific all-cause and cause-specific mortality for 240 causes of death, 1990–2013: a systematic analysis for the Global Burden of Disease Study 2013. *The Lancet*, 385(9963):117–171, 2015. 2, 57

[2] I.A. Adetunde. Mathematical Models for the Dynamics of Typhoid Fever in Kassena-Nankana District of Upper East Region of Ghana. *Journal of Modern Mathematics and Statistics*, 2:45–49, 2008. 49, 79, 95

[3] O. C. Akinyi, J.Y.T. Mugisha, A. Manyonge, C. Ouma, and K. Maseno. Modelling the impact of misdiagnosis and treatment on the dynamics of malaria concurrent and co-infection with pneumonia. *Applied Mathematical Sciences*, 7(126):6275–6296, 2013. 29

[4] M. Ali, A.R. Nelson, A.L. Lopez, and D.A. Sack. Updated global burden of cholera in endemic countries. *PLoS neglected tropical diseases*, 9(6):e0003832, 2015. viii, 3, 5

[5] G.D. Appiah, A. Chung, A.D. Bentsi-Enchill, S. Kim, J.A. Crump, V. Mogasale, R. Pellegrino, R.B. Slayton, and E.D. Mintz. Typhoid outbreaks, 1989–2018: implications for prevention and control. *The American journal of tropical medicine and hygiene*, 102(6):1296, 2020. xii, 6, 7

[6] B. Assan, F. Nyabadza, P. Landi, and C. Hui. Modeling the transmission of buruli ulcer in fluctuating environments. *International Journal of Biomathematics*, 10(5):1750063–1–1750063–22, 07 2017. 58

[7] A. S. Azman, K. E. Rudolph, D.A.T. Cummings, and J. Lessler. The incubation period of cholera: A systematic review. *Journal of Infection*, 66(5):432–438, 2013. 28, 52

[8] T. Baracchini, A. A. King, M. J. Bouma, X. Rodó, E. Bertuzzo, and M. Pascual. Seasonality in cholera dynamics: A rainfall-driven model explains the wide range of patterns in endemic areas. *Advances in Water Resources*, 108:357–366, 11 2016. 21, 87

[9] E. Bertuzzo, R. Casagrandi, M. Gatto, I. Rodriguez-Iturbe, and A. Rinaldo. On spatially explicit models of cholera epidemics. *Journal of the Royal Society Interface*, 7(43):321–333, 2010. 49, 95

[10] C.P. Bhunu, W. Garira, and Z. Mukandavire. Modeling HIV/AIDS and tuberculosis coinfection. *Bulletin of Mathematical Biology*, 71(7):1745–1780, 2009. 66

[11] S. Bilal and E. Michael. Effects of complexity and seasonality on backward bifurcation in vector–host models. *Royal Society Open Science*, 5(2):171971–, 02 2018. 9, 20

[12] K. Blayneh, Y. Cao, and H-D Kwon. Optimal control of vector-borne diseases: treatment and prevention. *Discrete & Continuous Dynamical Systems-B*, 11(3):587, 2009. 49, 79, 95

[13] P. S. Brachman and A. S. Evans. *Bacterial infections of humans*. Springer, 1998. 28

[14] L-M Cai, C. Modnak, and J. Wang. An age-structured model for cholera control with vaccination. *Applied Mathematics and Computation*, 299:127–140, 2017. 9, 13

[15] A.R.M. Carvalho and C.M.A. Pinto. A coinfection model for HIV and HCV. *Biosystems*, 124:46–60, 10 2014. 9, 22

[16] C. Castillo, Z. Feng, and W. Huang. On the computation of $\mathcal{R}_0$ and its role on global stability. *Mathematical Approaches for Emerging and Reemerging Infectious Disease: Models, Methods, and Theory, Springer-Verlag, Berlin*, 125:229–241, 2002. 66

[17] M. Chamuchi, J. Sigey, J. Okello, and J. Okwoyo. SII_cR model and simulation of the effects of carriers on the transmission dynamics of typhoid fever in KISII Town Kenya. *The SIJ Transactions on Computer Science Engineering & its Applications (CSEA)*, 02:86–93, 08 2014. 9, 16, 17

[18] N. Chitnis, D. Hardy, and T. Smith. A periodically-forced mathematical model for the seasonal dynamics of malaria in mosquitoes. *Bulletin of Mathematical Biology*, 74(5):1098–1124, 2012. 58

[19] C.T. Codeço. Endemic and epidemic dynamics of cholera: the role of the aquatic reservoir. *BMC Infectious Diseases*, 1(1):1, 2001. 49, 95

[20] G. Constantin de Magny, R. Murtugudde, M. R. P. Sapiano, A. Nizam, C. W. Brown, A. J. Busalacchi, M. Yunus, G. B. Nair, A. I. Gil, C. F. Lanata, J. Calkins, B. Manna, K. Rajendran, M. K. Bhattacharya, A. Huq, R. B. Sack, and R. R. Colwell. Environmental signatures associated with cholera epidemics. *Proceedings of the National Academy of Sciences*, 105:17676–17681, 2008. 86

[21] J.A. Crump and E.D. Mintz. Global Trends in Typhoid and Paratyphoid Fever. *Clinical Infectious Diseases*, 50(2):241–246, 2010. 2, 57

[22] J. Cui, Z. Wu, and X. Zhou. Mathematical analysis of a cholera model with vaccination. *Journal of Applied Mathematics*, 2014:1–16, 2014. 9, 12

[23] S. Del Valle, H. Hethcote, J.M. Hyman, and C. Castillo-Chavez. Effects of behavioral changes in a smallpox attack model. *Mathematical Biosciences*, 195(2):228–251, 2005. 58

[24] J.M. Epstein, J. Parker, D. Cummings, and R.A. Hammond. Coupled contagion dynamics of fear and disease: mathematical and computational explorations. *PLoS One*, 3(12):e3955, 2008. 58

[25] R.I. Glass, P.A. Blake, R.J. Waldman, M. Claeson, and N.F. Pierce. Cholera in africa: lessons on transmission and control for latin america. *The Lancet*, 338(8770):791–795, 1991. 3

[26] D. Greenhalgh, S. Rana, S. Samanta, T. Sardar, S. Bhattacharya, and J. Chattopadhyay. Awareness programs control infectious disease—multiple delay induced mathematical model. *Applied Mathematics and Computation*, 251:539–563, 2015. 58

[27] D.M. Hartley, J.G. Morris, and D.L. Smith. Hyperinfectivity: A Critical Element in the Ability of *V. cholerae* to Cause Epidemics? *PLoS Medicine*, 3(1):0063–0069, 2006. 49, 95

[28] T.R. Hendrix. The pathophysiology of cholera. *Bulletin of the New York Academy of Medicine*, 47(10):1169–1180, 1971. 49, 95

[29] D.L. Heymann. Control Of Communicable Diseases Manual. *American Public Health Association*, 18 edition, 2004. 2, 57

[30] M-T Ho, A. Datta, and S. Bhattacharyya. An elementary derivation of the Routh-Hurwitz criterion. *IEEE Transactions on Automatic Control*, 43(3):405–409, 1998. 65

[31] J.A. Jacquez and C.P. Simon. Qualitative theory of compartmental systems. *SIAM Review*, 35(1):43–79, 1993. 58

[32] D.T. Jamison, R.G. Feachem, M.W. Makgoba, E.R. Bos, F.K. Baingana, K.J. Hofman, and K.O. Rogo. *Disease And Mortality in Sub-saharan Africa*. World Bank Publications, 2 edition, 2006. 79

[33] M. A. Jensen, S. M. Faruque, J. J. Mekalanos, and B. R. Levin. Modeling the role of bacteriophage in the control of cholera outbreaks. *Proceedings of the National Academy of Sciences*, 103(12):4652–4657, 2006. 86

[34] M. Juga and F. Nyabadza. Modelling the ebola virus disease dynamics in the presence of interfered interventions. *Communications in Mathematical Biology and Neuroscience*, 2020:16, 07 2020. 58

[35] M.J. Keeling and P. Rohani. *Modeling Infectious Diseases in Humans and Animals*. Princeton University Press, 1 edition, 2007. 64

[36] M.A. Khan, M. Parvez, S. Islam, I. Khan, S. Shafie, and T. Gul. Mathematical analysis of typhoid model with saturated incidence rate. *Advanced Studies in Biology*, 7(2):65–78, 2015. 29

[37] A.A. King, E.L. Ionides, M. Pascual, and M.J. Bouma. Inapparent infections and cholera dynamics. *Nature*, 454(7206):877–880, 2008. 49, 95

[38] E. Kokomo and Y. Emvudu. Mathematical analysis and numerical simulation of an age-structured model of cholera with vaccination and demographic movements. *Nonlinear Analysis: Real World Applications*, 45:142–156, 02 2019. 9, 13

[39] G. Kolaye, I. Damakoa, S. Bowong, R. Houe, and D. Bekolle. A mathematical model of cholera in a periodic environment with control actions. *International Journal of Biomathematics*, pages S1793524520500254–, 02 2020. 9, 15

[40] K. Lee. The global dimensions of cholera. *Global Change and Human Health*, 2(1):6–17, 2001. 1, 2

[41] Y. Li, Z. Teng, S. Ruan, M. Li, and X. Feng. A mathematical model for the seasonal transmission of schistosomiasis in the lake and marshland regions of China. *Mathematical Biosciences & Engineering*, 14(5&6):1279–1299, 2017. 9, 19, 58

[42] K. MacKenzie, M. Palmer, W. Köster, and A. White. Examining the link between biofilm formation and the ability of pathogenic salmonella strains to colonize multiple host species. *Frontiers in Veterinary Science*, 4:1–19, 08 2017. viii, 5, 6

[43] S. Mandal, M. Mandal, and N. Pal. Cholera: A great global concern. *Asian Pacific journal of tropical medicine*, 4:573–80, 07 2011. viii, 3, 4

[44] L. Mari, E. Bertuzzo, L. Righetto, R. Casagrandi, M. Gatto, I. Rodriguez-Iturbe, and A. Rinaldo. Modelling cholera epidemics: the role of waterways, human mobility and sanitation. *Journal of the Royal Society Interface*, 9(67):376–388, 2012. 49, 95

[45] L. Matsebula, F. Nyabadza, and J. Mushanyu. Mathematical analysis of typhoid fever transmission dynamics with seasonality and fear. *Communications in Mathematical Biology and Neuroscience*, 2021(2021), 02 2021. 30, 87

[46] A. McLure, L. Furuya-Kanamori, A.C.A. Clements, M. Kirk, and K. Glass. Seasonality and community interventions in a mathematical model of clostridium difficile transmission. *Journal of Hospital Infection*, 102(2):157–164, 2019. 58

[47] M. Momba and M. Azab El-Liethy. Vibrio cholerae and cholera biotypes. *Global water pathogen project*, 2017. viii, 2, 3

[48] H.C. Moore, P. Jacoby, A.B. Hogan, C.C. Blyth, and G.N. Mercer. Modelling the Seasonal Epidemics of Respiratory Syncytial Virus in Young Children. *PLOS ONE*, 9(6):1–8, 06 2014. 58

[49] A.K. Mukhopadhyay, Y. Takeda, and G.B. Nair. Cholera outbreaks in the El Tor biotype era and the impact of the new El Tor variants. *Current Topics in Microbiology and Immunology*, 379:17–47, 2014. 2, 3

[50] P.M. Munro and R.R. Colwell. Fate of vibrio cholerae o1 in seawater microcosms. *Water Research*, 30(1):47–50, 1996. 49, 95

[51] J. Mushanyu, F. Nyabadza, G. Muchatibaya, P. Mafuta, and G. Nhawu. Assessing the potential impact of limited public health resources on the spread and control of typhoid. *Journal of Mathematical Biology*, 77(3):647–670, 2018. 59, 84, 87

[52] S. Mushayabasa. Impact of vaccines on controlling typhoid fever in Kassena-Nankana district of upper east region of Ghana: insights from a mathematical model. *Journal of Modern Mathematics and Statistics*, 5(2):54–59, 2011. 1, 2, 49, 57, 79, 95

[53] S. Mushayabasa. Modeling the impact of optimal screening on typhoid dynamics. *International Journal of Dynamics and Control*, 4(3):330–338, 2016. 49, 79, 95

[54] S. Mushayabasa, C.P. Bhunu, and N.A. Mhlanga. Modeling the Transmission Dynamics of Typhoid in Malaria Endemic Settings. *Applications & Applied Mathematics*, 9(1):121–140, 2014. 29, 87

[55] S. Mushayabasa, C.P. Bhunu, and E.T. Ngarakana-Gwasira. Assessing the Impact of Drug Resistance on the Transmission Dynamics of Typhoid Fever. *Computational Biology Journal*, 2013:1–13, 2013. 29, 49, 95

[56] J.M. Mutua, F-B Wang, and N.K. Vaidya. Modeling malaria and typhoid fever co-infection dynamics. *Mathematical Biosciences*, 264:128–144, 2015. 49, 79, 87, 95

[57] R.L.M. Neilan, E. Schaefer, H. Gaff, K.R. Fister, and S. Lenhart. Modeling optimal intervention strategies for cholera. *Bulletin of Mathematical Biology*, 72(8):2004–2018, 2010. 49, 95

[58] J. Nthiiri, O. Lawi, C. Akinyi, D. Oganga, C. Wachira, M. Musyoka, P. Otieno, and L. Koech. Mathematical modelling of typhoid fever disease incorporating protection against infection. *British Journal of Mathematics & Computer Science*, 14(1):1–10, 01 2016. 9, 16

[59] F. Nyabadza, B. T. Bekele, M. A. Rúa, D. M. Malonza, N. Chiduku, and M. Kgosimore. The implications of HIV treatment on the HIV-Malaria coinfection dynamics: A modeling perspective. *BioMed Research International*, 2015:1–14, 2015. 25

[60] N. Nyerere, L.S. Luboobi, S.C. Mpeshe, G.M. Shirima, and A. Kloczkowski. Modeling the Impact of Seasonal Weather Variations on the Infectiology of Brucellosis. *Computational and Mathematical Methods in Medicine*, 2020:1–19, 2020. 58

[61] H.S. N'cho, K.P. Masunda, I. Mukeredzi, et al. Notes from the Field: Typhoid Fever Outbreak — Harare, Zimbabwe. *MMWR Morb Mortal Wkly Rep 2019*, 68:44–45, 2019. 2

[62] K.O. Okosun and O.D. Makinde. Modelling the impact of drug resistance in malaria transmission and its optimal control analysis. *International Journal of the Physical Sciences*, 6(28):6479–6487, 2011. 49, 79, 95

[63] K.O. Okosun and O.D. Makinde. A co-infection model of malaria and cholera diseases with optimal control. *Mathematical Biosciences*, 258:19–32, 2014. 9, 26

[64] D.O Onyinge, N.O. Ongati, and F. Odundo. Mathematical model for co-infection of HIV/AIDS and pneumonia with treatment. *International Journal of Scientific Engineering and Applied Science*, 2(1):106–111, 2016. 29

[65] S. Osman and O.D. Makinde. A mathematical model for coinfection of listeriosis and anthrax diseases. *International Journal of Mathematics and Mathematical Sciences*, 2018:1–14, 08 2018. 9, 24

[66] O.J. Peter, O.A. Afolabi, F.A. Oguntolu, C.Y. Ishola, and A.A. Victor. Solution of a deterministic mathematical model of typhoid fever by variational iteration method. *Science World Journal*, 13(2):64–68, 2018. 15, 16

[67] T.A. Phan, J.P. Tian, and B. Wang. Dynamics of cholera epidemic models in fluctuating environments. *Stochastics and Dynamics*, 21(2):2150011, 2021. 58

[68] C. M. A. Pinto and A. Carvalho. Effects of treatment, awareness and condom use in a coinfection model for HIV and HCV in MSM. *Journal of Biological System*, 23(2):165–193, 06 2015. 9, 22, 23

[69] V.E. Pitzer, C.C. Bowles, S. Baker, G. Kang, V. Balaji, J.J. Farrar, B.T. Grenfell, and E.T. Ryan. Predicting the impact of vaccination on the transmission dynamics of typhoid in South Asia: A mathematical modeling study. *PLoS Neglected Tropical Diseases*, 8(1):e2642, 2014. 29

[70] D. Posny and J. Wang. Computing the basic reproductive numbers for epidemiological models in nonhomogeneous environments. *Applied Mathematics and Computation*, 242:473–490, 2014. 73, 81

[71] D. Posny and J. Wang. Modelling cholera in periodic environments. *Journal of Biological Dynamics*, 8(1):1–19, 2014. 9, 18, 58

[72] K. Prem, Y. Liu, T.W. Russell, A.J. Kucharski, R.M. Eggo, N. Davies, M. Jit, P. Klepac, S. Flasche, S. Clifford, C.A.B. Pearson, J.D. Munday, S. Abbott, H. Gibbs, A. Rosello, B.J. Quilty, T. Jombart, F. Sun, C. Diamond, A. Gimma, K. van Zandvoort, S. Funk, C.I. Jarvis, W.J. Edmunds, N.I. Bosse, and J. Hellewell. The effect of control strategies to reduce social mixing on outcomes of the COVID-19 epidemic in Wuhan, China: a modelling study. *The Lancet Public Health*, page S2468266720300736, 2020. 58

[73] N.J. Saad, V.D. Lynch, M. Antillón, C. Yang, J.A. Crump, and V.E. Pitzer. Seasonal dynamics of typhoid and paratyphoid fever. *Scientific Reports*, 8(1):6870, 2018. 59, 83

[74] R.P. Sanches, C.P. Ferreira, and R. A. Kraenkel. The role of immunity and seasonality in cholera epidemics. *Bulletin of Mathematical Biology*, 73(12):2916–2931, 2011. 49, 95

[75] J. Sepulveda, H. Gomez-Dantes, and M. Bronfman. Cholera in the Americas: an overview. *Infection*, 20(5):243–248, 1992. 49, 95

[76] P.D. Shapiro. How close is too close?: The negative relationship between knowledge of HIV transmission routes and social distancing tendencies. *The Social Science Journal*, 42(4):629–637, 2005. 58

[77] Z. Shuai, J.H. Tien, and P. van den Driessche. Cholera models with hyperinfectivity and temporary immunity. *Bulletin of Mathematical Biology*, 74(10):2423–2445, 2012. 49, 95

[78] H.L. Smith and P. Waltman. *The Theory of the Chemostat: Dynamics of Microbial Competition*. Cambridge Studies in Mathematical Biology. Cambridge University Press, 1995. 76

[79] A. Sommer, J. Katz, and I. Tarwotjo. Increased risk of respiratory disease and diarrhea in children with preexisting mild vitamin a deficiency. *The American journal of clinical nutrition*, 40(5):1090–1095, 1984. 86

[80] G-Q Sun, Z. Bai, Z-K Zhang, T. Zhou, and Z. Jin. Positive periodic solutions of an epidemic model with seasonality. *The Scientific World Journal*, 2013:1–10, 2013. 19, 71

[81] A. Taylor, A. Santiago, A. Gonzalez-Cortes, and E.J. Gangarosa. Outbreak of typhoid fever in Trinidad in 1971 traced to a commercial ice cream product. *American Journal of Epidemiology*, 100(2):150–157, 1974. 29, 52

[82] G. Teschl. *Ordinary differential equations and dynamical systems*, volume 140 of *AMS Graduate studies in mathematics*. American Mathematical Society, 2012. 58

[83] J.P. Tian and J. Wang. Global stability for cholera epidemic models. *Mathematical Biosciences*, 232(1):31–41, 2011. 9, 11

[84] G.T. Tilahun, O.D. Makinde, and D. Malonza. Co-dynamics of pneumonia and typhoid fever diseases with cost effective optimal control analysis. *Applied Mathematics and Computation*, 316:438–459, 2018. 1, 57, 87

[85] B. Traoré, B. Sangaré, and S. Traoré. A mathematical model of malaria transmission with structured vector population and seasonality. *Journal of Applied Mathematics*, 2017:1–15, 2017. 58

[86] A.C. Tsai, D.R. Bangsberg, S.M. Kegeles, I.T. Katz, J.E. Haberer, C. Muzoora, E. Kumbakumba, P.W. Hunt, J.N. Martin, and S.D. Weiser. Internalized stigma, social distance, and disclosure of HIV seropositivity in rural Uganda. *Annals of Behavioral Medicine*, 46(3):285–294, 2013. 58

[87] P. van den Driessche and J. Watmough. Reproduction numbers and subthreshold endemic equilibria for compartmental models of disease transmission. *Mathematical biosciences*, 180(1-2):29–48, 2002. 64

[88] M. Wameko, P. Koya, and A. Wodajo. Mathematical model for transmission dynamics of typhoid fever with optimal control strategies. *International Journal of Industrial Mathematics*, 12(3):283–296, 2020. 9, 17

[89] W. Wang and X-Q Zhao. Threshold dynamics for compartmental epidemic models in periodic environments. *Journal of Dynamics and Differential Equations*, 20(3):699–717, 2008. 71, 72, 73, 75, 76

[90] X. Wang, D. Gao, and J. Wang. Influence of human behavior on cholera dynamics. *Mathematical Biosciences*, 267:41–52, 09 2015. 9, 14, 58

[91] X. Wang, L. Zanette, and X. Zou. Modelling the fear effect in predator–prey interactions. *Journal of Mathematical Biology*, 73(5):1179–1204, 2016. 58

[92] World Health Organisation. Diarrhoeal Diseases, Cholera, key facts. https://www.who.int/news-room/fact-sheets/detail/cholera, 2021. Accessed: 2021-01-29. 1, 3

[93] World Health Organisation. Diarrhoeal Diseases, Salmonella (non-typhoidal). https://www.who.int/news-room/fact-sheets/detail/salmonella-(non-typhoidal), 2021. Accessed: 2021-10-29. 6

[94] World Health Organisation. Diarrhoeal Diseases, Typhoid Fever. https://web.archive.org/web/20111102190825/http://www.who.int/vaccine_research/diseases/diarrhoeal/en/index7.html, 2021. Accessed: 2021-01-11. 2, 57

[95] X. Yang, L. Chen, and J. Chen. Permanence and positive periodic solution for the single-species nonautonomous delay diffusive models. *Computers & Mathematics with Applications*, 32(4):109–116, 1996. 62

[96] F. Zhang and X-Q Zhao. A periodic epidemic model in a patchy environment. *Journal of Mathematical Analysis and Applications*, 325(1):496–516, 2007. 72